AD-A042 276 IRT CORP SAN DIEGO CALIF F/G 18/4
NEUTRON DOSIMETRY STANDARD.(U)
MAR 77 V V VERBINSKI DNA001-74-C-0163
UNCLASSIFIED INTEL-RT-8106-054 DNA-4128F NL

1 OF 2
ADA
042276

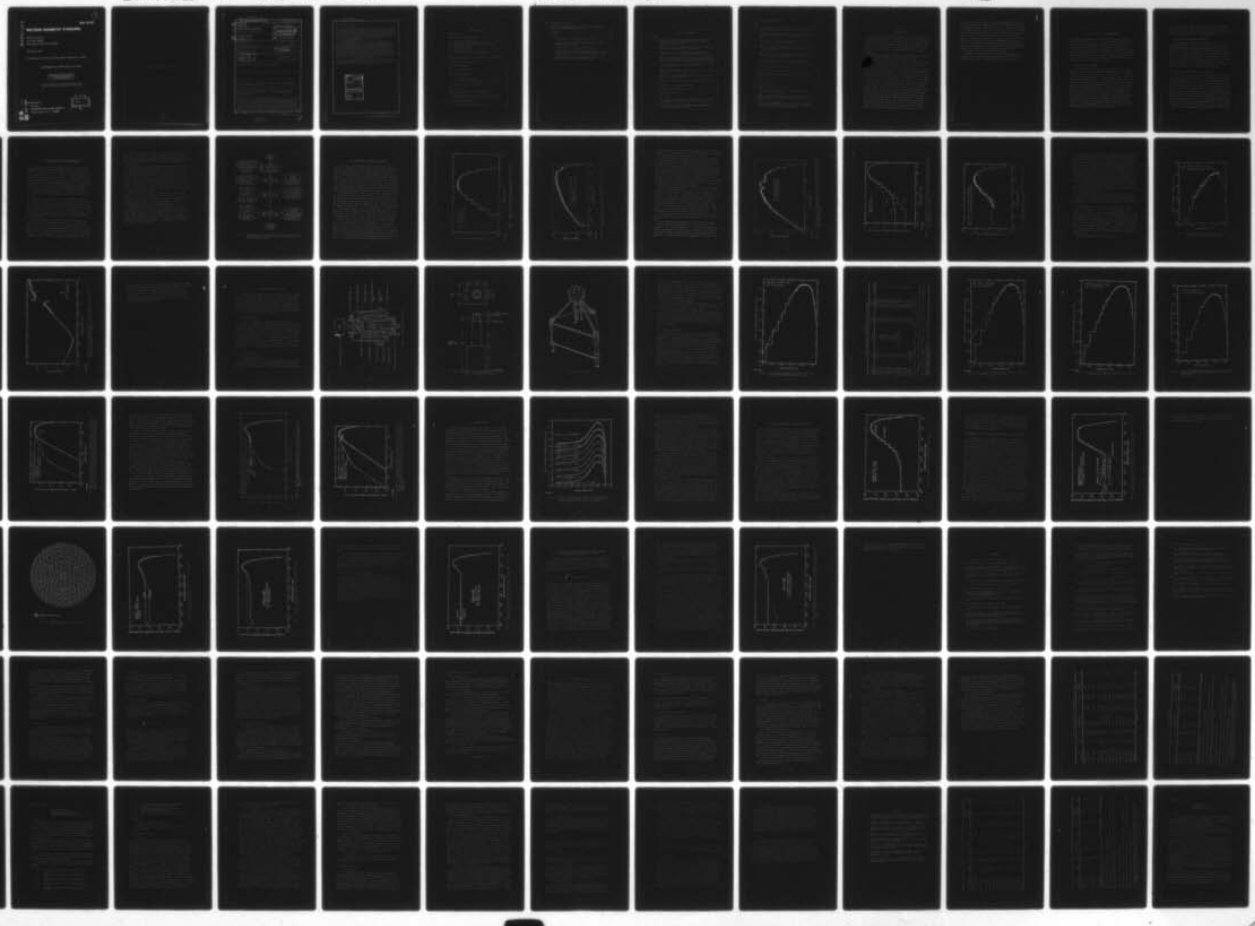

(12)

DNA 4128F

NEUTRON DOSIMETRY STANDARD

IRT Corporation
P.O. Box 80817
San Diego, California 92138

15 March 1977

Final Report for Period 1 May 1974—30 October 1975

CONTRACT No. DNA 001-74-C-0163

THIS WORK SPONSORED BY THE DEFENSE NUCLEAR AGENCY
UNDER RDT&E RMSS CODE B323075464 Z99QAXTE06241 H2590D.

Prepared for
Director
DEFENSE NUCLEAR AGENCY
Washington, D. C. 20305

Destroy this report when it is no longer needed. Do not return to sender.

UNCLASSIFIED

SECURITY CLASSIFICATION OF THIS PAGE (When Data Entered)

REPORT DOCUMENTATION PAGE

READ INSTRUCTIONS BEFORE COMPLETING FORM

1. REPORT NUMBER: DNA 4128F	2. GOVT ACCESSION NO.
3. RECIPIENT'S CATALOG NUMBER	
4. TITLE (and Subtitle): NEUTRON DOSIMETRY STANDARD	5. TYPE OF REPORT & PERIOD COVERED: Final Report for Period 1 May 74—30 Oct 75
6. PERFORMING ORG. REPORT NUMBER: INTEL-RT-8106-054	
7. AUTHOR(s): V. V. Verbinski	8. CONTRACT OR GRANT NUMBER(s): DNA 001-74-C-0163
9. PERFORMING ORGANIZATION NAME AND ADDRESS: IRT Corporation, P.O. Box 80817, San Diego, California 92138	10. PROGRAM ELEMENT, PROJECT, TASK AREA & WORK UNIT NUMBERS: Subtask Z99QAXTE062-41
11. CONTROLLING OFFICE NAME AND ADDRESS: Director, Defense Nuclear Agency, Washington, D.C. 20305	12. REPORT DATE: 15 March 1977
	13. NUMBER OF PAGES: 124
14. MONITORING AGENCY NAME & ADDRESS (if different from Controlling Office): 116p.	15. SECURITY CLASS (of this report): UNCLASSIFIED
	15a. DECLASSIFICATION/DOWNGRADING SCHEDULE

16. DISTRIBUTION STATEMENT (of this Report)

Approved for public release; distribution unlimited.

17. DISTRIBUTION STATEMENT (of the abstract entered in Block 20, if different from Report)

18. SUPPLEMENTARY NOTES

This work sponsored by the Defense Nuclear Agency under RDT&E RMSS Code B323075464 Z99QAXTE06241 H2590D.

19. KEY WORDS (Continue on reverse side if necessary and identify by block number)

Standard Neutron Spectrometry Method
Selection of Neutron Spectrometry Method for Si Damage
Radiation Damage Function
Spectral Characterization

20. ABSTRACT (Continue on reverse side if necessary and identify by block number)

The neutron spectrometry program described in this report was carried out in support of a set of draft ASTM standards (included as Appendix A) prescribing a standard method of measuring neutron spectra and characterizing the spectra in terms of their effectiveness in producing radiation damage in silicon. The neutron fluence is characterized in terms of ϕ_{eq}, the number of near-1-MeV neutrons required to produce the same radiation damage, and the spectral shape in terms of ϕ_{eq}/ϕ, the equivalent 1-MeV

→ next page

DD FORM 1 JAN 73 1473 EDITION OF 1 NOV 65 IS OBSOLETE

UNCLASSIFIED

SECURITY CLASSIFICATION OF THIS PAGE (When Data Entered)

409388

20. ABSTRACT (Continued)

fluence per unit fluence of neutrons above 0.01 MeV. Since there are no useable thresholds between 0.01 and 0.5 MeV, the spectrum is, to a large extent, indeterminate below ~1 MeV. However, it was found that reactor spectra can be parameterized by fitting a 1/E tail to a fission or GODIVA-core spectrum, the fitting point being determined by the threshold-foil data. In this way, the uncertainty interval can be reduced to yield accuracies in ϕ_{eq}/ϕ and ϕ_{eq} of ~5 and 10%, respectively.

The program included an evaluation of many candidate methods of specifying a neutron field, a selection of the most suitable method (threshold-foil spectrometry), a measurement of three different spectra, a comparison of the measurements with "known" spectra to determine the accuracy of the method, a comparison of threshold-foil measurements carried out by two different laboratories to evaluate the precision of the method, a variational study to determine the factors that most sensitively impact the accuracy, and folding the spectra in with a recently calculated silicon radiation damage function D(E) to express the accuracy in terms of a single parameter ϕ_{eq} or ϕ_{eq}/ϕ.

The work is of interest in planning irradiation schedules, for parts screening, or for sample-specification tests, and in comparing radiation damage studies carried out in different neutron fields.

TABLE OF CONTENTS

TABLE OF CONTENTS (Continued)

LIST OF ILLUSTRATIONS

Figure

LIST OF ILLUSTRATIONS (Continued)

Figure

1. INTRODUCTION

The objectives of this task are the selection of a standard method of measuring and characterizing neutron spectra in terms of the permanent radiation damage produced in silicon semiconductor devices and the evaluation of the accuracy of the method. The accuracy was determined by comparing the measured results to the "known" spectrum for three different spectra, and by carrying out a variational study of the measurement technique.

The detailed procedure for quantifying the neutron field is presented as five ASTM draft standards. They are included as Appendix A.

This report covers the work completed in Phase I (Task 4) which was carried out during the period May 1, 1974 to February 28, 1975, and Phase II (Task 13), which was completed October 30, 1975. In Section 2, a brief review is given of the advantages and shortcomings of several candidate methods of neutron spectrometry. The reasons for choosing the foil-activation method are cited there. Section 3 presents the detailed method of obtaining a neutron spectrum with foil activation data, using the SAND II unfolding code with its threshold-foil cross-section set, and selecting a suitable "start" spectrum for SAND II input. Section 4 covers the work done to obtain the "best known" spectrum for comparison with the SAND II results. Section 5 presents the method of obtaining ϕ_{eq}/ϕ, the fluence of 1-MeV neutrons required to produce the same radiation damage as a unit fluence of neutrons from the spectrum being characterized. In Section 6 the method of obtaining two experimental spectra from the White Sands Missile Range Fast Burst Reactor (WSMR FBR) is described. Included is a description of work done to assess the importance of selecting a good starting spectrum – one that includes all the physics of the neutron source, the shielding, and the nearby scattering material. Section 7 presents the results of the variational study. The precision of the

measuring technique was evaluated by remeasuring the WSMR FBR spectra in the glory hole, and 50 cm from the reactor. The measurements were made by a different experimental group with their own foils, detector, and gamma-ray calibration sources. The results are presented in Section 8. A TRIGA reactor spectrum (much softer) was measured and compared with a calculated spectrum. Also, the systematics of measuring reactor spectra became apparent (selecting the trial spectrum). These are discussed in Sections 8 and 9, where the results of the recent measurements are presented. In addition, a discussion of the relationship between the precise spectral characterization (where the "known" spectrum is folded in with the "known" damage function), and that of utilizing the spectral index [SI = (ϕ >0.01 MeV)/(ϕ >3 MeV)] is presented in Section 10.

The detailed methodology of the "Neutron Dosimetry Standard", the summary of this report, the conclusions, and the assessment of the precision and accuracy of the method are well covered in Appendix A.

2. SELECTION OF A SPECTROMETRY METHOD

The most promosing neutron spectrometry methods for application to radiation damage studies in silicon (0.01 to 14 MeV neutron energy interval) are the time-of-flight (TOF) method, the organic scintillation spectrometer with pulse-shape gamma-ray discrimination properties, the proton-recoil proportional counter spectrometer, coincidence spectrometers utilizing nuclear reactions such as $^{3}He(n,p)^{3}H$ and $^{6}Li(n,\alpha)^{3}H$ with coincidence counting of the two reaction products, the proton-recoil spectrometer telescope, proton-recoil nuclear emulsions, threshold-foil-activation spectrometry, and silicon itself as a dosimeter.

2.1 TIME-OF-FLIGHT SPECTROMETRY

The TOF method is by far the most accurate, since it gives a direct measure of the velocity of each neutron detected; there is no unfolding to be done, and good energy resolution is feasible (Ref. 1). The detector efficiency versus neutron energy is the only critical input, and this has been obtained with good accuracy in a coordinated effort utilizing measurements and calculations (Ref. 2). However, to be useful in the pertinent energy range, a nanosecond pulsed-neutron source, a 50- to 200-m flight path, a detector with nanosecond time resolution, and a neutron assembly with short neutron dieaway time must be available. The method is very expensive and few such facilities are readily available. Nonetheless, the verification of the "known" or "standard" spectrum for this work was carried out with the TOF method, as discussed in Section 4. With the skillful use of good geometry shielding and/or gamma-ray-insensitive detectors, reasonably good gamma-ray rejection can be achieved. Energies of thermal through 200 MeV can readily be measured.

For the case of "reactor spectra", however, the neutron dieaway time is a very serious problem. The TOF measurements are only possible for fast subcritical assemblies with k_{eff} ~0.9 or less, with a long flight path, and with complex dieaway time corrections (Refs. 3,4).

2.2 PROTON-RECOIL SCINTILLATION SPECTROMETER

The proton-recoil scintillation spectrometer (Ref. 5) is useful where TOF measurements are not feasible, and where good geometric efficiencies are important to obtaining statistically significant results (Refs. 6,7). However, the gamma-ray rejection capability with pulse-shape discrimination is not adequate for reactor environments unless the reactor is a zero-power assembly that has not been subjected to high-power gamma-ray buildup. The detector response must be very accurately known as a function of neutron energy; otherwise, error propagation to low energies severely limits the energy range of the spectrometer. Spectra have been reported for ~0.5 to ~15 MeV with this method.

2.3 PROTON-RECOIL PROPORTIONAL COUNTER SPECTROMETER

Detectors utilizing proton-recoil proportional counters have been applied with good success from ~5 keV to ~2 MeV (Refs. 8,9) in reactor cores, and up to about 10 MeV (Ref. 10) in "beam" geometries where the neutrons are parallel to the axis of a long, gas-filled proportional counter. Again, gamma-ray discrimination is a serious problem except in a "cold" reactor core – one that is not very gamma radioactive. This method is generally considerably more expensive than the threshold-foil method, requiring very long counting times at many gas gain settings and an on-line computer for best gamma-ray discrimination capabilities. Earlier methods utilized a series of counters with increasingly higher pressures to cover increasingly higher neutron energies with good gamma discrimination over a limited range, but few, if any, reliable spectra spanning a large energy range have been reported with this technique.

2.4 ^{3}He AND ^{6}Li COUNTERS

Counters using exoergic nuclear reactions of light particles, such as $^{3}He(n,p)^{3}H$ and $^{6}Li(n,\alpha)^{3}H$, have been used with coincidence-measurement of the two reaction products (Ref. 11). The gamma-ray rejection can be reasonably good in a shielded diode configuration (Ref. 11), but is otherwise generally inadequate. One of the main problems in a very low counter efficiency, requiring long reactor times for a good measurement. Energy ranges of ∿100 keV to 5 to 10 MeV have been reported. At high energies, reaction-product background, multiparticle breakup, and the very forward angular distributions severely limit the accuracy of the coincidence-counting method.

2.5 PROTON-RECOIL TELESCOPE

The proton-recoil telescope consists of a hydrogeneous scatterer of a given diameter separated by a detector several diameters away. This is placed in a neutron beam incident along the common axis of the scatterer and detector. Background estimates are made by replacing the hydrogeneous scatterer (usually CH_2) with a carbon scatterer. The method gives the neutron spectrum directly because the forward scattered protons have an energy equal to the incident neutron energy. This method can operate only in a beam geometry. It requires a number of measurements, each with a different scatterer thickness, to cover a large range of neutron energy. The background determinations are, in most cases, very inaccurate because of high-energy neutron interactions with all the surrounding material, especially the material near the scatterer; the detector efficiency is very low; gamma backgrounds are unmanageable for most reactor-type measurements; and the "splicing" together of several segments of a spectrum is nearly always problematic. Energy ranges of ∿2 to ∿10 MeV have been achieved in measurements where the gamma-ray backgrounds are low.

2.6 NUCLEAR EMULSIONS

Proton-recoil nuclear emulsions have been used for early reactor-spectrum measurements in the 2- to 10-MeV energy range. They also have

low efficiencies, are subject to gamma-ray darkening, and require laborious, manual recoil-track measurements for each exposed emulsion.

2.7 THRESHOLD-FOIL-ACTIVATION SPECTROMETRY

This method, currently useful for the neutron energy range of thermal to ∿15 or 20 MeV, is applicable to both pulsed and steady-state neutron fields, and has a remarkably high tolerance to gamma-ray fields. Two notable exceptions exist. These apply to (γ, fission) and (γ,γ') reactions, which seriously complete with (n, fission) and (n,n') reactions in the same foils. These gamma reactions are important (a) for Linac-type (γ,n) sources, where the Linac bremsstrahlung is very intense and energetic (the γ,f thresholds are at $\sim E_{\gamma} \simeq 6$ MeV), and (b) for reactor spectra in low-Z neutron shields, such as water, at 1 to 2 feet in the shield or deeper.

The foil-activation method was of very limited usefulness before the advent of an evaluated, consistent cross-section set, an unfolding code that retards spurious structure, and reliable neutron transport codes (and cross-section sets) to provide a physically meaningful trial spectrum. These are discussed in more detail in the next section.

2.8 USE OF SILICON ITSELF AS A DOSIMETER

This has been ruled out as impractical because of difficulties in measuring the number of dislocation centers. The silicon would have to be kept cold (at liquid-nitrogen temperatures or colder) during and after radiation. Damage-annealing from all sources would have to be correctly accounted for. It can vary with the type of device, the current drain, temperature, gamma-ray dose rate, and perhaps even the neutron dose rate.

3. CHARACTERISTICS AND OPERATING PRINCIPLES OF THE THRESHOLD-FOIL-ACTIVATION SPECTROMETER

Threshold-foil neutron spectrometry became a useful tool when an evaluated reference cross-section library (Ref. 12) became available. The set discussed in Reference 12 includes 23 new and revised cross sections comprising a consistent set. This set is generally adequate for reactor spectra from thermal through 15 MeV. In addition to the availability of an evaluated set of consistent cross sections (Refs. 13,14), the development of an iterative unfolding code (Ref. 13), with modifications (Ref. 14, SAND II code) that retard the formation of spurious structure while preserving real structure (known input structure, such as a resonance "dip" or a 14-MeV source "peak"), made it feasible to obtain accurate reactor spectra when a good trial spectrum is input to the code.

With the present state of the art of neutron transport codes, it is not difficult to calculate a trial spectrum that contains all the reactor physics (usually the "transport-hardened" fission-source term, the 1/E and low-energy thermal components of a moderated reactor or the E component of an unmoderated reactor core spectrum, plus resonance structure). When all the basic structure is present, the code will usually converge in only a few iterations without generating a good deal of nonphysical structure (see Section 6).

Thus, the threshold-foil spectrometry method is not truly a spectrometer system, it is a perturbation system. This is all that can be expected of a system in which only a few activation numbers are input to the code. There is simply not enough input information to specify a spectrum over many decades of neutron energy without injecting a considerable amount of *a priori* information. In fact, below 1 MeV there are no useful thresholds except the ^{237}Np (n, fission) reaction (threshold energy ≈ 0.5

MeV), and the single strong-resonance foils with resonances above that for gold (~5 eV) generally have a very large scattering-to-absorption ratio. Thus, before reliable neutron transport codes became available for furnishing a good trial spectrum, the threshold foil activation method was of limited usefulness.

When utilizing the SAND II unfolding code, the best trial spectrum is used. The zeroth iteration output provides a consistency test for the many foil activations (counts) that have been input; the activation ratios are calculated for the input spectrum and compared to the ratios of the measured (input) activations, so that a spurious input value is immediately apparent. With a reasonable amount of *a priori* information about the spectral shape (obtained from a calculation or from some accurate measurement of a closely related assembly), bad counting data can be detected and removed in the interest of obtaining a rapid convergence and thus avoiding the generation of spurious structure.

Two threshold foils that have nearly the same shape and threshold value can also give rise to a large number of iterations if the input values of the two are inconsistent. The foil yielding the spurious activation value can usually be spotted by comparing the input activation ratios to those calculated for each spectral iteration (perturbation).

Another useful technique in applying unfolding codes was developed in the present application. It involves the sequential combination of the proper amount of the moderated 1/E component and the thermal-neutron component with the GODIVA core-type (glory hole) spectrum to obtain the reactor-plus-room-scattered components that characterize the FBR spectrum outside the reactor core (see Section 6). A flow diagram illustrating this procedure is shown in Figure 1.

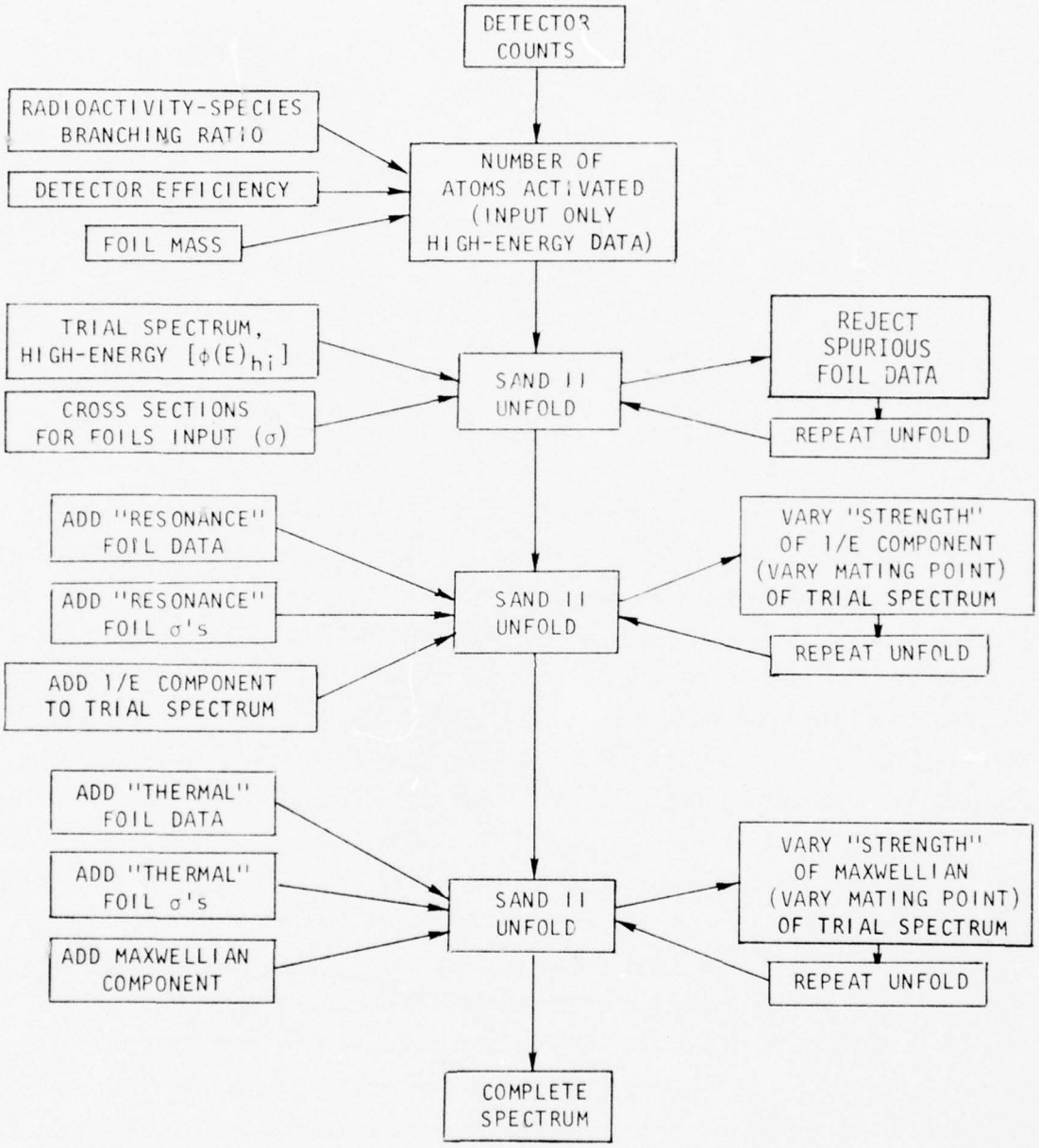

Figure 1. Flow diagram (progressive unfolding from high energy to 1/E to thermal regions) for adding correct wall scattering to FBR spectra outside the reactor

4. THE STANDARD OR BEST-KNOWN FBR SPECTRUM

Figure 2 shows a TOF measurement and an early calculation for the central core spectrum (Ref. 15) of a GODIVA-type FBR. The reactor is the APFA-III, and the calculation is a 1DF neutron transport calculation (Ref. 16) utilizing an early cross-section compilation, ENDF/B, Version I (ENDF/B-1). The measurement and calculation are in reasonably good agreement, in spite of the early cross-section set utilized. The calculation shows a somewhat softer spectrum above 1 MeV, but even so, the spectrum can serve as a good trial spectrum for the SAND II unfolding code because there are many foils with threshold above 1 MeV that will allow SAND II to make any necessary adjustment of this small magnitude with good accuracy.

The foil-activation data of McElroy et al. (Ref. 17) agree well with the TOF data at the core center shown in Figure 2. The comparison of the two outside the reactor is complicated by nearby scattering walls and by the fact that the foil data are 4π data, while the TOF data are angular flux data normal to the surface of the APFA-III FBR. The APFA-III, like the WSMR and the SPR-II FBRs, is a ^{235}U metal-fueled reactor. The APFA-III is a 7-inch-diameter spherical reactor, the WSMR-FBR is a cylindrical assembly 8 inches in diameter x 7-5/8 inches high, and SPR-II is a cylindrical FBR 8 inches in diameter x 8.2 inches high. The latter two have 10% Mo added to the fuel. All three contain 93.2% ^{235}U-enriched fuel.

Figure 3 shows a comparison of the 1DF calculation with TOF data (Ref. 18) and a proton-recoil proportional-counter (p-recoil) spectrum (Ref. 19) for the STSF-1A reactor central core region. The 1DF code agrees very well with an average of the two measurements in the 0.01- to 6-MeV energy region, the region that contributes most of the Si radiation damage. The p-recoil data are of questionable validity for 4π counters above 1.8 to 2 MeV and, for such a hard spectrum, below 0.01 MeV (Ref. 20). Above 6 MeV, the TOF data show a harder spectrum than the early 1DF

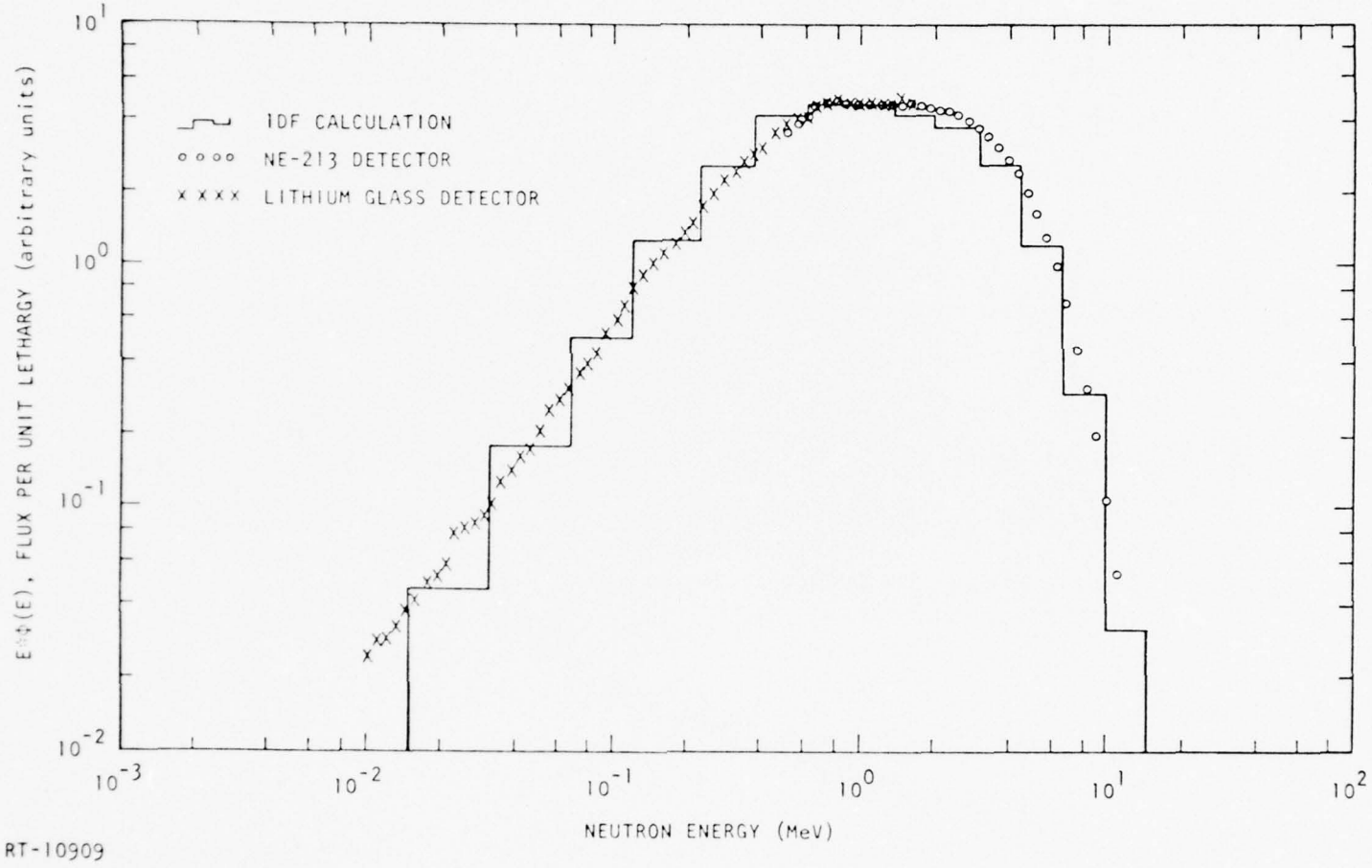

Figure 2. Comparison of time-of-flight measurements (200-m flight path) with 1DF calculated spectrum for APFA reactor

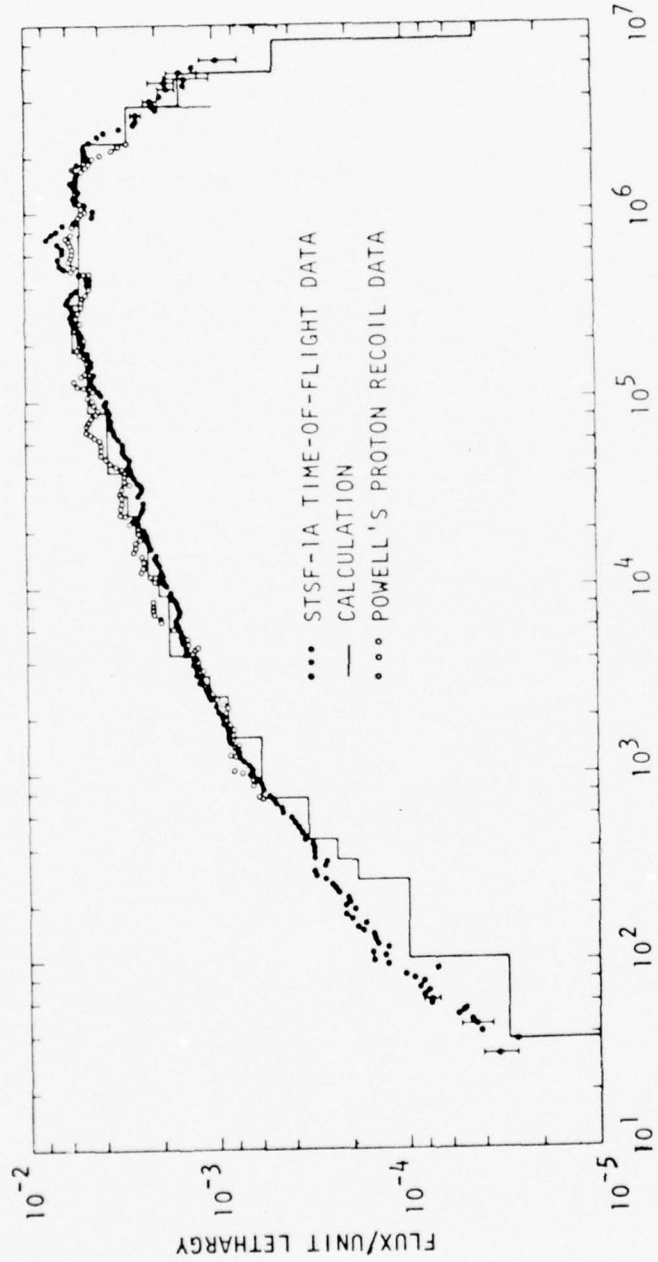

Figure 3. Comparison of time-of-flight spectrum and proton-recoil spectrum to 1DF calculation for STSF-1A subcritical assembly

calculations that utilized ENDF/B-1 cross-section data set. The STSF-1A is roughly a 50:50 mixture of 93% enriched ^{235}U and depleted uranium plates with ∿70 volume percent BeO moderator and an iron reflector.

Recent 1DF calculational results shown in Figure 4 for a different fuel loading configuration, are compared to TOF data and to some recent p-recoil work (Ref. 21). The p-recoil work was part of an extensive study wherein the detector responses were accurately measured, the carbon-recoil (in CH_4-gas-filled counters) effects measured and quantified, and the p-recoil errors assessed (Ref. 20). The calculations utilized ENDF/B-4 cross sections. The three sets of data are in excellent agreement above 0.01 MeV, the region of importance to Si radiation damage, and strongly indicate that the 1DF calculation with the use of the updated cross-section set will provide a good "standard" or "known" spectrum for comparison with the WSMR-FBR foil-activation spectrometry results.

Such calculations were carried out for both the glory-hole region and the region outside the WSMR-FBR reactor (Ref. 22). They were also performed for the SPR-II reactor (the WSMR-FBR and SPR-II spectra were identical). Figure 5 shows the results of the 1DF calculation for several distances from the WSMR-FBR reactor, with an 18-cm-thick 4π concrete scattering wall located 12 meters from the reactor. This modeled the scattering from the concrete floor ∿2 meters below the reactor. The radius of the 18-cm-thick wall was varied until a spectrum was obtained that gave a best fit to the low-energy foil data measured at 50 cm from the WSMR-FBR (Au, bare, Au in Cd cover, and Na in Cd cover).

Note the presence of the 1/E wall-scattering component in Figure 5. This is represented as a flat region at low energies in the $\phi(u) = E^*\phi(E)$ plots.

One of these spectra calculated at 74 cm from the SPR-II reactor is compared with Powell's measurements at 76 cm from the SPR-II (see Figure 6). Even if we ignore the p-recoil spectrum above 1.5 MeV, where the wall and end effects corrections for long p-recoil tracks cannot be determined accurately (especially when the 4π correction of Bennett is applied to a cylindrical counter in a beam geometry irradiation), a much

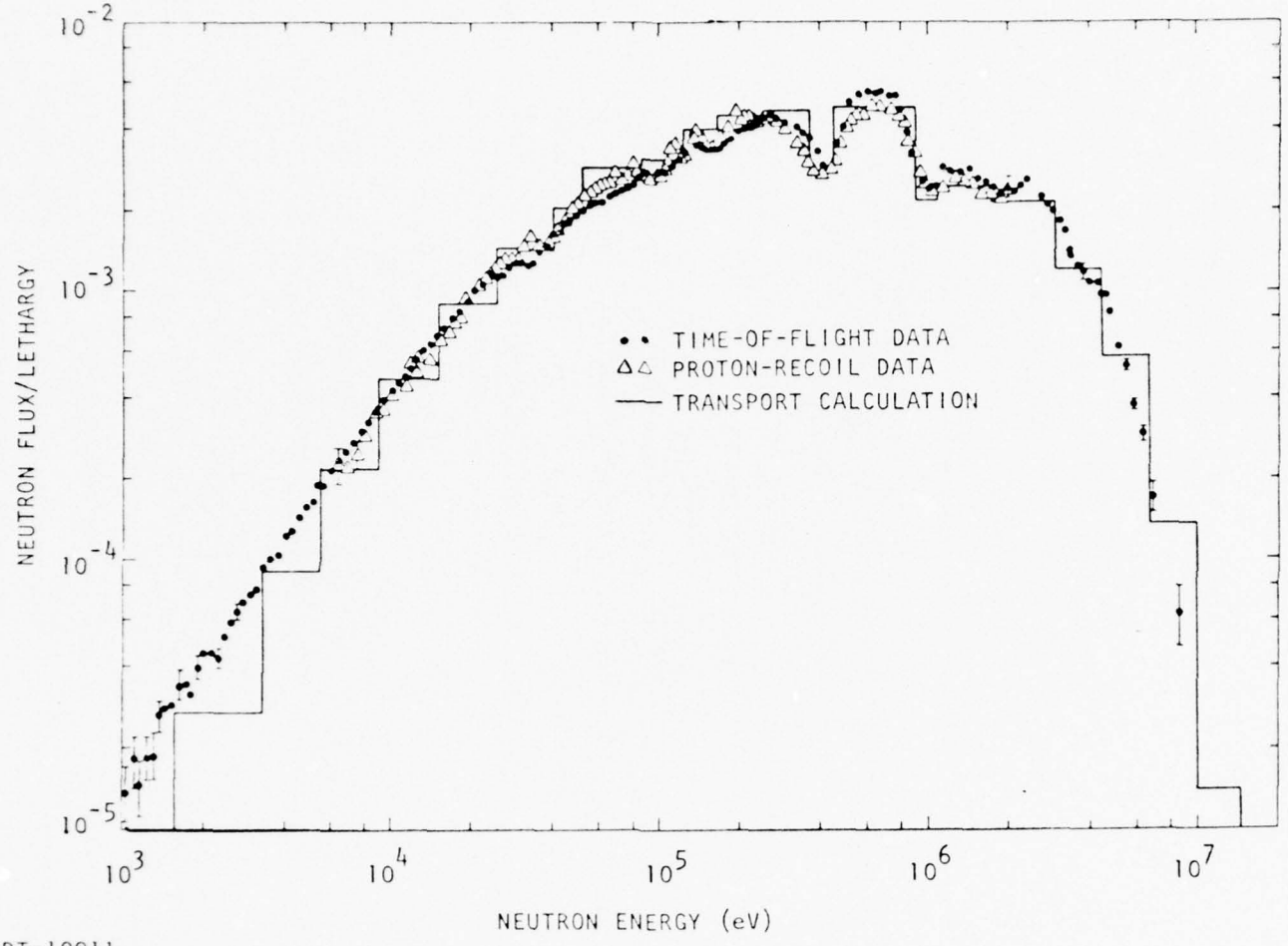

Figure 4. STSF-9 angular-flux calculation compared directly to TOF data and to 4π proton-recoil data that were heterogeneity-modified and corrected for different average positions of the counter

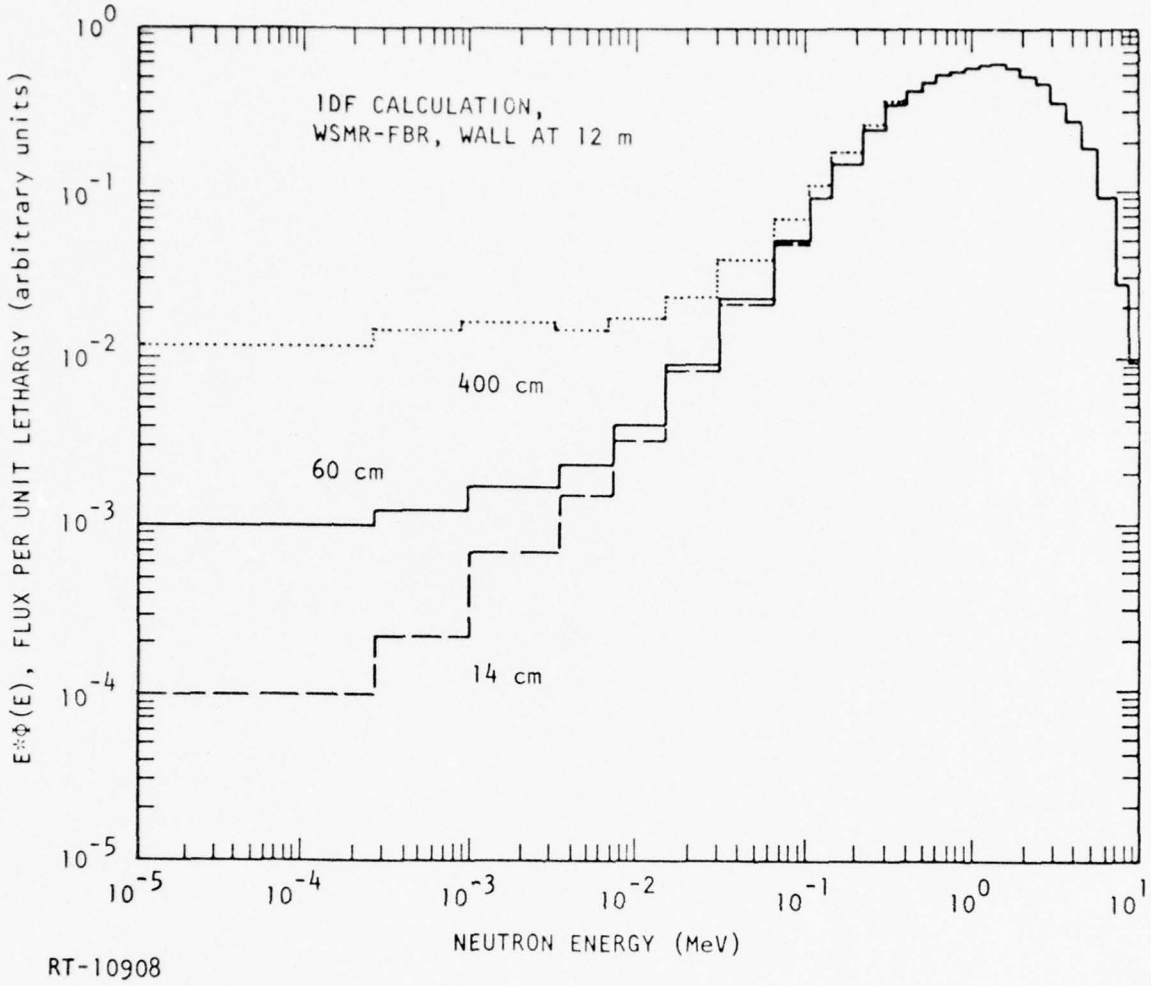

Figure 5. IDF calculational results for WSMR-FBR with spherical concrete wall 12 meters away. The wall-moderated component, which increases as one approaches the wall, is the flat region at low neutron energy.

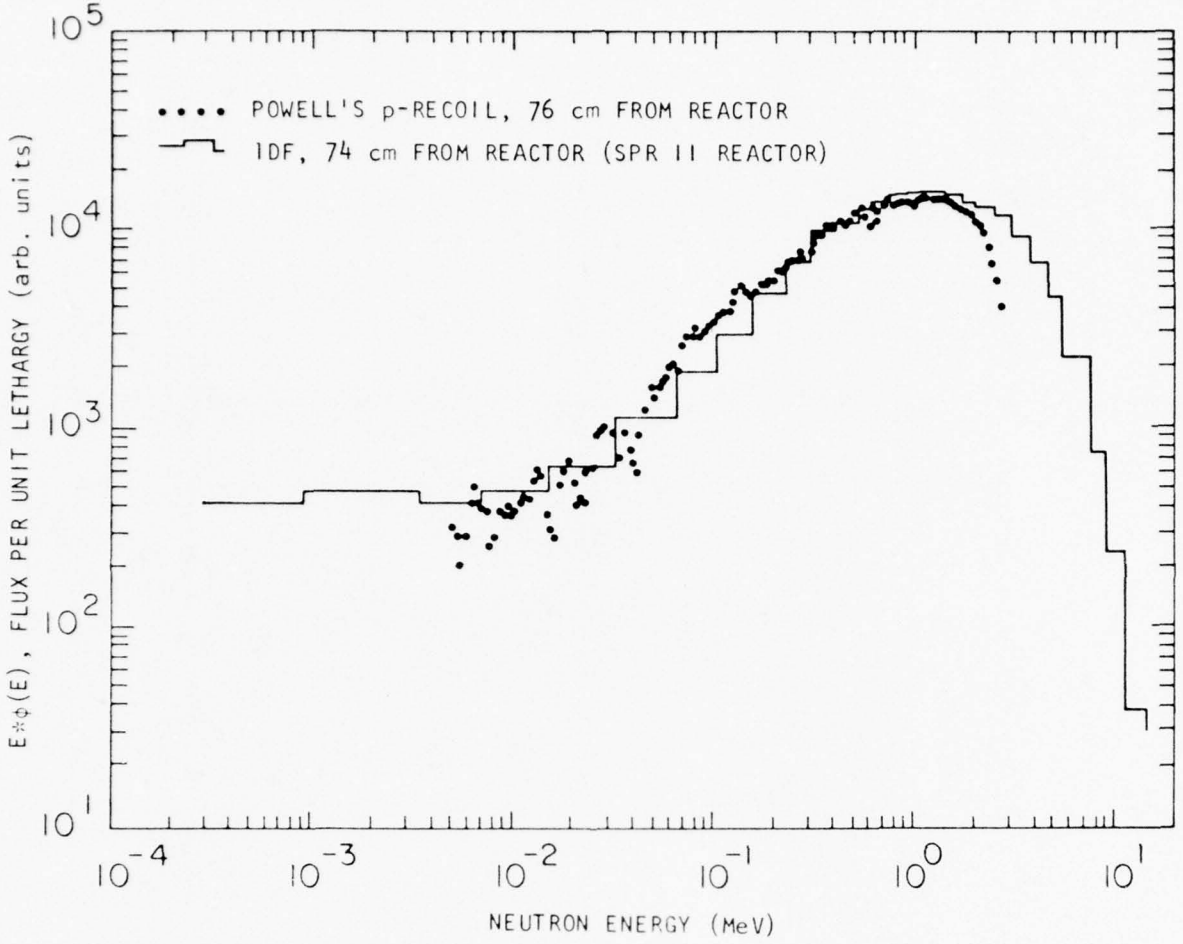

Figure 6. SPR-II reactor spectrum: 1DF calculation (74 cm) and p-recoil measurements (76 cm from reactor)

softer spectrum for the p-recoil data is obtained. On the other hand, the p-recoil spectrum inside the glory hole is much harder (<2 MeV) than the 1DF calculation (see Figure 7). But the form of the 1DF spectrum above about 0.1 MeV is similar both inside and outside the SPR-II. This seems intuitively correct, except from some wall-scattering component that begins to soften the spectrum below 0.1 MeV. The WSMR-FBR foil data will later bear this out. Thus, the p-recoil data are too soft outside the core (and also in Figure 3 for a "cold," zero-power reactor core) and too hard inside the glory hole. Here, the high gamma-ray background effects of the non-zero-power reactor might explain the enormous difference in hardness from that of the outside spectrum for the same p-recoil counter.

We conclude from these data and from the threshold-foil-activation-spectrometry results presented in Section 6 that the 1DF data provide the best "standard" spectrum for evaluating the accuracy of the foil-activation method of neutron spectrometry.

The one-dimensional S_n transport theory code DTR-IV (Ref. 16) was used to calculate the neutron spectrum inside and outside the WSMR-FBR and the SPR-II. In addition, it was used to calculate the APFA-III FBR spectrum and the spectra for several split-bed subcritical reactor assemblies at IRT.

The WSMR-FBR and SPR-II criticality calculations used spherical geometry, an S_8 quadrature, P_3 scattering, 30 energy groups, and six material zones. These six material zones represented the glory hole (air), glory hole liner (stainless steel), core (93% ^{235}U-enriched uranium + 10% Mo + homogenized SS bolts), shroud (^{10}B + Aℓ + resin, all thin), air, and 4π concrete wall. The flux-weighted cross sections were obtained with the use of the GGC-5 code (Ref. 23) using infinite dilute ENDF/B-3 cross sections for all components except ^{238}U (^{238}U is a minor constituent of the 93% ^{235}U-enriched uranium + 10% Mo fuel). The ^{238}U cross sections were calculated by GGC-5 using ENDF/B-3 resonance parameters in the Nordheim integral method.

1DF is an IRT modification of the DTF-IV code.

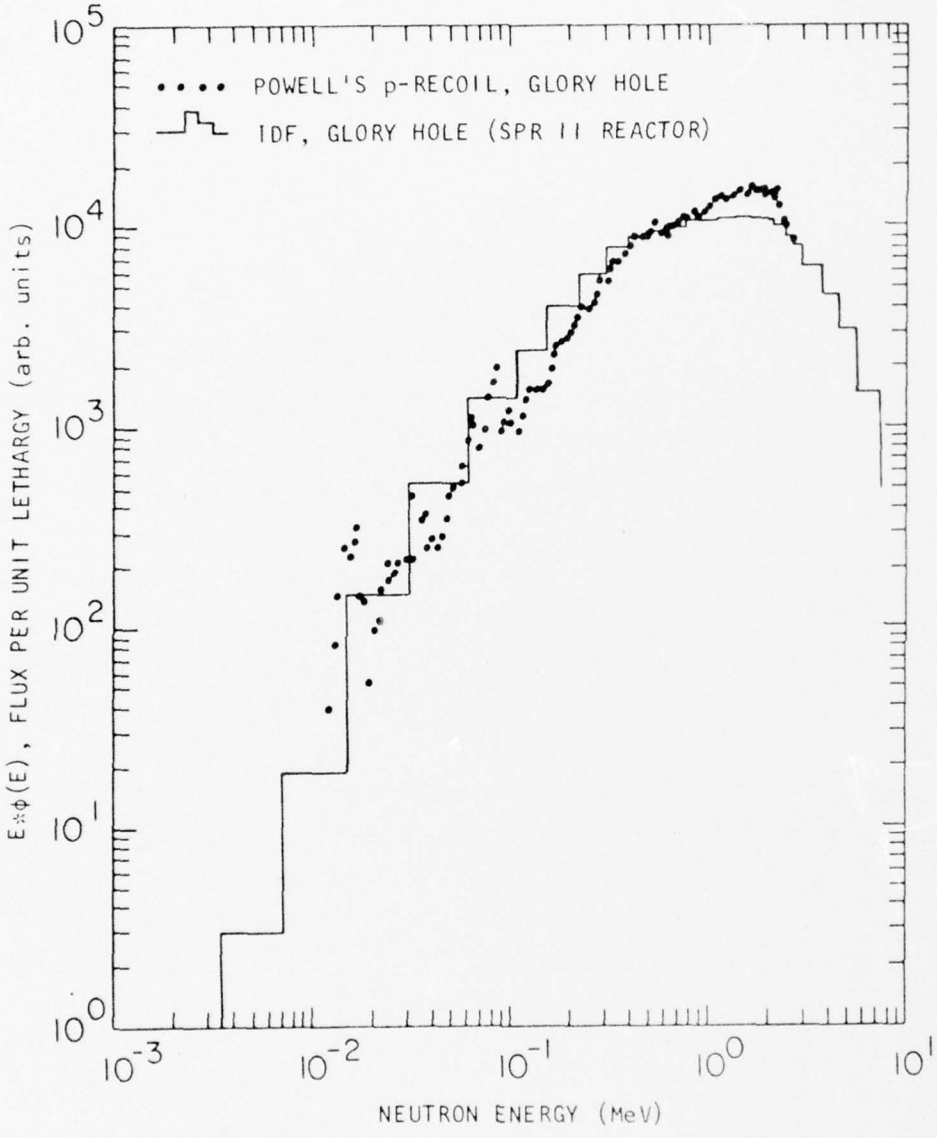

Figure 7. Comparison of 1DF neutron spectrum calculation and p-recoil data for SPR-II FBR glory hole

5. SPECTRUM CHARACTERIZATION

For application to radiation damage in silicon, the neutron field is characterized by ϕ_{eq}, the number of 1-MeV neutrons required to produce the same radiation damage, and the hardness parameter ϕ_{eq}/ϕ, the number of 1-MeV neutrons required to produce an amount of permanent damage equivalent to that of a unit fluence of neutrons from the radiation field being characterized. The value of ϕ_{eq} is obtained by folding in the neutron spectrum in question, $\phi(E)$, with the damage function D(E) for silicon:

$$\phi_{eq} = \frac{\int \phi(E)\ D(E)\ dE}{D\ (1\ MeV)} \quad , \tag{1}$$

and

$$\phi_{eq}/\phi = \frac{\int \phi(E) D(E) dE}{D\ (1\ MeV) \int \phi(E) dE} \quad ,$$

All integrals are taken from 0.01 to 18 MeV, where nearly all the damage occurs. D (1 MeV) is the average value of D over the interval of 0.85 to 1.15 MeV (see Method E XX4, Appendix A).

One such D(E) curve that has often been used is that of R. R. Holmes et al., shown in Figure 8. This was calculated using early cross-section data. For the work presented here, the D(E) data recently calculated (Ref. 24) under contract at IRT was utilized. Figure 9 shows a plot of an early calculation of D(E) for silicon. It exhibits the characteristic

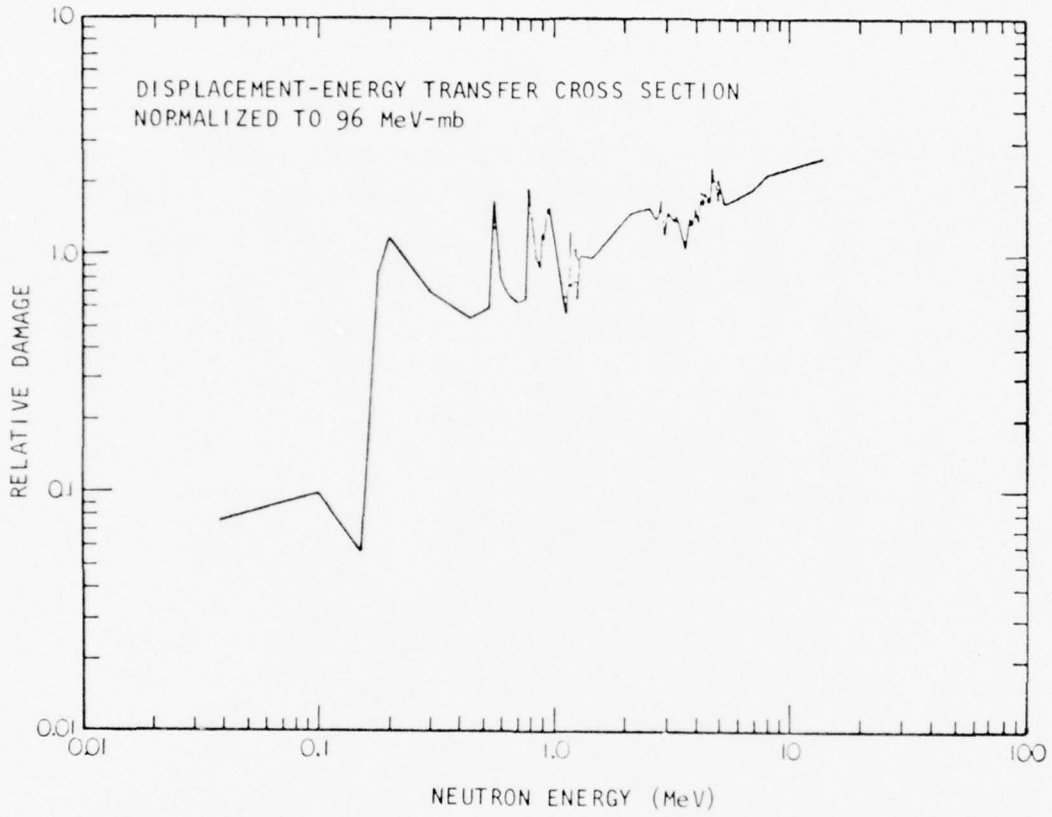

Figure 8. Relative neutron effectiveness for displacement production in silicon (figure developed from data in "Weapons Effects Studies, Vol. II, Radiation Effects on Interceptor Electronics," ABMDA Development Program, Bell Telephone Laboratories, October 1970)

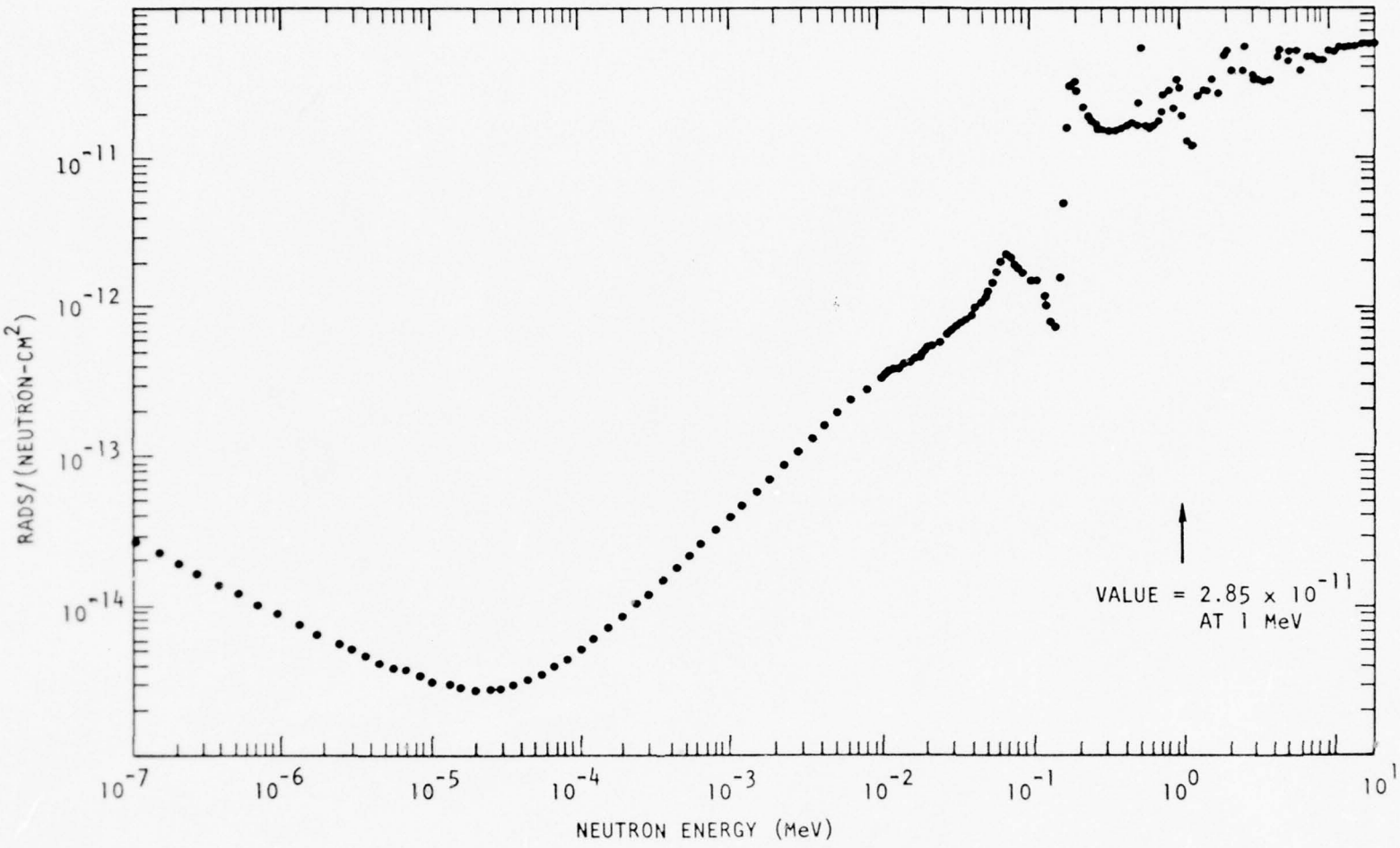

RT-10916

Figure 9. Calculated silicon displacement KERMA. Multiply all data by 1.24 to correct for underestimate of displacement partition. Tabulated values (correct) are in Appendix A, ASTM Method E XX4 (also Ref. 31).

shape of the D(E) function. It consists of a silicon displacement KERMA calculated with the latest ENDF/B-4 cross-section set (MAT 1194, May 1974), but with an underestimate of the partition of neutron-recoil energy resulting in collisions. Although the shape of the curve is reasonably accurate, all values are ∿22% too low, the correct values being given in Table I of Appendix A, Method E XX4. The correct curve is in preparation, and will be presented in Ref. 31.

6. OBTAINING THE WSMR-FBR SPECTRA

A number of trial spectra were used in an effort to obtain an output spectrum with the SAND II code (Ref. 25) that was physically meaningful. Thus, the dependence of SAND II on a trial spectrum was investigated. It was found that reliable output spectra were obtained only if the input spectrum contained all the physics of the problem. In addition to SAND II, the SPECTRA code of Halblieb et al. (Refs. 26-28) of Sandia was utilized. Thus, to a limited extent, the sensitivity of the foil-activation method to the unfolding code utilized was investigated.

6.1 FAST BURST REACTORS

The core of the WSMR-FBR is shown in Figure 10 for the earlier version without the glory hole. The recently added glory hole is 1-inch i.d. and has a 0.060-inch-thick stainless-steel wall. The fuel region is 8 inches in diameter and 7.6 inches high. It contains 92.4 kg of uranium alloyed with 10 wt % of molybdenum. The uranium is 93.2% ^{235}U. Figure 11 shows the FBR critical dimensions. The core of SPR-II is similar to that of the WSMR-FBR, except that it is 8 inches in diameter and 8.2 inches high, and contains 105 kg of uranium (same enrichment). It has a stainless-steel-lined glory hole 1.625 inches i.d. The APFA-III FBR, shown in Figure 12, is a 7-inch-diameter sphere fabricated with 60 kg of uranium (93.2% ^{235}U).

6.2 GLORY HOLE SPECTRUM

6.2.1 SAND II Code Results

The suitable trial spectrum for the glory hole foil-activation data (generously provided by H. L. Wright of the WSMR Dosimetry Section) was the GODIVA-type spectrum contained in the SAND II library of trial spectra

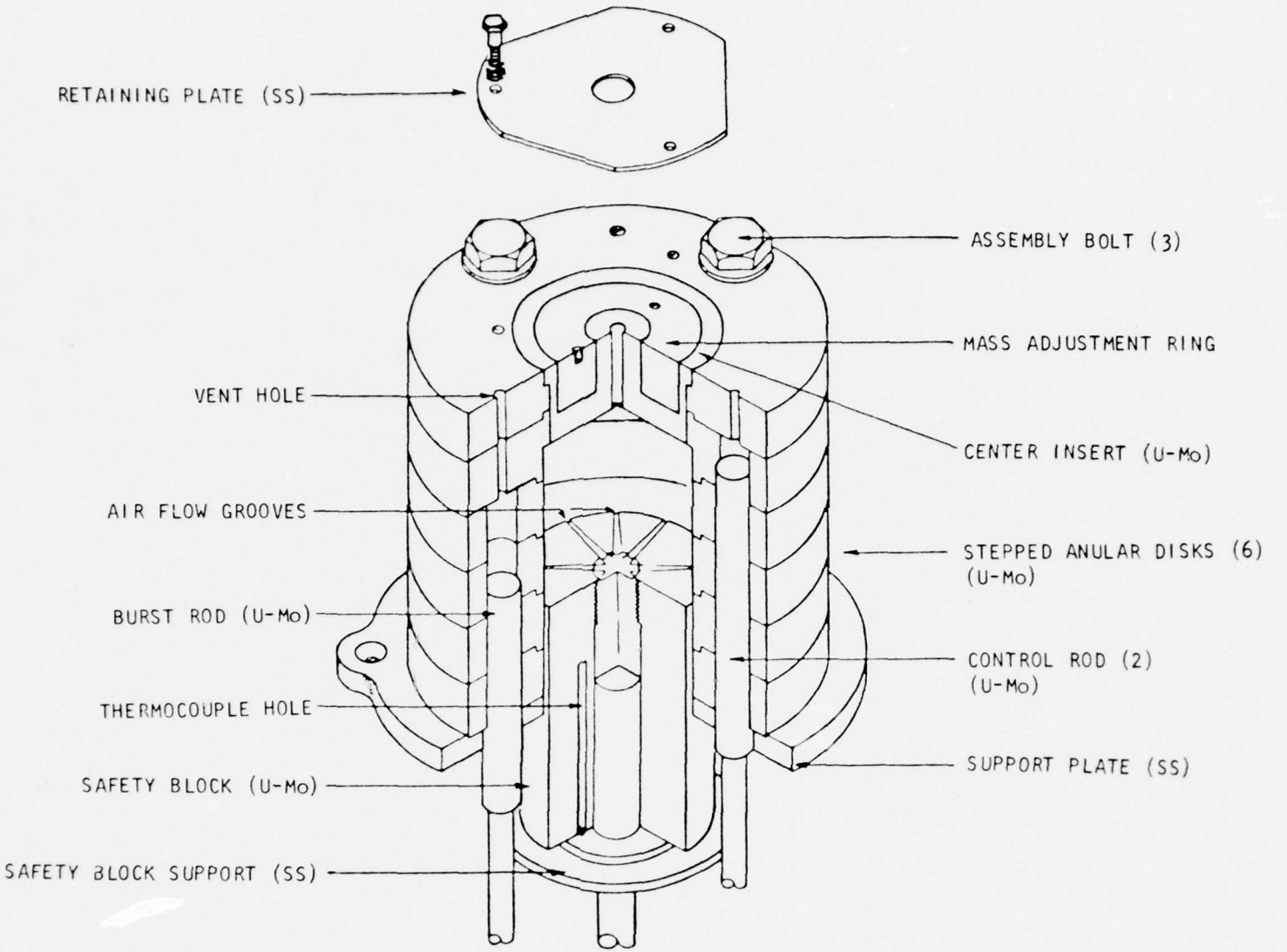

Figure 10. Isometric section of FBR core

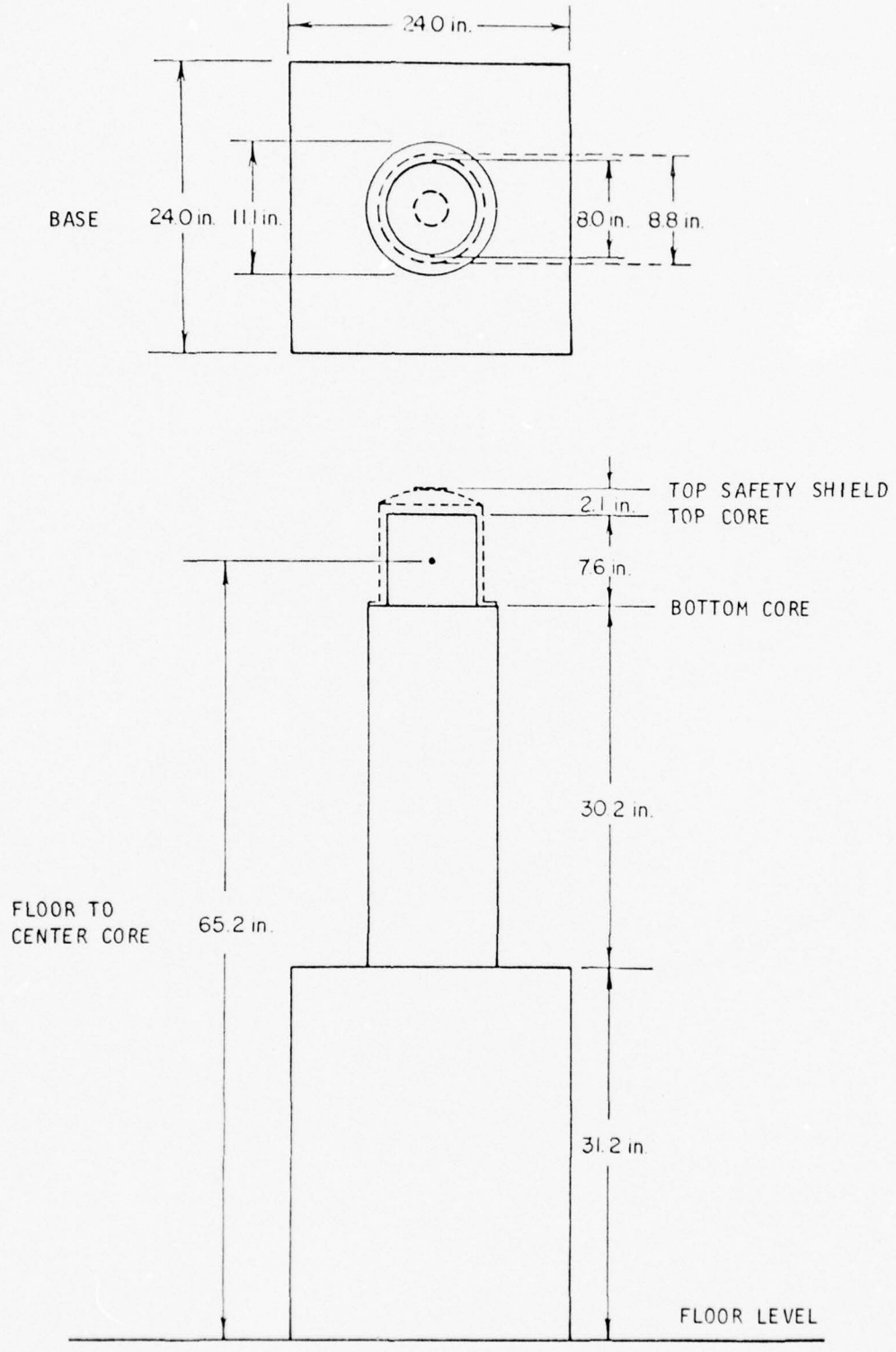

Figure 11. FBR critical dimensions

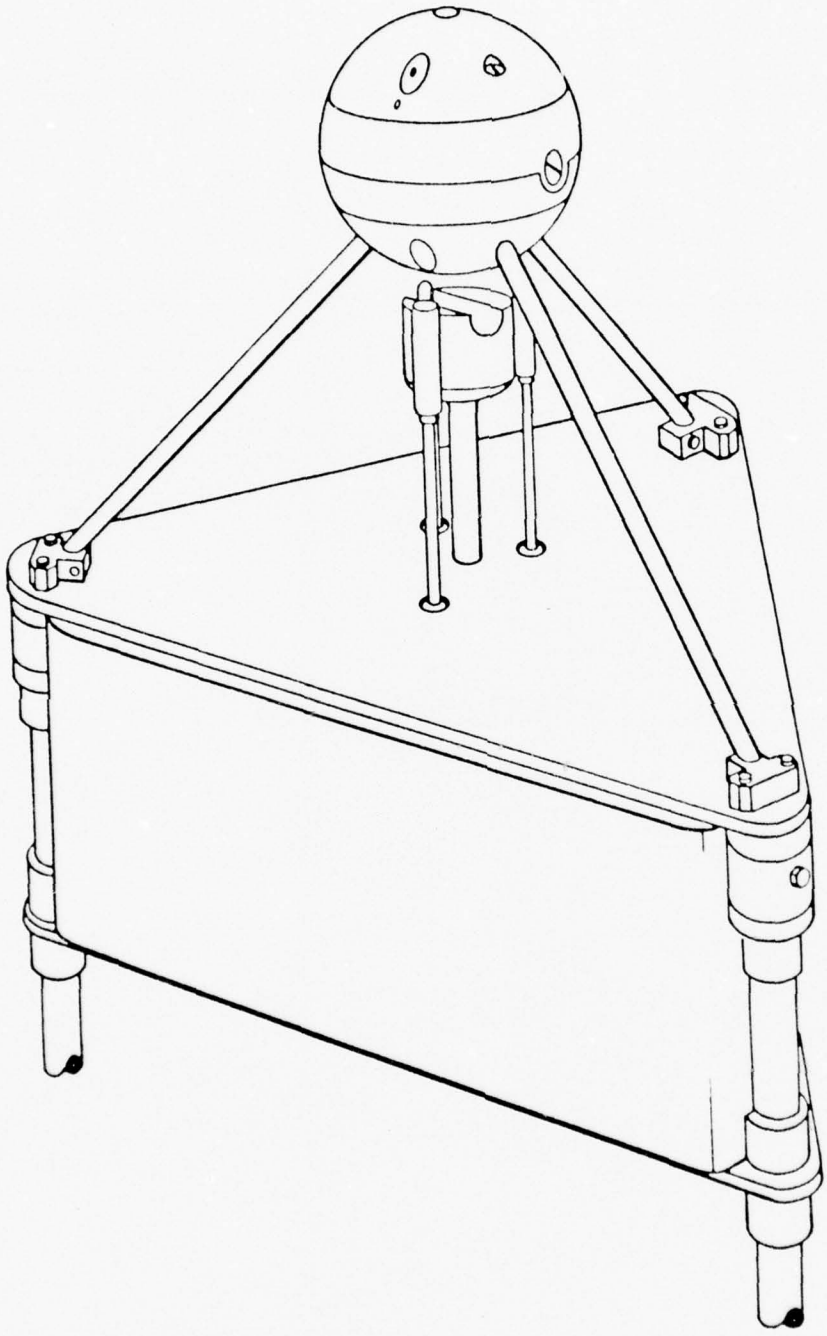

Figure 12. APFA assembly

[spectrum 5, constructed by C. S. Shapiro (Ref. 29)]. The results of SAND II with trial spectrum 5 are shown in Figure 13 compared to the IDF-calculated core spectrum. The agreement is very good. This is spectrum S of Table 1. Only four iterations of SAND II were required. The radiation damage produced by a unit fluence of neutrons having the SAND II output (trial spectrum number 5 of the SAND II library of trial spectra) is the same as that produced by a fluence of 1.058 1-MeV neutrons, while ϕ_{eq}/ϕ = 1.086 for trial spectrum number 5.

For a Watt fission spectrum (SAND II trial spectrum 1), ϕ_{eq}/ϕ = 1.246. Utilizing this as a trial spectrum leads to a SAND II output spectrum (Figure 14, spectrum T of Table 1) with ϕ_{eq}/ϕ = 1.064.

Figure 15 shows the results of a SAND II unfolding operation using the IDF calculation as a trial spectrum (Ref. 30). The foil data and the calculation are in excellent agreement in spectral shape and also in terms of a silicon radiation damage equivalence. The value of ϕ_{eq}/ϕ for this SAND II result (spectrum B, Table 1) is 1.037 compared to ϕ_{eq}/ϕ = 1.031 for the IDF spectrum.

6.2.2 SPECTRA Code Results

The same foil-activation data were used with the SPECTRA unfolding code, except for the foil utilizing the $^{90}Zr(n,2n)^{89}Zr$ reaction. Its threshold is at ~14 MeV and has negligible effect on the output spectrum and on ϕ_{eq}/ϕ. Inclusion of Zr produced mathematical difficulties in the SPECTRA code with the IDF input spectrum. The results are shown in Figure 16 and correspond to spectrum R in Table 1. They yield good comparative values of ϕ_{eq}/ϕ = 1.037 for the SPECTRA output compared to 1.031 for the IDF glory hole spectrum. The SPECTRA code required 16 iterations, by which time it began to produce some spurious structure. This is seen as an "oscillation" which nets a positive overshoot at 0.3 to 0.1 MeV, negative at 0.1 to 0.25 MeV, and positive again at 0.25 to 0.5 MeV. It is both possible and likely for oscillations to have no net effect on ϕ_{eq}/ϕ.

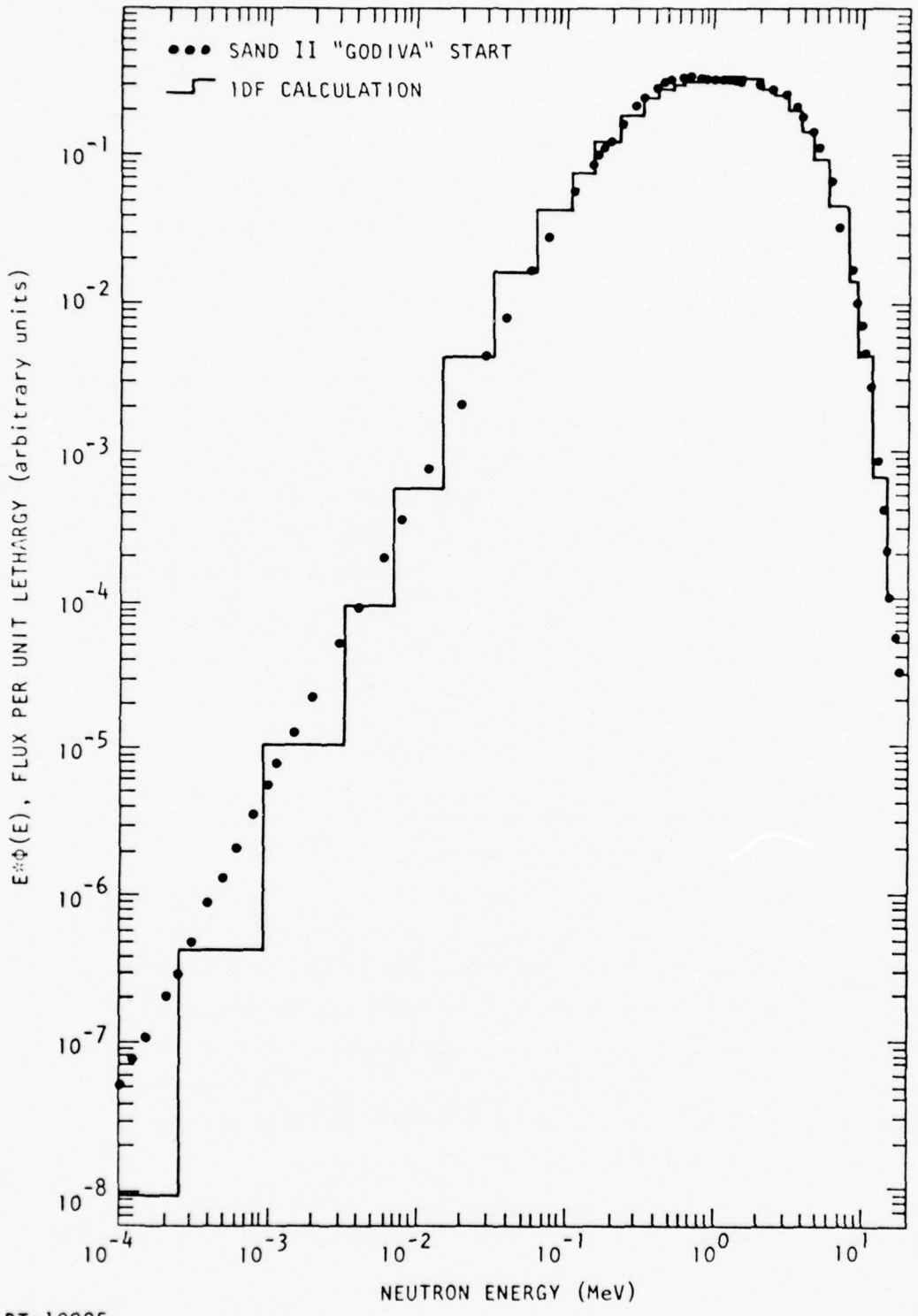

Figure 13. 1DF calculation and SAND II spectrum (GODIVA start spectrum) for WSMR-FBR glory hole; 10 foils

Table 1

SPECTRAL CHARACTERISTICS FOR WSMR-FBR FOIL-ACTIVATION RESULTS

Spectrum	Foils	Variation	ϕ_{eq}/ϕ (SAND II)	ϕ_{eq}/ϕ (Start)	Iterations
A (50 cm)	1-10	-	1.097	1.070 (1DF)	3
B (0 cm)	1-4, 11-16	-	1.037	1.031 (1DF)	3
C (50 cm)	1-9	None	1.075	1.070 (1DF)	2
D (50 cm)	1-9	1.15 Pu	1.063	1.070 (1DF)	3
E (50 cm)	1-9	1.25 Pu	1.048	1.070 (1DF)	10
F (50 cm)	1-9	1.15 U8	1.089	1.070 (1DF)	2
G (50 cm)	1-9	1.25 U8	1.095	1.070 (1DF)	2
H (50 cm)	1-9	1.15 S	1.083	1.070 (1DF)	3
I (50 cm)	1-9	1.25 S	1.084	1.070 (1DF)	5
J (50 cm)	1-9	1.25 Mg	1.075	1.070 (1DF)	2
K (50 cm)	1-9	1.25 Fe	1.070	1.070 (1DF)	8
L (50 cm)	1-9	1.25 U8, Mg	1.102	1.070 (1DF)	3
M (50 cm)	1-9	1.25 U8, 0.75 Mg	1.128	1.070 (1DF)	10
N (50 cm)	1-8	-	0.629	1.031 (15)	15
O (50 cm)	1-9	-	0.929	0.486 (15)	6
P (50 cm)	1-9	-	0.818	1.086 (5)	22
Q (50 cm)	1-9	-	0.847	1.246 (1)	13
R (0 cm)	1-4, 11-15	-	1.037[a]	1.031 (1DF)	16
S (0 cm)	1-4, 11-16	-	1.058	1.086 (5)	4
T (0 cm)	1-4, 11-16	-	1.064	1.246 (1)	7

Foil 1 = ^{58}Ni(n,p); 2 = ^{24}Mg(n,p); 3 = ^{127}I(n,2n); 4 = ^{56}Fe(n,p); 5 = ^{239}Pu(fiss) (in ^{10}B); 6 = ^{238}U(fiss) (in ^{10}B); 7 = ^{235}U(fiss) (in ^{10}B); 8 = ^{32}S(n,p); 9 = ^{197}Au (in Cd); 10 = ^{237}Np(fiss) (in ^{10}B); 11 = ^{239}Pu(fiss) (in Cd); 12 = ^{238}U(fiss) (in Cd); 13 = ^{235}U(fiss) (in Cd); 14 = ^{237}Np(fiss) (in Cd); 15 = ^{54}Fe(n,p); 16 = ^{90}Zr(n,2n).

[a] ϕ_{eq}/ϕ with SPECTRA unfolding code.

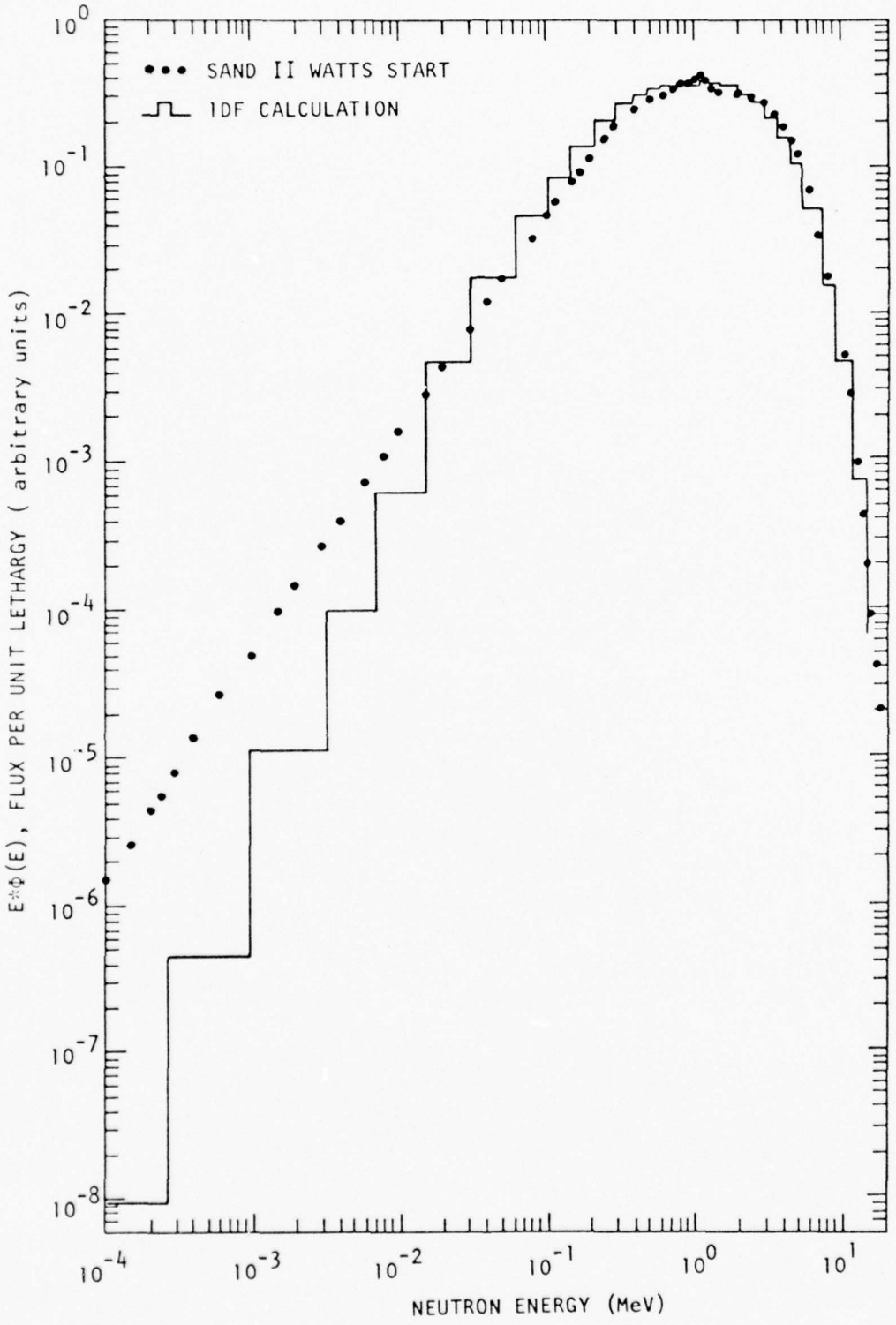

RT-10904

Figure 14. 1DF calculation and SAND II spectrum (Watt start spectrum) for WSMR-FBR glory hole; 10 foils

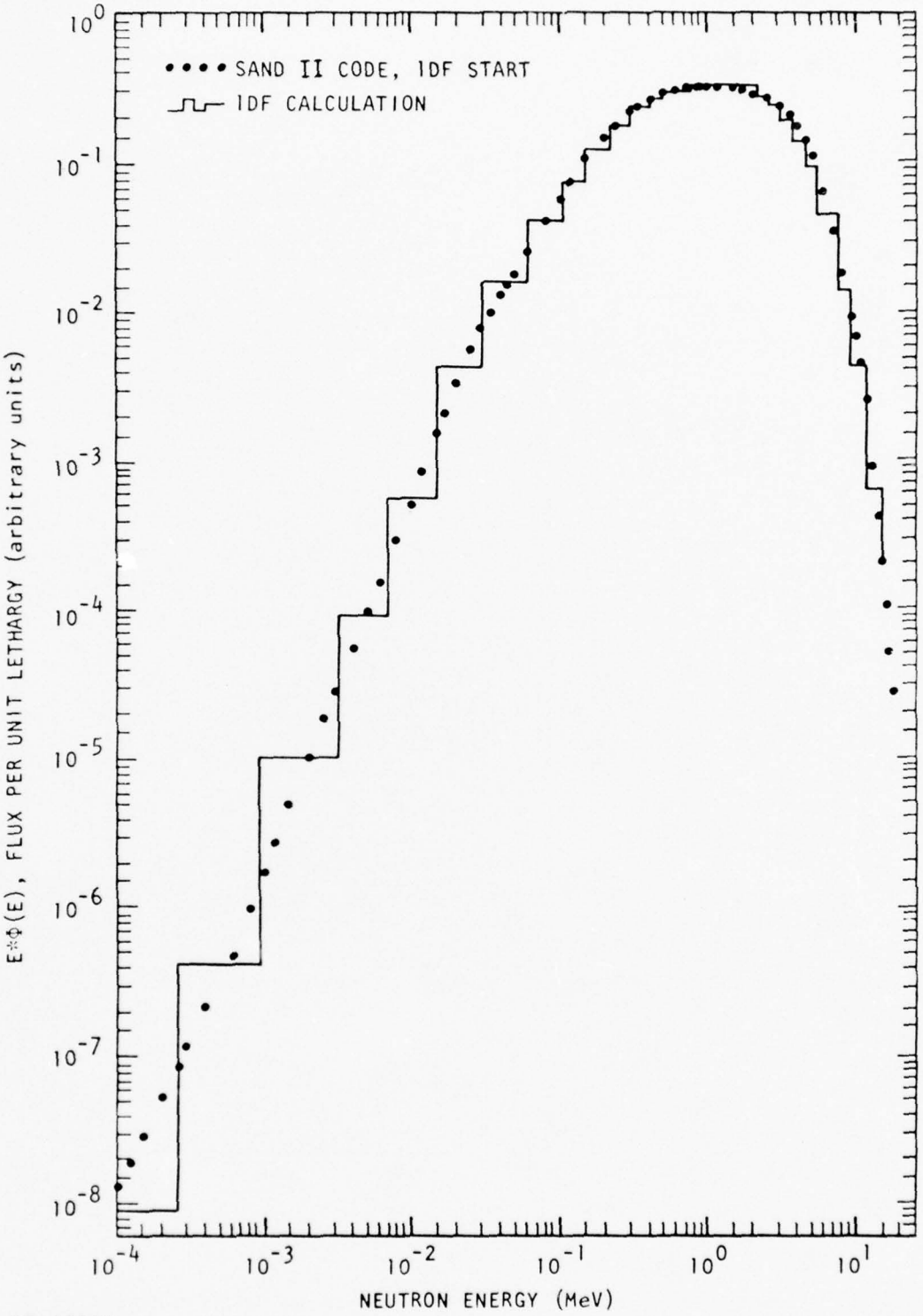

RT-10903

Figure 15. 1DF calculation and SAND II spectrum (1DF start spectrum) for WSMR-FBR glory hole; 10 foils

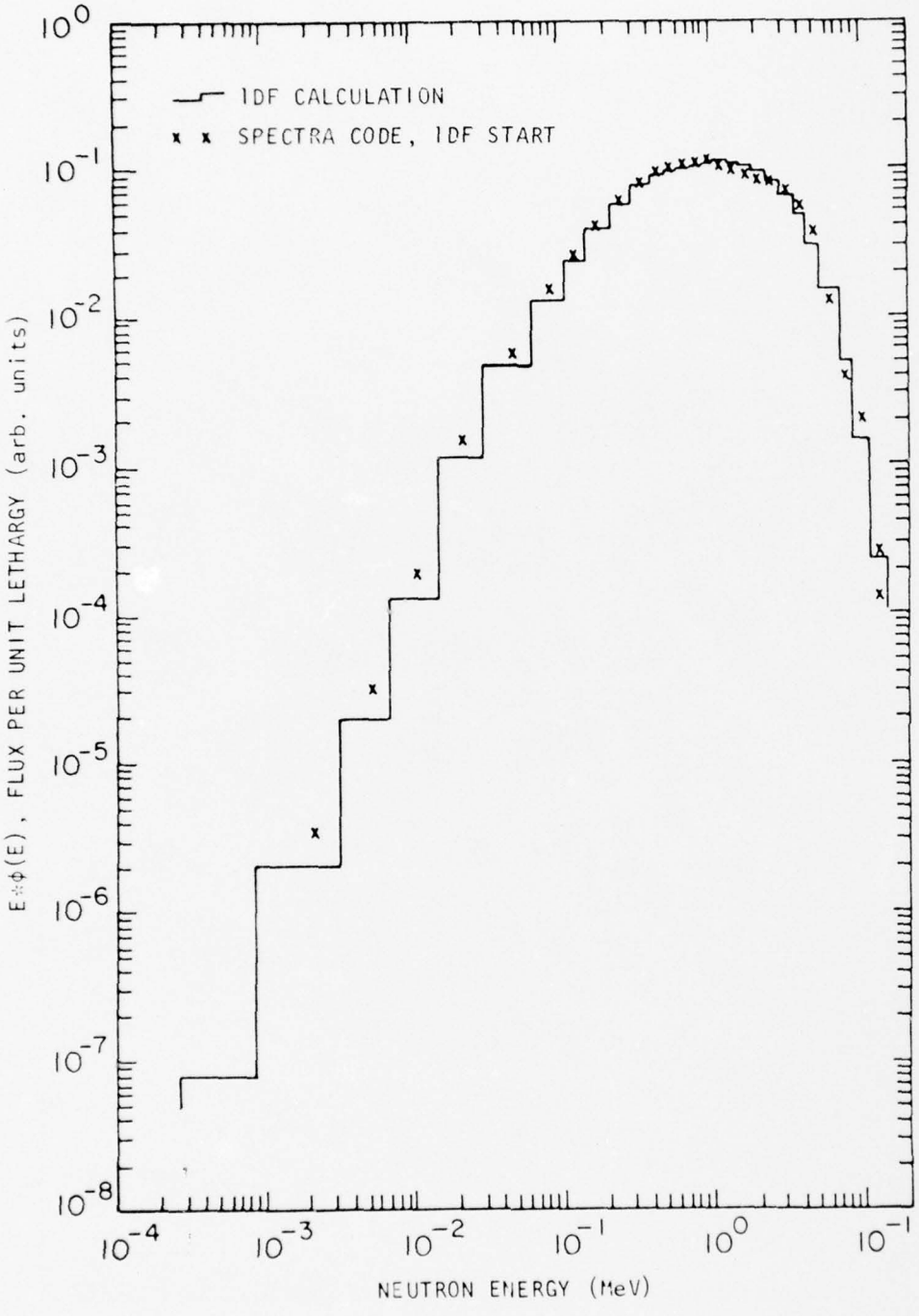

Figure 16. Comparison of WSMR-FBR glory hole spectra: 1DF calculation and activation foil data unfolded with SPECTRA code, 1DF trial spectrum

6.2.3 Choice of Unfolding Codes

Consequently, the SAND II version (Ref. 14) of the SAND code (Ref. 13) does tend to suppress the growth of spurious structure, as described in the users' manual. Code comparison was carried no further. Because of these considerations, the many options available in the SAND II code, and the convenient output format, we selected SAND II as the working code for Task 4.

6.3 WSMR-FBR SPECTRUM AT 50 cm FROM THE REACTOR

As seen in Figure 5, the WSMR-FBR spectrum outside the core is essentially a hard glory-hole-type spectrum with a 1/E moderated (wall-scattering) component that becomes significant (>10%) at energies of about 10^{-2} MeV and lower for a distance from the reactor of about 50 cm. Since none of the SAND II trial spectra (of the library of 59) had a 1/E component normalized to a GODIVA-type spectrum at $\sim 10^{-2}$ MeV, the unfolding became problematic.

Note first (Figure 17 and spectra A of Table 1) that when the 1DF spectrum at 50 cm from the WSMR-FBR is used as a trial spectrum, the unfolded spectrum agrees well with the trial spectrum, yielding ϕ_{eq}/ϕ = 1.097 and 1.070, respectively. The foil data are in good accord with the 1DF calculation.

When the GODIVA-type spectrum (SAND II library spectrum 5) was used and the low-energy gold foil data were input to SAND II, the code required 22 iterations. By this time, the code had built in a considerable amount of unreal (spurious) structure in seeking a solution consistent with the foil-activation data. This is shown by the spectrum plotted with x's in Figure 18 (spectrum P of Table 1, ϕ_{eq}/ϕ = 0.818 for SAND II versus 1.086 for trial spectrum 5). When the low-energy data are omitted from SAND II, the unfolded spectrum (dots) agrees reasonably well with the input spectrum (solid line), and this is, of course, a physically incomplete result. It is clear that a physically meaningful solution cannot be obtained in this case without adding varying amounts of 1/E component (a flat-line

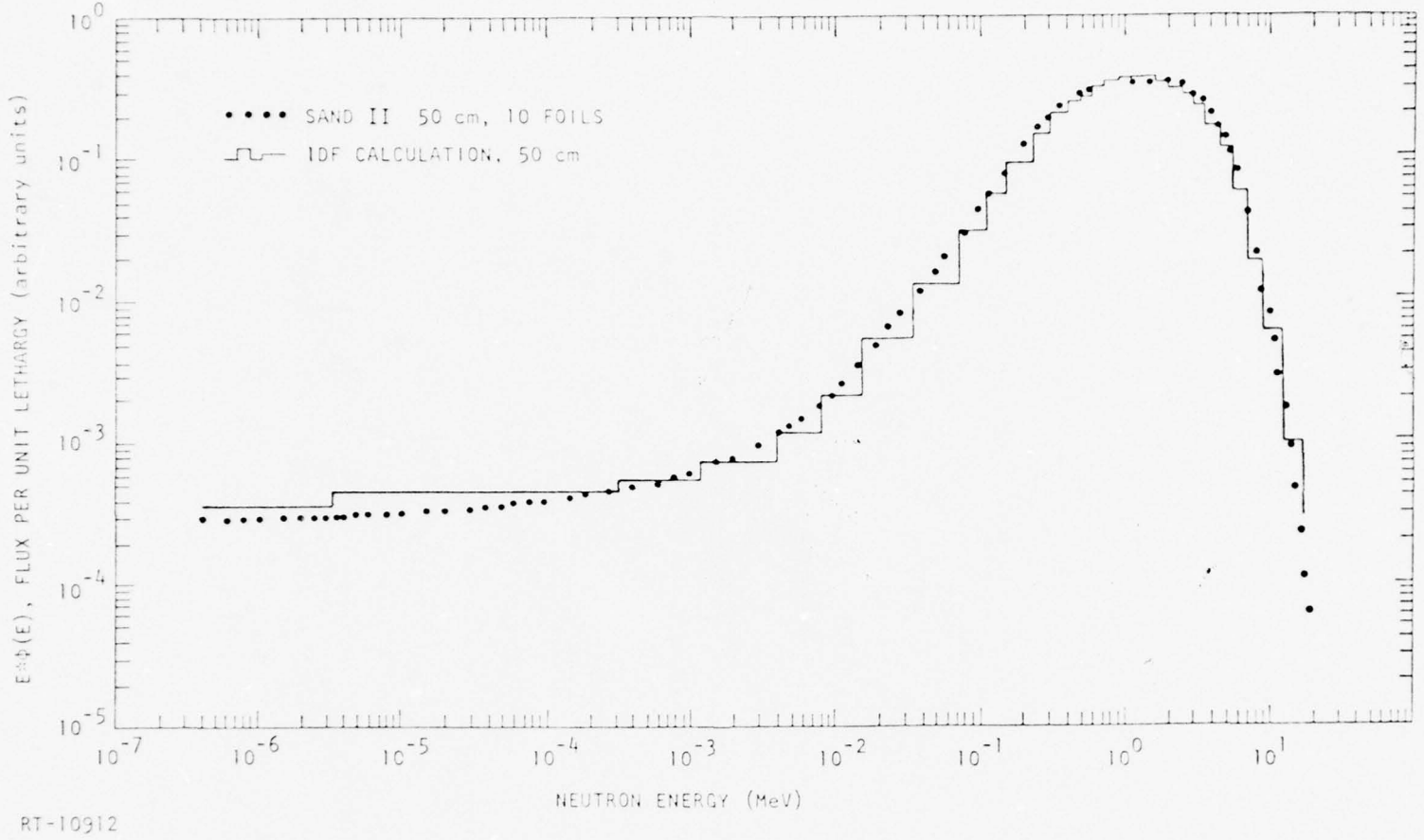

Figure 17. Comparison of 1DF calculation and SAND II results using the 1DF calculation as a starting spectrum. The low-energy gold-foil data and the Np data were used with SAND II.

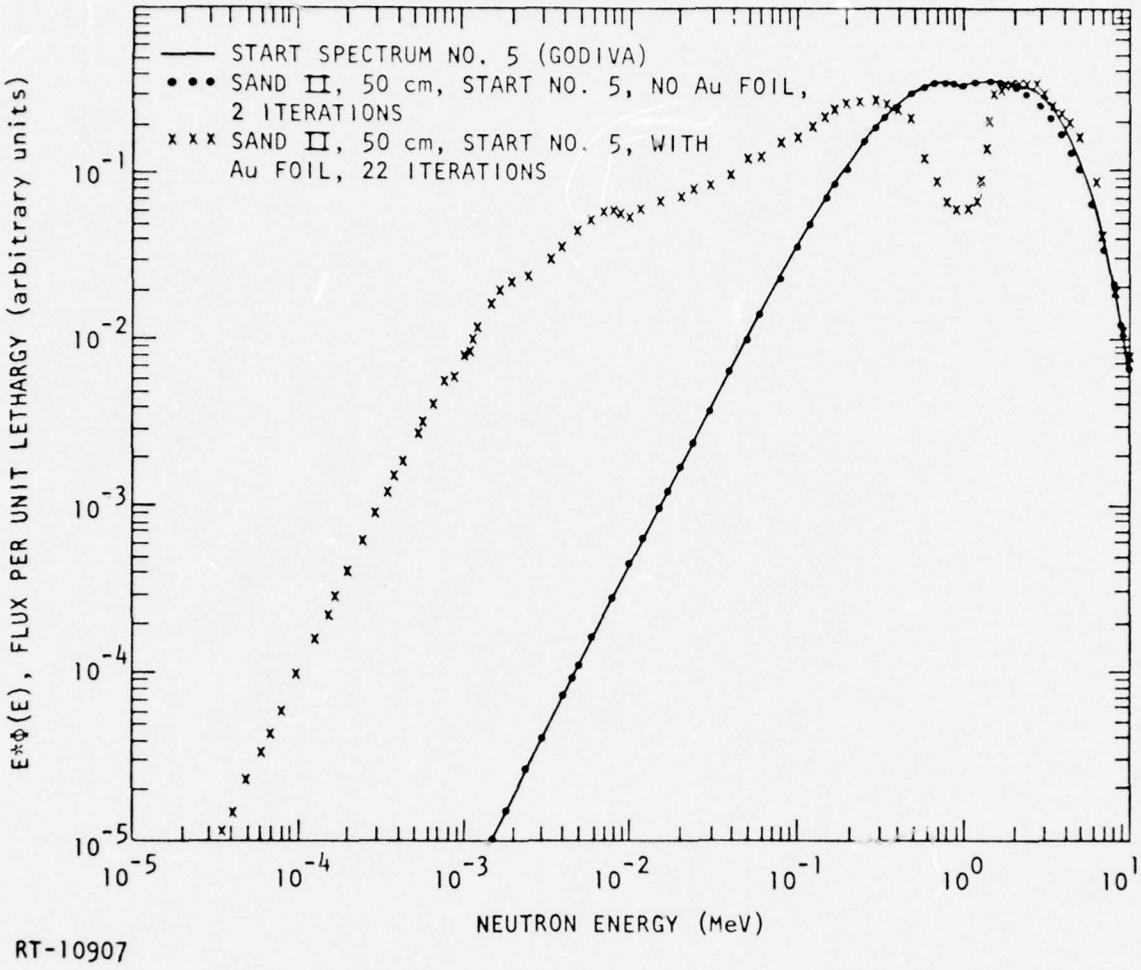

Figure 18. SAND II results for spectrum at 50 cm from WSMR-FBR for SAND II run with GODIVA start spectrum which has no low-energy wall-moderated component. The output agrees well with the start spectrum when the gold-foil data are not included, but the results are meaningless when we unfold with the low-energy foil data included.

component in the E* (E) plots) until the resultant trial spectrum agrees with the SAND II output. The flow diagram of Figure 1 outlines this procedure in which the trial spectrum must be specified down to the Cd cutoff energy. Also, Cd-covered low-energy foils must be used for fitting the 1/E component to the fission component so that the thermal (Maxwellian) peak can be fitted later with the bare-foil data.

Figure 19 shows the effect of utilizing a trial spectrum (solid line) that has too large a value of 1/E component. When the unfolding is carried out with the low-energy gold-foil data input to SAND II, a physically unreal spectrum is obtained (open circles, Figure 19, and spectrum 0 of Table 1). The starting spectrum was spectrum 15 of the SAND II trial-spectrum library. It consists of a GODIVA-type spectrum with a 1/E component normalized to it at 0.5 MeV. The solution immediately suggests that the normalizing point for the trial spectrum be moved down to an energy well below 0.5 MeV. Again, as per the flow chart of Figure 1, this is accomplished iteratively until the trial spectrum and the SAND II output agree. Note that the trial spectrum has a ϕ_{eq}/ϕ value of 0.486, while the solution with gold foil (spectrum 0, Table 1) yields $\phi_{eq}/\phi = 0.929$.

The solid points in Figure 19 depict the result of a SAND II run without the gold-foil activation. Even without the gold foil, the ^{239}Pu and ^{235}U fission foils have caused the output (spectrum N, Table 1) to show a smaller 1/E component than trial spectrum 15. For this case, ϕ_{eq}/ϕ is only 0.629 for the SAND II output spectrum without gold-foil data.

In addition to unfolding with an overmoderated trial spectrum (15) and an undermoderated GODIVA trial spectrum (5), some unfolding was done with a Watt trial spectrum (1) for foil-activation data at 5 cm from the WSMR-FBR. The results (Figure 20 and spectrum Q of Table 1 for gold-foil data) are much like those for trial spectrum 5, and do not warrant further discussion here.

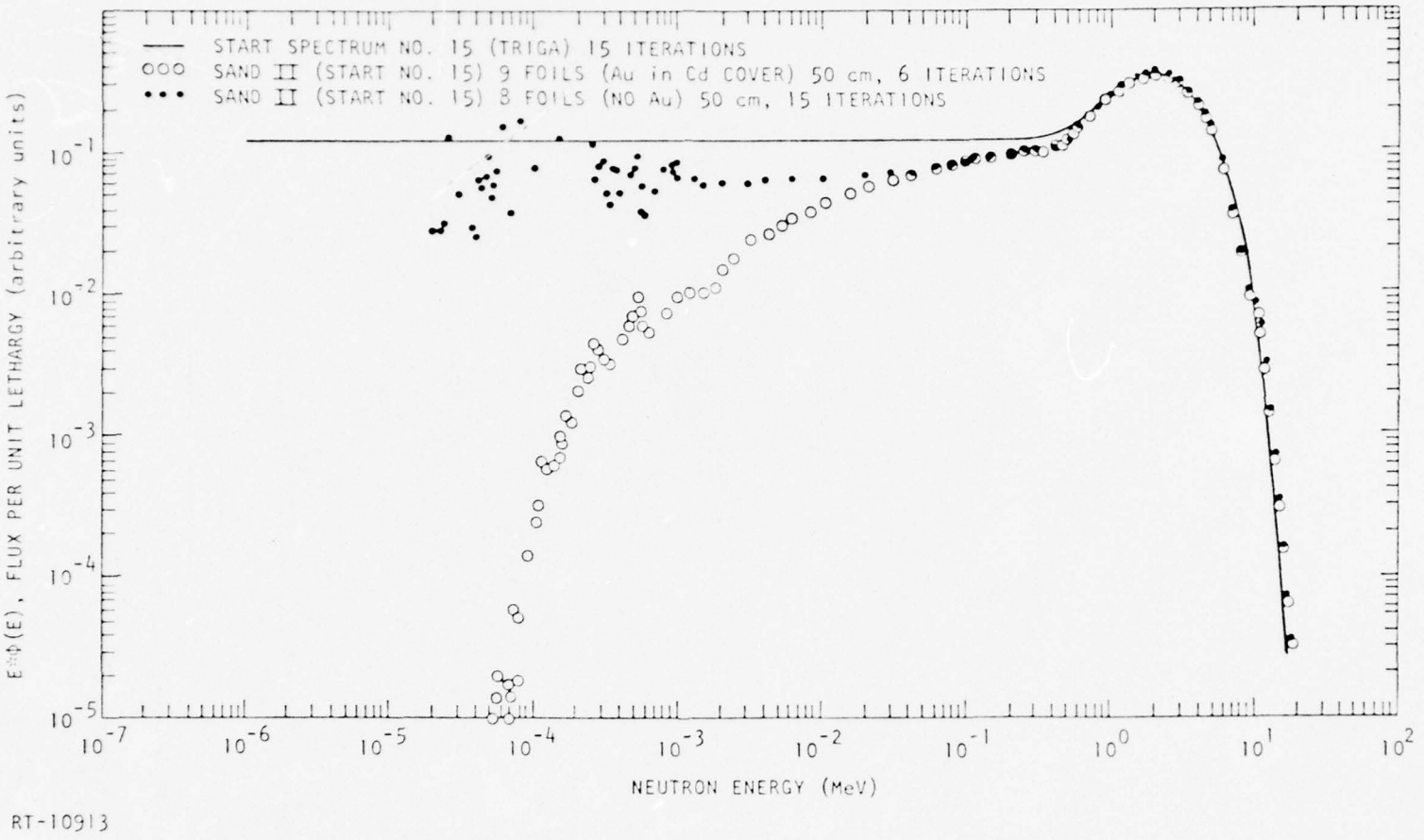

Figure 19. SAND II results with and without the use of the low-energy (gold foil) data when an overmoderated (TRIGA-type) spectrum is used for a SAND II start spectrum

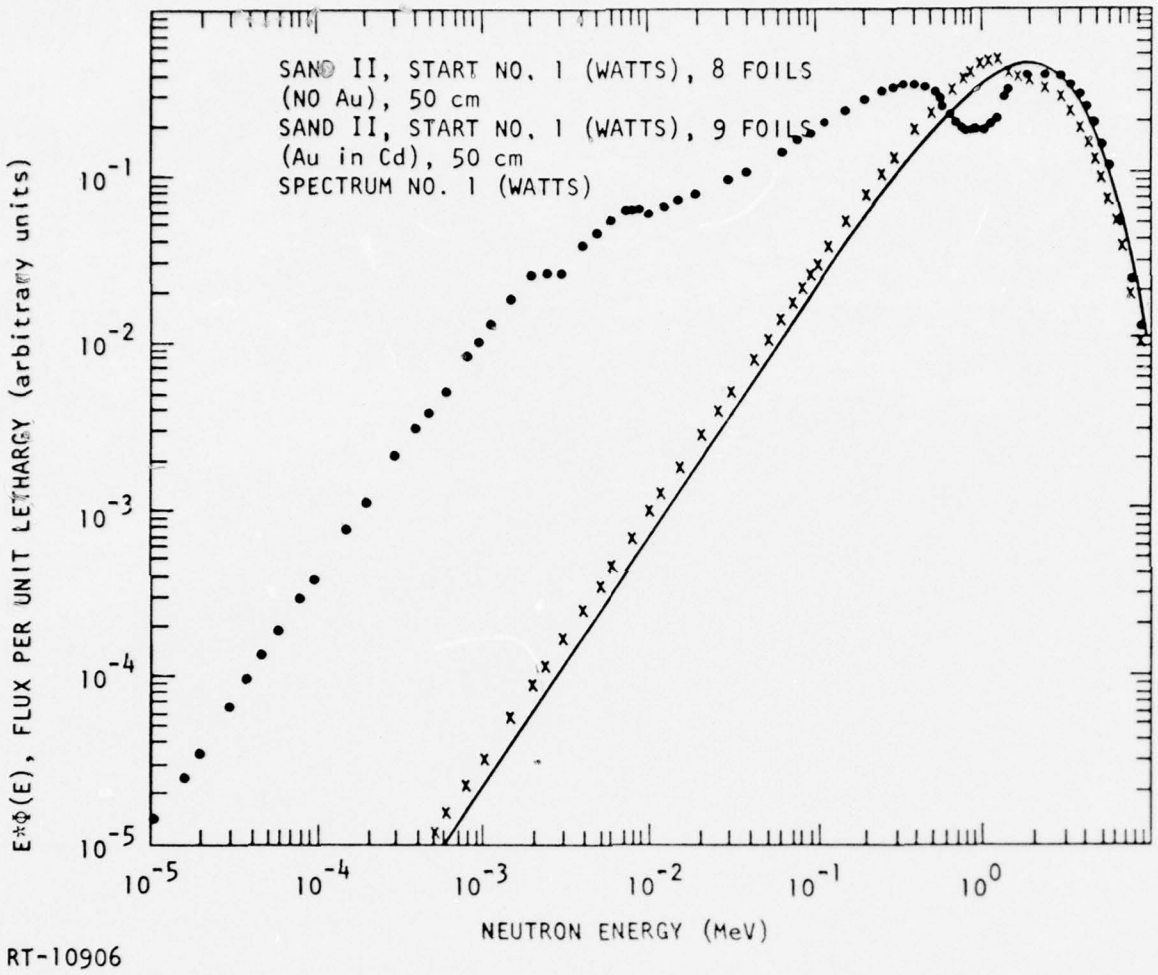

Figure 20. Two SAND II unfolding results compared to the Watt start spectrum (solid line) which has no wall-moderated component. There is approximate agreement when the low-energy (gold foil) data are omitted, but an almost meaningless spectrum results when the foil data include a low-energy contribution not included in the start spectrum.

7. VARIATIONAL STUDY

A number of variational studies of the effects of cross-section uncertainties on unfolding have been made over the past several years. In some of these studies, the reaction cross section for a given foil was varied at random over the neutron energy region above threshold. These showed that a random variation over many energy groups has almost no net effect on the output spectrum. In the work described here, the variational studies were accomplished by changing the magnitude of each individual cross section in a preselected manner. This change can be representative of a cross-section error, an incorrect branching ratio, or an uncertainty in the fission-fragment yield used in calculating back from count rate observed to activations actually produced. This cross-section change was simulated by changing the input activation number used in SAND II. In fact, this variational study simultaneously evaluates the effects of counting, foil weighing, and self-absorption-correction errors, as well as cross-section uncertainties. The effect of varying the activation (or "cross section") input to SAND II on the 1-MeV silicon equivalent fluence was evaluated by folding the resulting SAND II output spectrum with the neutron energy-dependent damage function D(E) for silicon shown in Figure 9.

It should be pointed out that any future updating of the data on D(E) or on the activation cross sections does not invalidate this study. The 1-MeV equivalent specification can simply be updated with the improved data. Nor will the procedural specifications written up in Appendix A be invalidated by such improvements in cross section.

In Figure 21 is shown the result of a series of SAND II unfolding operations with the cross sections varied by 15 and 25%, individually for most cases and in pairs for the ^{238}U and ^{24}Mg foils. For the pairs, in one case both the ^{238}U and ^{24}Mg activations were increased, and in the

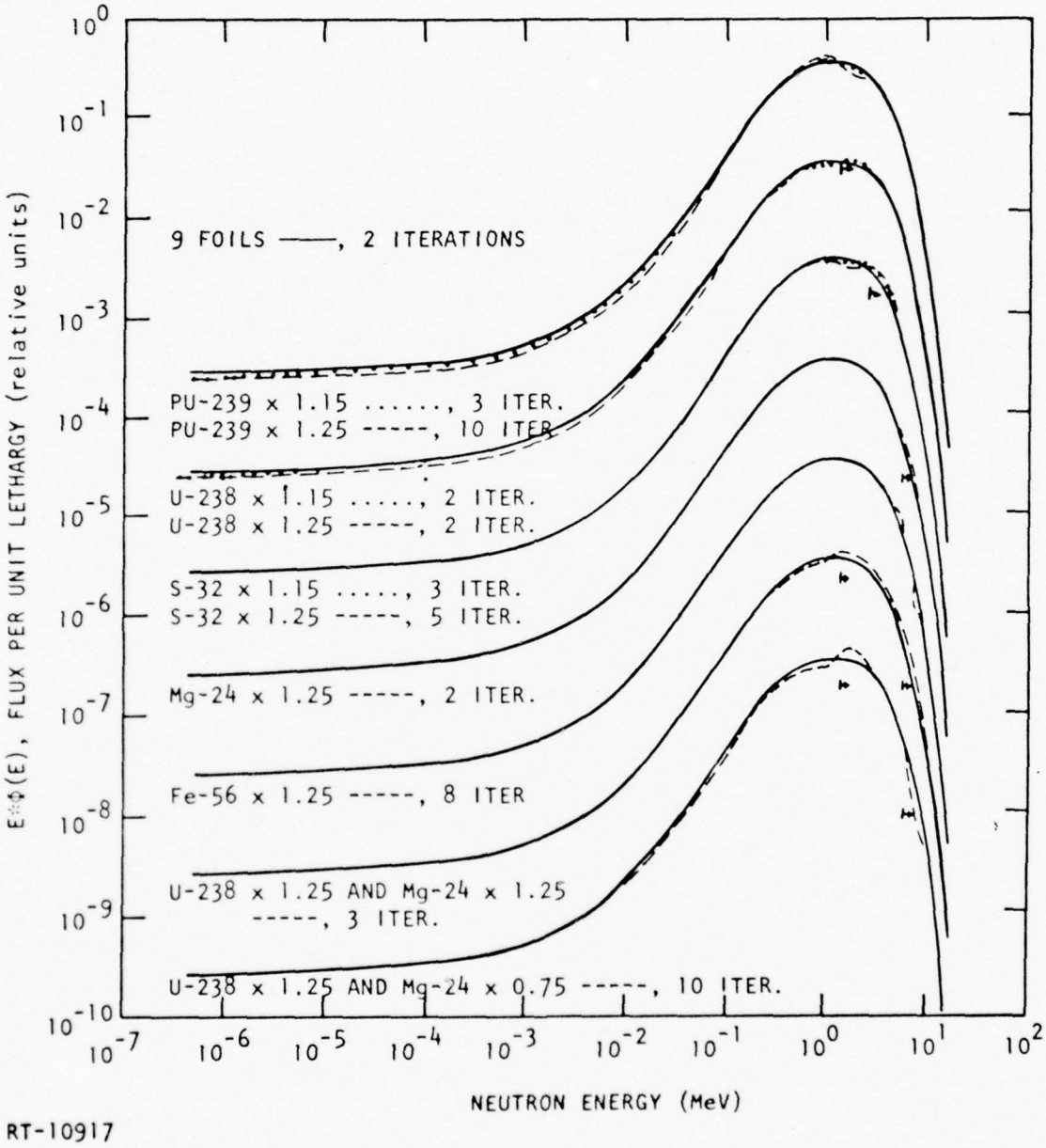

Figure 21. Effect of varying foil activation (or, equivalently, the cross section) on SAND II spectra. Solid curve is for unperturbed data in each case (the "standard" run).

other the ^{238}U activation was increased and the ^{24}Mg decreased. A total of nine foils was used. These are ^{239}Pu, ^{238}U, and ^{235}U fission foils covered with boron, a cadmium-covered gold foil to provide low-energy data, and foils utilizing the following reactions: $^{32}S(n,p)^{32}P$, $^{58}Ni(n,p)^{58}Co$, $^{56}Fe(n,p)^{56}Mn$, $^{24}Mg(n,p)^{24}Na$, and $^{127}I(n,2n)^{126}I$.

The bare gold foil and the Cd-covered sodium foil were not included because they caused the SAND II code to iterate a large number of times to produce the local structure at low energies required to fit these three activations to the final curve. One should either include this local structure in the start spectrum or use only the "average" foil (in this case, the Cd-covered gold foil) for serious studies at high energies. The local structure in the low-energy region can later be modified by varying the strength of the thermal peak that is superposed on the 1/E component below $\sim 10^{-6}$ MeV. Bare low-energy foils are now used (Figure 1).

The perturbed spectra in Figure 18 are shown compared to the unperturbed spectrum (solid line). The threshold energy of the foil cross section being varied is depicted by a vertical bar and horizontal arrow located below the corresponding curve. Note that the effect of varying one of the activations (or cross sections) is very local for those foils that have thresholds near the threshold energies of the other foils. The ^{239}Pu and the ^{238}U foils have a slight effect on the low-energy data as well, probably because no other thresholds exist between the ^{239}Pu (0.01 MeV) and ^{238}U (1.5 MeV) thresholds and the gold-foil region ($\sim$5 eV) in the present group of nine foils.

In Table 1 is shown a list of 1-MeV equivalent values for the variational studies shown in Figure 21. These are spectra C through M in Table 1. These data indicate that for foils with thresholds below 2 MeV, where few thresholds exist, a 25% increase in cross-section or foil activation produces $\sim$2% decrease in ϕ_{eq}/ϕ; for foils with thresholds just above 2 MeV, where the neutron flux is still high and the thresholds are close together, a 25% increase in cross section of one foil produces about a 1% or less increase in ϕ_{eq}/ϕ; for foils with thresholds well above 2 MeV, a 25% increase in cross section results in a 0 to +0.4% ϕ_{eq}/ϕ change.

8. WSMR-FBR REMEASUREMENTS: PRECISION EVALUATION

The measurements presented in Section 6 were carried out at the White Sands Missile Range FBR by the Nuclear Operations and Effects Branch personnel (Ref. 34) with their own set of foils, gamma-ray detector, and gamma-ray calibration standards. The measurements were repeated by IRT personnel with their foils, detector, and calibration sources. The IRT foils were all obtained from Reactor Experiments, Inc. (Ref. 35), except for ^{237}Np and ^{235}U foils, which were obtained from the Oak Ridge National Laboratory Isotopes Division, and ^{127}I, which was in the form of 2-Iodoacetamide, and contained in a thin aluminum encapsulation. The reproducibility of the WSMR results is taken as the precision of the measuring technique.

A SAND II unfolding calculation was carried out with the IRT data, using the 1DF calculated spectrum as a trial spectrum. The SAND II spectrum was nearly identical in shape to both the 1DF calculation and the SAND II results obtained with the WSMR data (Figure 15). The spectral shapes, as expressed in terms of ϕ_{eq}/ϕ, were also nearly the same: ϕ_{eq}/ϕ = 1.037 for the WSMR data and 1.023 for the IRT results. In both cases, the questionable ^{232}Th fission foil data were omitted because they systematically disagreed with the other foils (^{237}Np, ^{115}In, and ^{238}U), with threshold energies E_t near that of ^{232}Th [$E_t(^{232}\text{Th})$ = 1.75 MeV]. (This is probably due to the difficulty in counting thorium fission via the mass-140 chain, because of interference by thorium natural radioactivity. ^{232}Th was therefore omitted from the recommended set of foils, ASTM Standard Method E XXI, Appendix A.)

At 50 cm from the WSMR reactor, the agreement in spectral shape (see Figure 22) is again very good. The hardness parameter ϕ_{eq}/ϕ is 1.076 1-MeV (±0.15 MeV) neutrons/unit fluence (silicon equivalent) for the WSMR foil results, and ϕ_{eq}/ϕ = 1.062 for the IRT data.

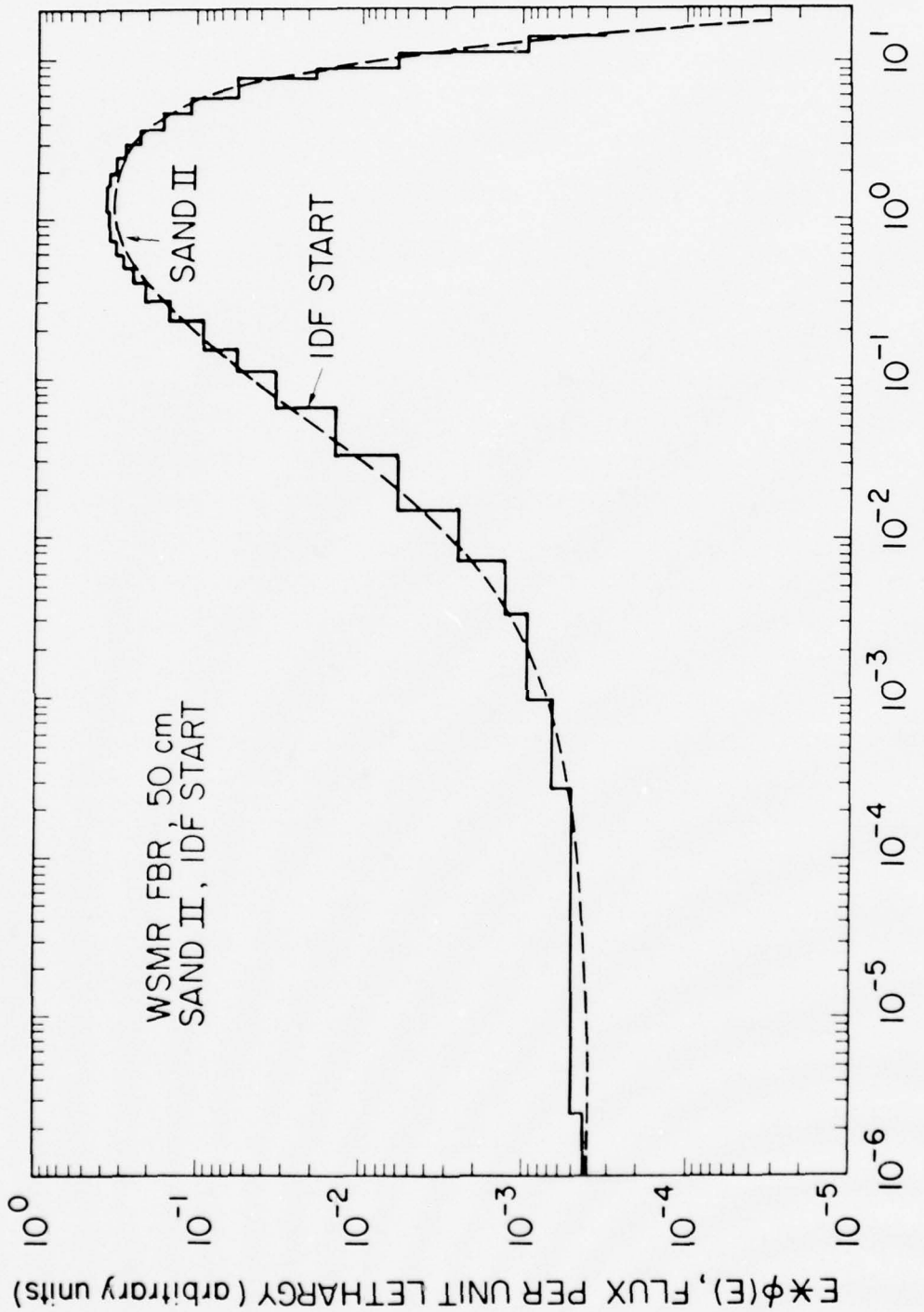

Figure 22. Spectrum at 50 cm from the WSMR FBR, (1975 results)

Thus, for both sets of measurements, a precision of ~0.01 in ϕ_{eq}/ϕ is indicated. With standard techniques (see Appendix A), a precision of 5% is probably attainable with well-developed techniques in foil selection, exposure, counting, and data analysis, and perhaps 10% with nominal care. This assumes that the trial spectrum $\phi_{tr}(E)$ is chosen according to the prescription of Method E XXI, Appendix A.

8.1 STANDARD METHOD OF SELECTING TRIAL SPECTRUM $\phi_{tr}(E)$ FOR REACTOR SPECTRA

It was observed that all WSMR-FBR spectra can be approximated by a GODIVA spectrum (see Figure 13) with a 1/E low-energy component that becomes larger as the distance from the reactor increases [see IDF calculations at different distances (Figure 5)]. The same was seen to hold true for the TRIGA spectrum presented in Section 9. Thus, a good trial spectrum can probably be generated by simply attaching a 1/E component at the proper point on the GODIVA spectrum. Figure 23 shows a GODIVA spectrum (Start No. 5), and the results of SAND II unfolding with a 1/E component normalized to the GODIVA at 0.005, 0.01, and 0.02 MeV. (These were unfolded with the ^{232}Th foil data, which tends to produce a dip at ~1 MeV. A dip or peak at this energy has no effect on ϕ_{eq}/ϕ to first order, so that these data provide a valid test.) After unfolding, the test case of $\phi_{tr}(E)$ = GODIVA + 1/E normalized at 0.01 MeV provides an output spectrum that is nearly identical to the $\phi_{tr}(E)$. In addition, ϕ_{eq}/ϕ for both this $\phi_{tr}(E)$ and the respective SAND II output shown in Figure 23 are nearly the same, i.e., ϕ_{eq}/ϕ = 1.080 for $\phi_{tr}(E)$ in all three cases, and ϕ_{eq}/ϕ = 1.041, 1.081, and 1.154, respectively, for SAND II run with GODIVA + 1/E normalized at 0.005, 0.01, and 0.02 MeV, respectively. Thus, the 0.01-MeV normalizing point was found to be the best for $\phi_{tr}(E)$ in the case of the spectrum at 50 cm from the FBR reactor (165 cm above the concrete floor).

The validity of this procedure should be checked by further comparing these values of ϕ_{eq}/ϕ to those for (a) the IDF FBR calculation at 50 cm, and (b) the SAND II output with this IDF spectrum used as $\phi_{tr}(E)$. The respective values of ϕ_{eq}/ϕ are 1.074 and 1.063. Thus, the accuracy

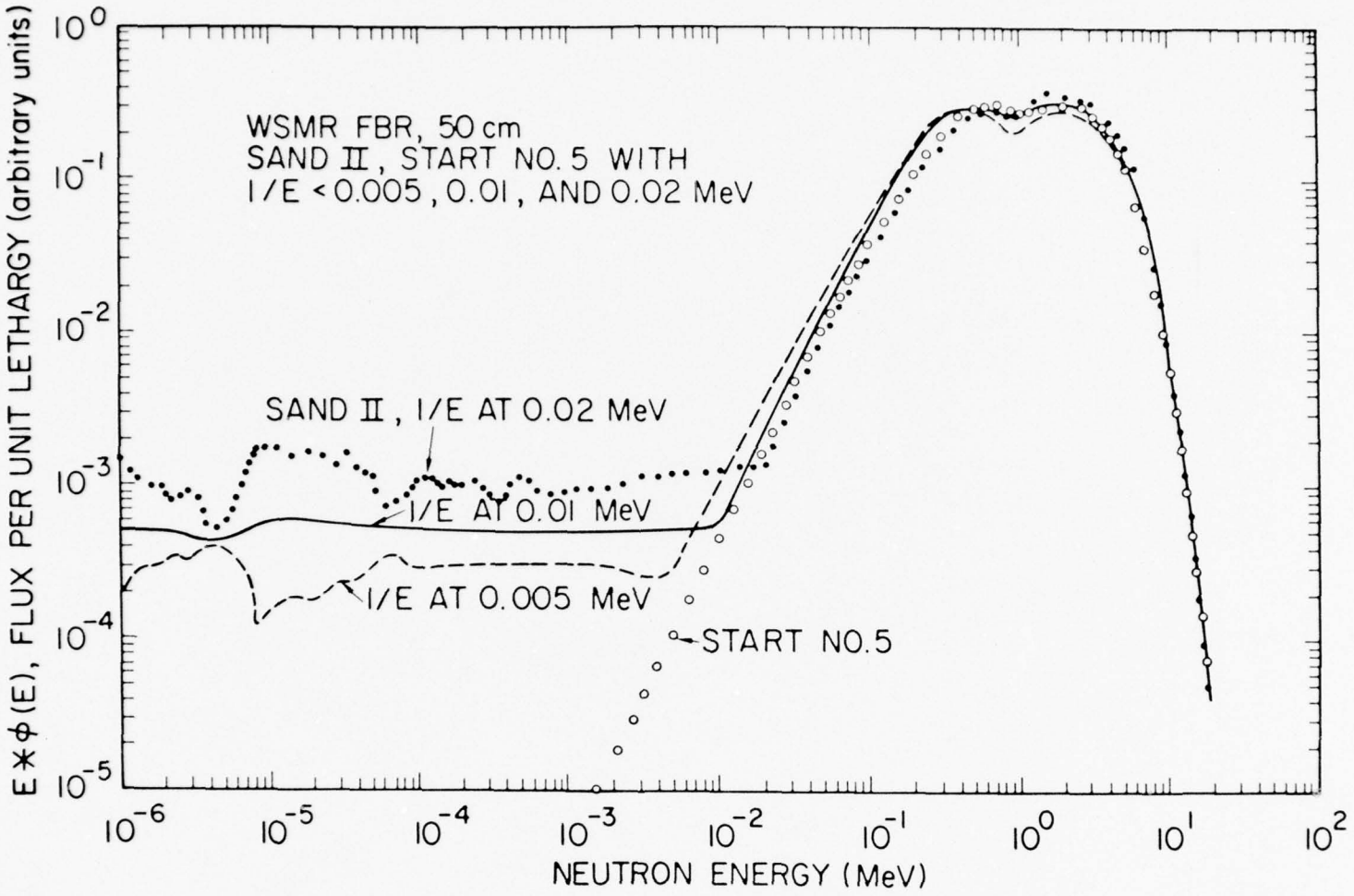

Figure 23. SAND II unfolding with GODIVA (Start No. 5) plus 1/E spectrum used as trial spectrum. Results are shown for 1/E-tail juncture at three different energies.

achieved with the 1/E fitting appears to be ~1% (1.081 versus 1.074 for the "known" spectrum. A similar comparison will be made in Section 9, where the TRIGA results are presented.

9. THE TRIGA J-TUBE MEASUREMENT

A set of threshold activation foils was exposed to the General Atomic TRIGA reactor, inside the J-tube which abuts the reactor core (see Figure 24) adjacent to fuel element G-1 shown in Figure 25. A 3-inch lead shield separates the J-tube irradiation chamber from the reactor core, and a boral shield (~0.6 cm) covers all sides of the chamber. The total fluence was $\sim 5 \times 10^{11}$ n/cm^2, which represents about the lower limit in terms of acceptable counting statistics.

The TRIGA J-tube spectrum was calculated with the GAZE code, and the GAZE spectrum was used as the trial spectrum, $\phi_{tr}(E)$, for SAND II unfolding. The results, shown in Figure 26, yielded a spectrum that is everywhere lower than the GAZE calculation below about 400 keV. This indicates that the GAZE code predicts a spectrum that is somewhat too high below this energy. The respective values of ϕ_{eq}/ϕ for the GAZE spectrum and the SAND II result are 0.942 and 0.993, which is consistent with a GAZE spectrum that is too soft compared to the threshold-foil data.

Next, SAND II was run with trial spectrum No. 7 of the SAND II library of start spectra. This is simply a GODIVA spectrum (Start No. 5) with a 1/E tail normalized at 500 keV. This is also too soft a trial spectrum, as can be seen from the plot of trial spectrum No. 7 and the accompanying SAND II result shown in Figure 27.

The results of a more recent calculation for a similar water-moderated reactor (Ref. 37) were used for $\phi_{tr}(E)$ in the SAND II unfolding program. The calculation was carried out with a finer group structure than the GAZE calculation (Ref. 36), and was able to reproduce much of the resonance structure above 0.5 MeV, the low-energy cutoff. Except for this resonance structure, the spectrum was found to be nearly identical to the GODIVA spectrum which was used for extrapolation down to the 0.15-MeV point of

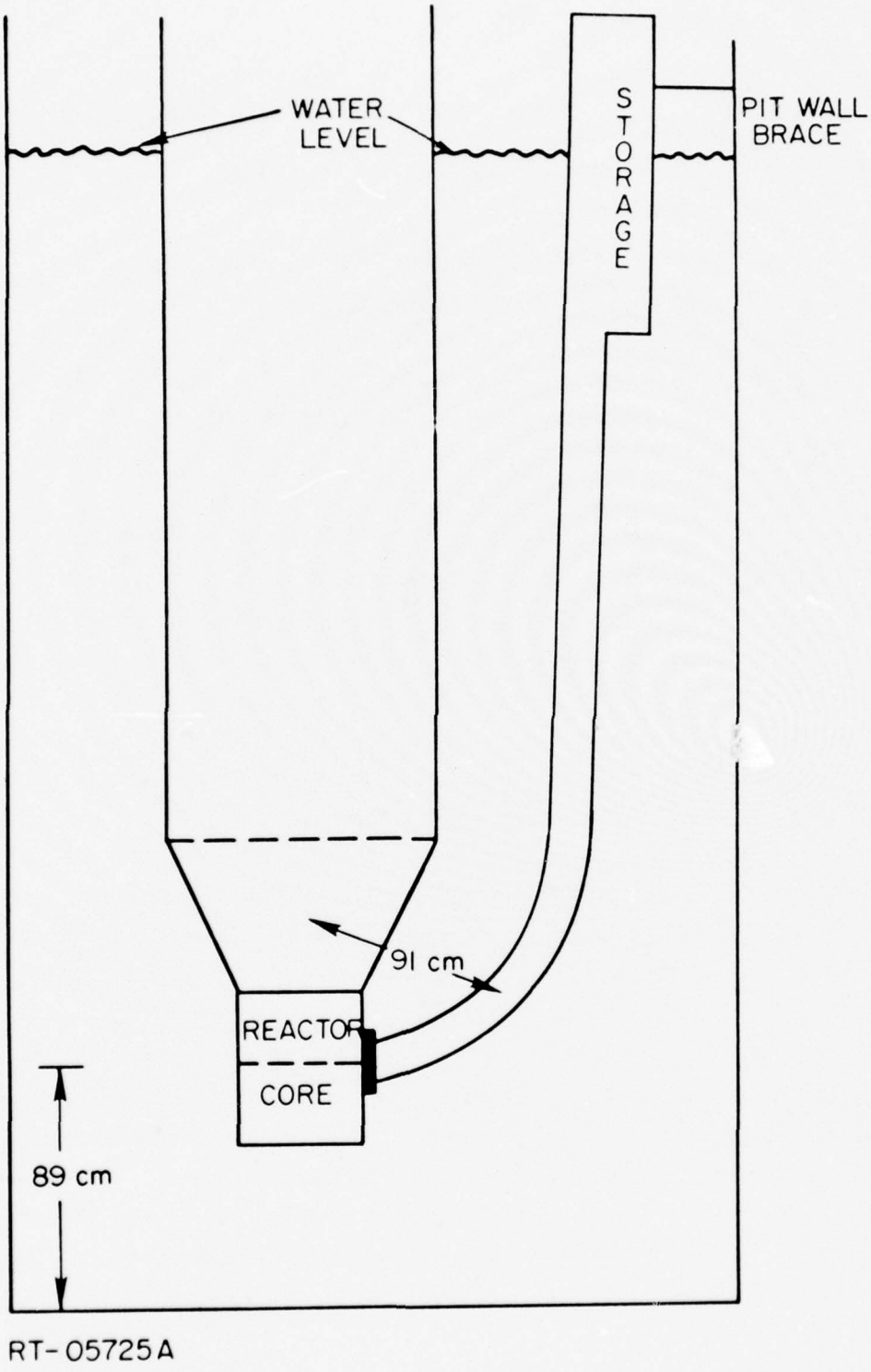

Figure 24. TRIGA J-tube geometry

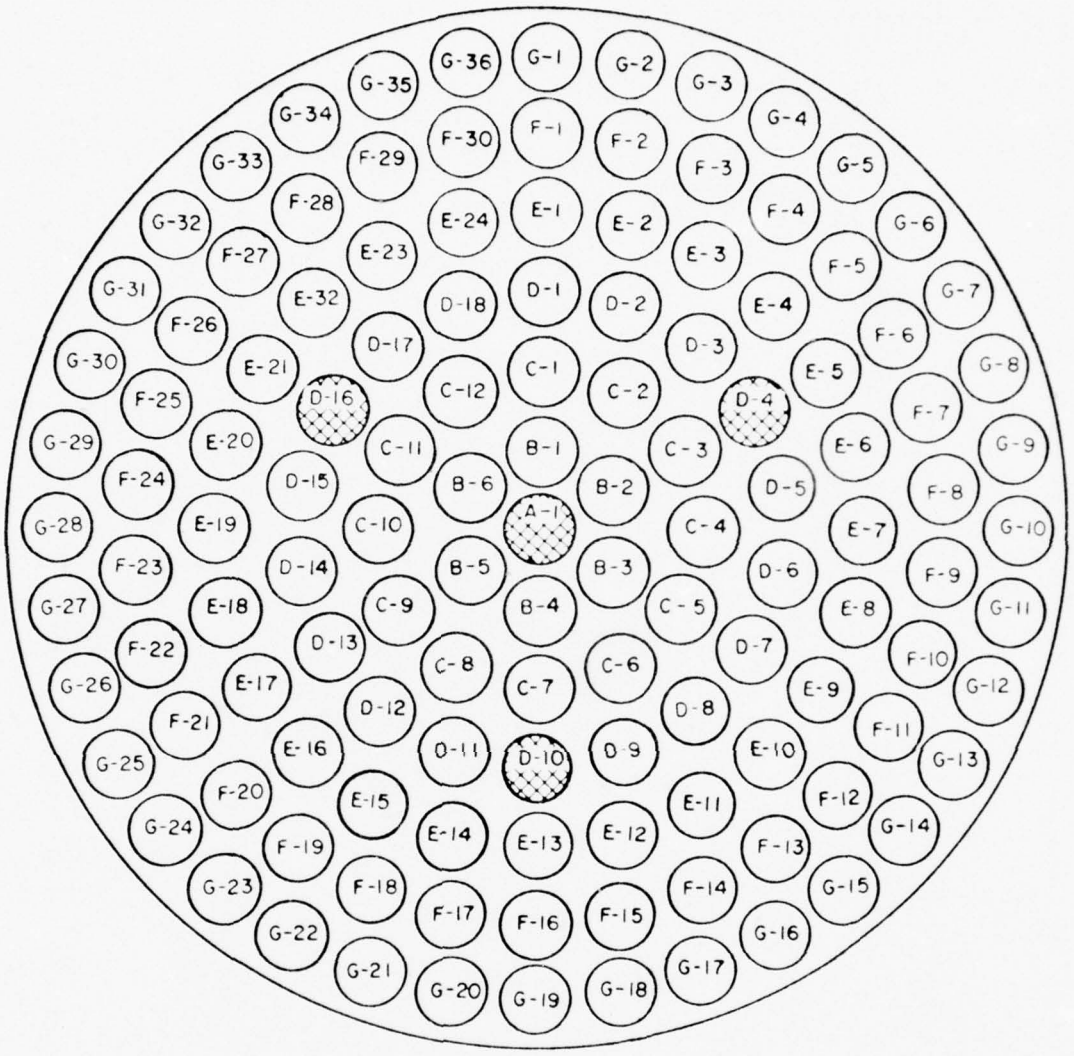

Figure 25. TRIGA fuel loading. J-tube lead shield is adjacent to fuel cell G-1

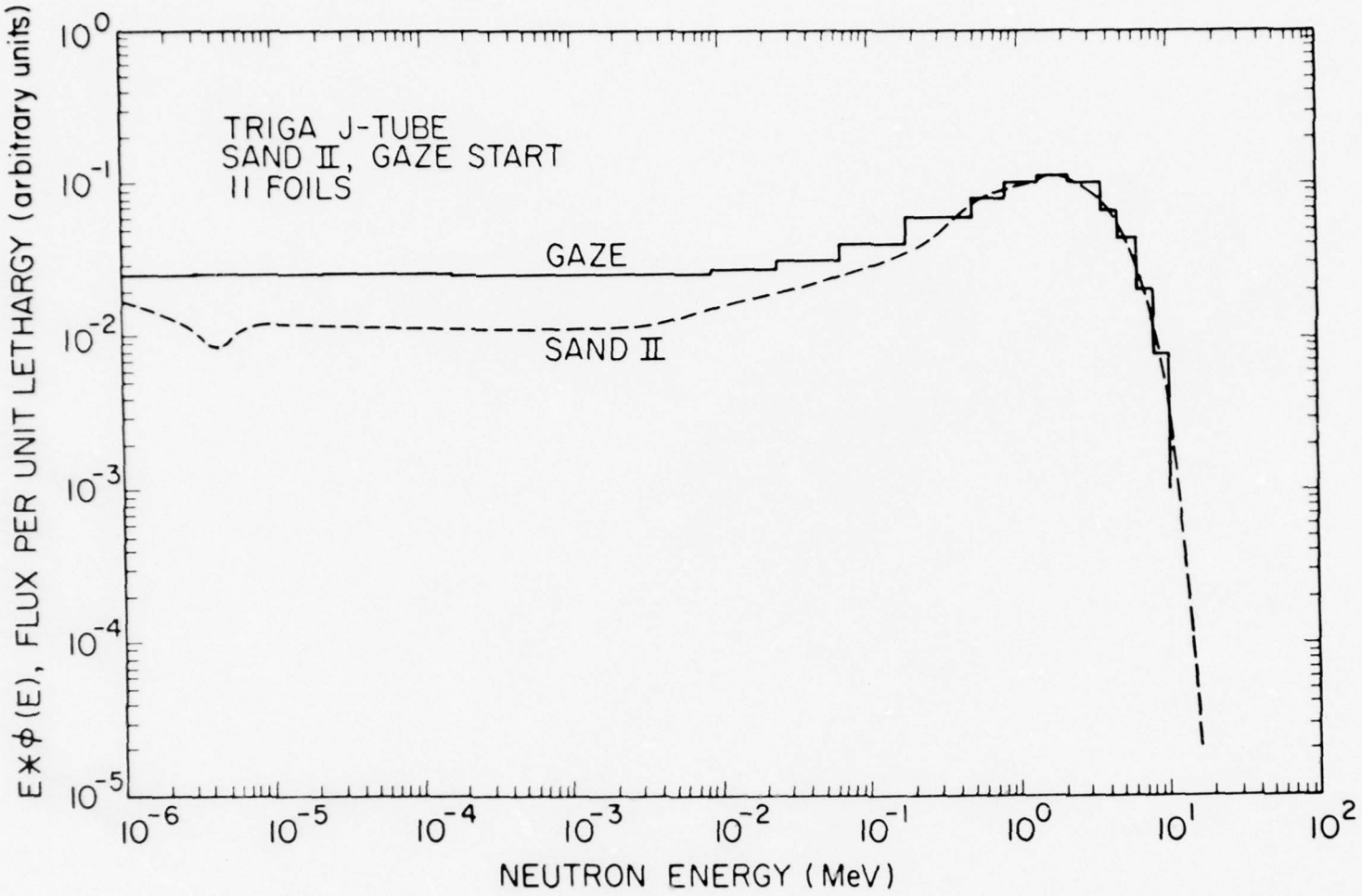

Figure 26. SAND II unfolded spectrum with GAZE. Calculated spectrum used as trial spectrum.

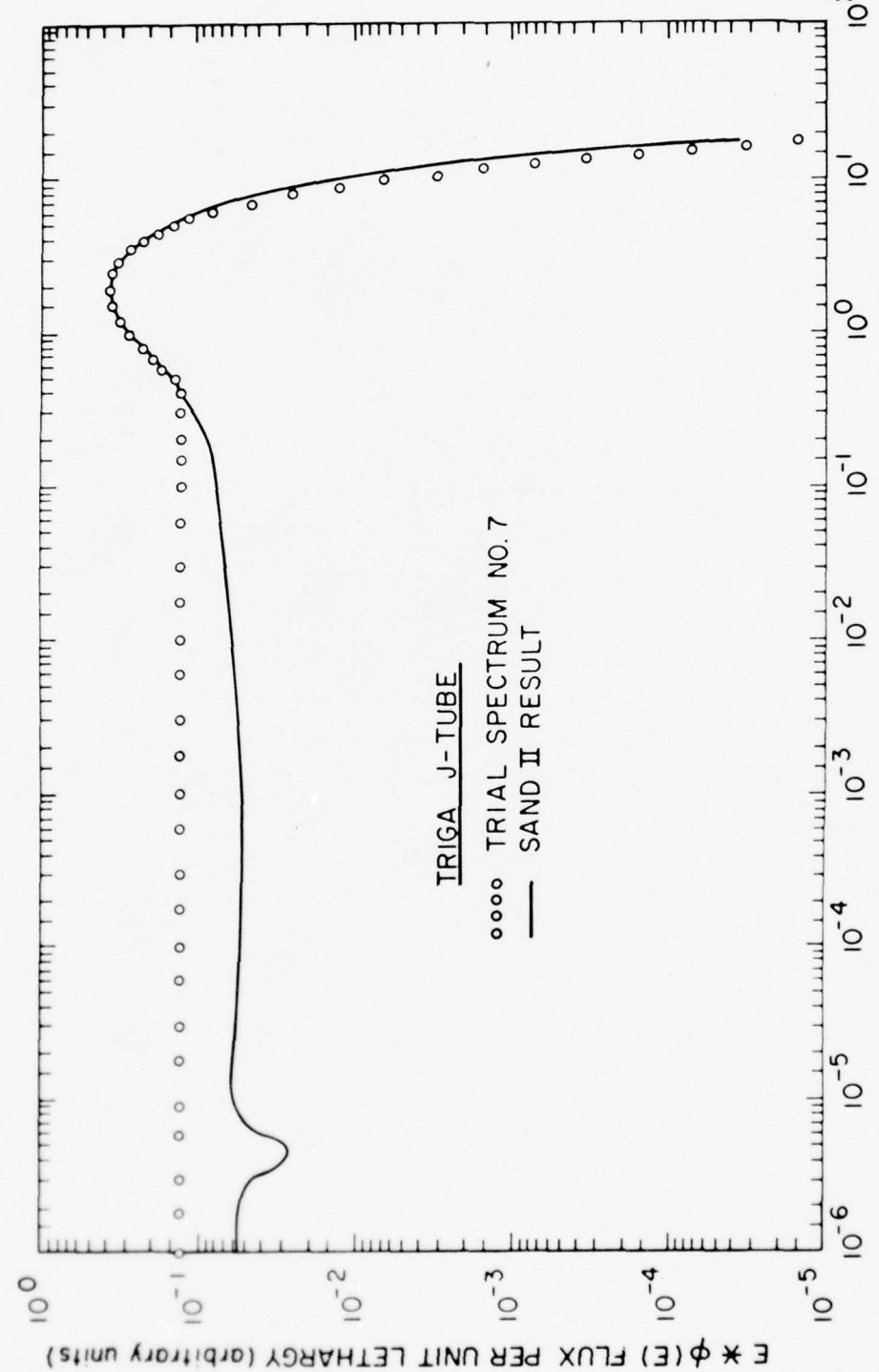

Figure 27. SAND II spectrum for TRIGA J-tube, with GODIVA trial spectrum plus 1/E tail below 0.5 MeV

the 1/E-spectrum juncture. This spectrum (Figure 28) is consistent with the threshold-foil data, as seen by the excellent agreement between the two.

Thus, a 1/E juncture at 0.15 MeV is called for when tailoring a GODIVA and 1/E spectral combination to obtain a reliable $\phi_{tr}(E)$ for input to SAND II. The corresponding juncture points E_j would be at 0 MeV for a FBR glory-hole spectrum, and 0.01 MeV at 50 cm from the reactor, with E_j increasing with distance away from the reactor and nearer the source of the floor- and wall-scattering component.

9.1 GOLD-FOIL SELF-SHIELDING CORRECTION

The low-energy end of the SAND II spectrum (Figure 28) shows the results of varying the correction for gold foil self absorption. While a factor-of-two correction repairs the "dip" at very strong 5 eV gold resonance, the influence on ϕ_{eq}/ϕ was ~1%, almost negligibly small. The measured self-absorption correction for a 0.0025-cm-thick cadmium-covered gold foil is ~2.3 for isotropic flux (Ref. 38). These corrections (Ref. 39) are only important for low-energy spectrometry, but should nevertheless be made to avoid the possibility of the SAND II code making compensating changes in the wrong part of the spectrum, where D(E) for silicon may be drastically different.

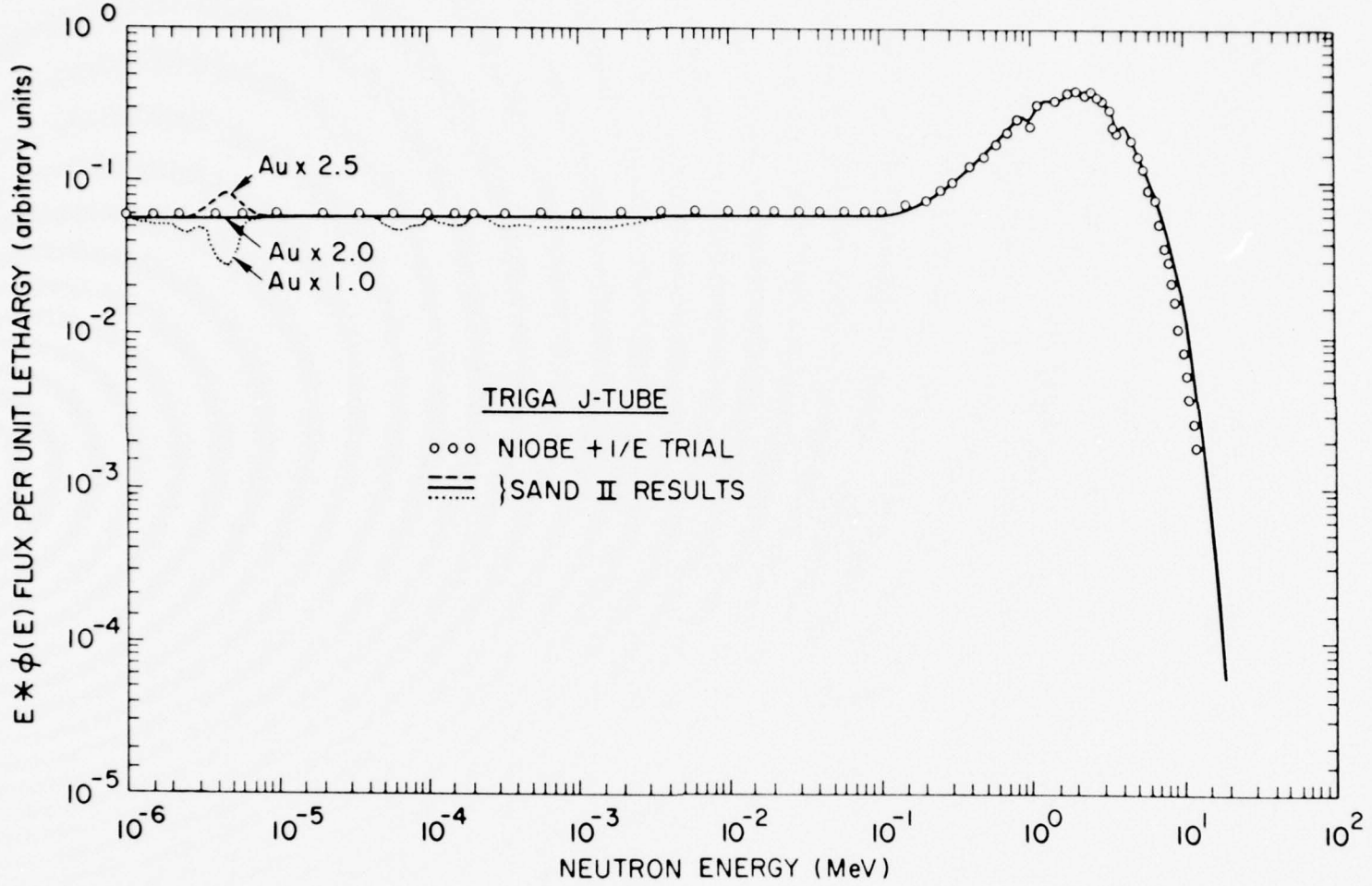

Figure 28. SAND II spectrum for TRIGA J-tube, with $\phi_{tr}(E)$ = NIOBE calculation 0.5 MeV, GODIVA between 0.15 and 0.5 MeV, and 1/E below 0.15 MeV

10. SPECTRAL-INDEX CHARACTERIZATION OF THE NEUTRON SPECTRUM FOR PRODUCING RADIATION DAMAGE IN SILICON

Note that the high-energy end of the spectrum for the NIOBE calculation (Figure 28) is lower than the SAND II output. The same is true for the GODIVA spectrum (Figure 27) and the GAZE (Figure 26), although less so for the latter. In examining the activations calculated with SAND II for the input spectrum $\phi_{tr}(E)$,

$$A_x(\text{calc}) = \int_0^{18\ \text{MeV}} \phi_{tr}(E)\ \sigma_x(E)\ dE \quad , \tag{3}$$

one finds that Δ_o, the percentage difference between measured and calculated activations, consistently increases with the threshold energy E_t of the foil for $E_t > 3$ MeV. Thus, the early calculations appear to underpredict the high-energy flux in a consistent manner. (This discrepancy is not important to obtaining accurate SAND II results, because the code easily and rapidly corrects the spectrum here, where many values of E_t exist and when the discrepancy increases with E_t.) This has a direct impact on the popular procedure of characterizing the neutron spectrum by the spectral index (SI), which is defined as the ratio of neutron flux above 10 keV to the flux above 3 MeV. The SI is often used to characterize the radiation damage effectiveness of the spectrum which is, in a way, an approach to estimating ϕ_{eq}/ϕ. If the results of a poor calculation are used to infer SI from $\phi_{calc}(E)$, a large error can ensue. This can be seen from the following comparison of the calculated and measured values of the SI and of ϕ_{eq}/ϕ. For the glory-hole spectrum, $\phi_{eq}/\phi = 1.031$ for the IDF calculation and 1.023 for the SAND II result using this calculation as $\phi_{tr}(E)$. This is a 1% agreement. The respective SI are 8.99 and 6.79, or a 32% difference. Thus, a very large difference in SI can occur for two

spectra with nearly identical silicon radiation damage effectiveness. This is due to the SI being a characterization that compares the total neutron fluence to that above 3 MeV, where there are only a few neutrons, and therefore little contribution to the radiation damage. (A 1-MeV dividing line would give a much more sensitive measure of radiation damage effectiveness.)

For the WSMR-FBR 50-cm spectrum, ϕ_{eq}/ϕ (1DF) = 1.074 and ϕ_{eq}/ϕ(meas) = 1.064, which is a 1% agreement. The respective SI are 7.74 and 6.42, a 21% difference.

For the TRIGA J-tube, ϕ_{eq}/ϕ(GAZE) = 0.942, ϕ_{eq}/ϕ(meas) = 0.993, yielding a 5% difference. The respective SI are 7.19 and 6.54, which differ by 10%.

While it is clear from these comparisons that the SI representation may be 10 to 30% off, a spectrum characterization by an imprecise threshold-foil spectrum measurement may be worse. For example, a measurement of the TRIGA spectrum was made two years ago, utilizing six foils (^{197}Au, E_t = 0; ^{239}Pu, E_t = 0; ^{237}Np, E_t = 0.5 MeV; ^{238}U, E_t = 1.45 MeV; ^{32}S, E_t = 2.9 MeV; and ^{27}Al(n,α), E_t = 8.7 MeV). No express care was taken to choose $\phi_{tr}(E)$ with all the physical characteristics, a choice that is most necessary for obtaining a good spectrum from 10^{-8} to 20 MeV with only six input numbers! The SI so obtained was 9.24 (ϕ_{eq}/ϕ was 0.844). This solution was so non-physical that when used in SAND II as $\phi_{tr}(E)$, the parameters became even worse (10.99 for SI and 0.660 for ϕ_{eq}/ϕ). A comparison of the 1973 and the 1975 results is given in Figure 29. The latter data were obtained with a hybrid $\phi_{tr}(E)$ consisting of the NIOBE calculation above 0.85 MeV, GAZE between 0.1 and 0.85 MeV, and 1/E <0.1 MeV. SI = 6.8 and ϕ_{eq}/ϕ = 0.974. The SAND II result was in good agreement with this trial spectrum $\phi_{tr}(E)$. For this case, ϕ_{eq}/ϕ = 1.019 and SI = 6.25. It is clear from these results that the standard procedure for measuring $\phi(E)$ (Appendix A) must be spelled out in enough detail to ensure good reproducibility and accuracy. It is also clear (see Figure 29) that a log-log plot in the form of $E*\phi(E)$ versus E is important in showing up even small aberrations in the solution; the 1/E component is a flat line, and the high-energy component, above ~2 MeV,

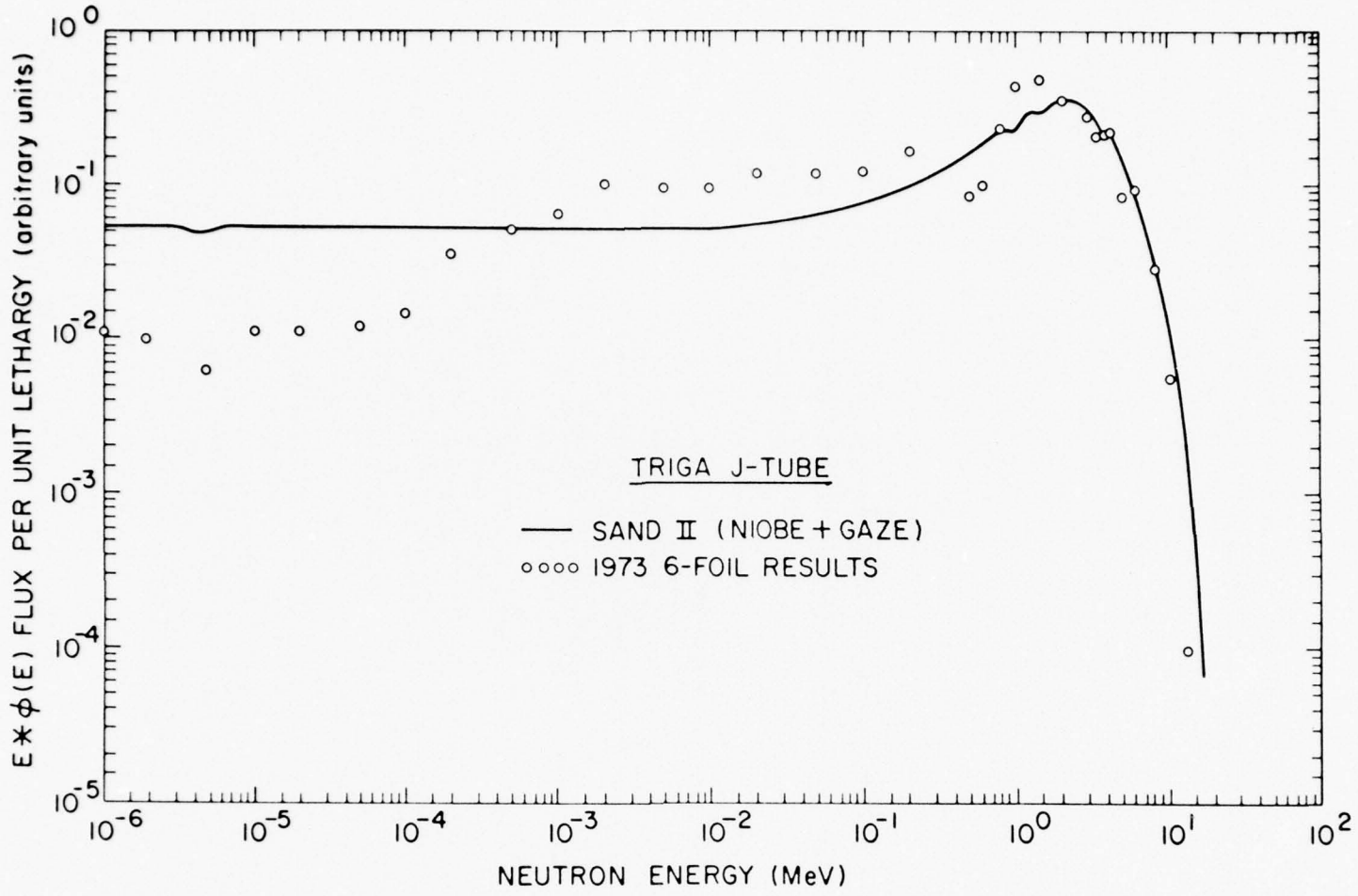

Figure 29. 1973 six-foil SPECTRA-code results for TRIGA J-tube compared to 1975 results with SAND II using NIOBE above 0.8 MeV, GAZE between 0.1 and 0.8 MeV, and 1/E below 0.1 MeV

has a less steep slope. The disagreement between the 1973 results and earlier calculations [such as the GAZE prediction of $\phi(E)$] is not very apparent on a log-log $\phi(E)$ versus E plot.

REFERENCES

1. V. V. Verbinski and J. C. Courtney, Nucl. Phys. 73, 398 (1965).

2. V. V. Verbinski, et al., Nucl. Inst. and Meth. 63, 8 (1968).

3. J. M. Young, J. M. Neill, P. d'Oultremont, E. L. Slaggie, and C. A. Preskitt, Nucl. Sci. Eng. 48, 45 (1972); P. d'Oultremont, J. C. Young, J. M. Neill, and C. A. Preskitt, Nucl. Sci. Eng. 45, 141 (1971).

4. P. d'Oultremont, D. H. Houston, and J. C. Young, "CAGE-BIRD-SPEC," Gulf-RT-10195, Gulf Radiation Technology, San Diego, California (1970).

5. W. R. Burrus and V. V. Verbinski, Nucl. Inst. and Meth. 67, 181 (1969).

6. V. V. Verbinski and W. R. Burrus, Phys. Rev. 177, 1671 (1969).

7. V. V. Verbinski, et al., Phys. Rev. 170, 916 (1968).

8. E. F. Bennett, Nucl. Sci. and Eng. 27, 16 (1967); R. Gold and E. F. Bennett, Nucl. Inst. and Meth. 63, 285 (1967); E. F. Bennett and T. J. Yule, Nucl. Inst. and Meth. 98, 393 (1972).

9. V. V. Verbinski and R. Giovannini, Nucl. Inst. and Meth. 114, 205 (1974).

10. H. Werle, Nucl. Inst. and Meth. 99, 295 (1972).

11. V. V. Verbinski and M. S. Bokhari, Nucl. Inst. and Meth. 46, 309 (1966).

12. For an early summary, see R. L. Simon and W. N. McElroy, "Evaluated Reference Cross Section Library," BNWL-1312, Battelle Memorial Institute, Richland, Washington 99352, May 1970.

13. W. N. McElroy, et al., "A Computer-Automated Iterative Method for Neutron Flux Spectra Determination by Foil Activation," AFWL-TR-67-41, Vol. I, Air Force Weapons Laboratory, Kirtland AFB, New Mexico, September 1967.

14. S. Berg and W. N. McElroy, ibid., Vol. II.

15. J. C. Young, IRT Corporation (private communication); also, "Fast Reactor Spectrum Measurements and Their Interpretation," IAEA-138 (Summary of Meeting of Specialists, Argonne National Laboratory, November 10-13, 1970), ed. B. K. Malaviya and V. V. Verbinski.

16. K. D. Lathrop, "DTF-IV Code, a FORTRAN-IV Program for Solving the Multi-Group Transport Equation with Anisotropic Scattering," USAEC Report LA-3373, Los Alamos Scientific Laboratory, July 1974 (IDF is an IRT modification of the DTF-IV code).

17. W. N. McElroy, et al., Nucl. Sci. and Eng. 48, 51-71 (1972).

18. J. C. Young, et al., ibid., 45-50 (1972).

19. J. E. Powell, Trans. Amer. Nucl. Soc. 12, 712 (1969).

20. V. V. Verbinski and R. Giovannini, Nucl. Inst. and Meth. 114, 205-231 (1974).

21. V. V. Verbinski, et al., Nucl. Sci. and Eng. 52, 330-342 (1973).

22. The IDF calculations and the GGC-5 calculation of the flux-weighted cross sections were carried out by C. Rindfleisch and D. Houston at IRT Corporation, San Diego, California 92111.

23. D. R. Mathews, et al., "GGC-5, A Computer Program for Calculating Neutron Spectra and Group Constants," GA-8871, General Atomic, September 1971.

24. V. C. Rogers, et al., "Displacement and Ionization KERMA of Silicon for Neutron Energies from 10^{-5} eV to 20 MeV," IEEE Conf. Nuclear Space and Radiation Effects, Arcata, California, July 14-17, 1975, IEEE Trans. Nucl. Sci. NS-22 No. 6,2326 (1975). Erratum, ibid. NS-23, No. 1, 875 (1976). For useful tabular data, see Appendix A, Method E XX4, and Reference 33.

25. SAND II is available at the Radiation Shielding Information Center, Oak Ridge National Laboratory, Oak Ridge, Tennessee.

26. J. A. Halblieb, J. V. Walker, and C. L. Greer, "Neutron Spectroscopy by Foil Activation in Radiation Effects Studies," SC-R-67-1157, Sandia Laboratories, Albuquerque, New Mexico, July 1967,

27. J. A. Halblieb, "Theory and Application of the Generalized SPECTRA Code," SC-RR-70-251, Sandia Laboratories, April 1970.

28. SPECTRA is available at the Radiation Shielding Information Center.

29. C. S. Shapiro, "GODIVA Test Series Dosimetry Techniques," IBM, A. D. 234769 (1960).

30. E. Watt, Phys. Rev. 87, 1037 (1952).

31. H. L. Wright, Dosimetry Section, White Sands Missile Range, White Sands, New Mexico (private communication).

32. Proc. Consultants Meeting on Nuclear Data for Reactor Neutron Dosimetry, INDC (NDS) - 56/U, IAEA, Vienna, September 10-12, 1973.

33. V. V. Verbinski, N. A. Lurie and V. C. Rogers, "Threshold-Foil Measurements of Reactor Spectra for Radiation Damage Applications," (submitted for publication in Nucl. Sci. Eng.).

34. J. T. Harvey, J. L. Meason, J. C. Hogan, and H. L. Wright, "Gamma-Ray Intensities for the Radioactive Decay of ^{140}Ba and ^{140}La," Nucl. Sci. and Eng. 58, 431 (1975).

35. Reactor Experiments, Inc., 963 Terminal Way, San Carlos, California 94070.

36. G. B. West, "Calculated Fluxes and Cross Sections for TRIGA Reactors," GA-4361, General Atomic, San Diego, California (1963).

37. V. V. Verbinski, M. S. Bokhari, J. C. Courtney, and G. E. Whitesides, Nucl. Sci. Eng. 27, 283 (1967).

38. G. S. Sanford and J. H. Seckinger, "Thickness Corrections for Neutron-Activated Gold Foils," ANL-7545, Argonne National Laboratory, Argonne, Illinois 60439.

39. ANL 5800, Reactor Physics Constants, Argonne National Laboratory, Argonne, Illinois 60439, February 1969.

APPENDIX

Designation: E XX1

Standard Method for
UNFOLDING NEUTRON SPECTRA

1. Scope

1.1 This method describes a set of standard procedures for unfolding a neutron spectrum $\phi(E)$ with the SAND II code, using as input data a set of threshold-foil activations, with threshold energies E_t effectively ranging from cadmium cutoff ($\sim 3 \times 10^{-7}$ MeV) to $\sim$14 MeV.

1.2 The selection and exposure of a set of activation foils is covered in ASTM Method E XX2, "Method of Irradiating a Standard Set of Neutron Threshold Activation Foils." In addition, a minimum set of reliable foils is presented in that method.

1.3 The measurement of the specific activities of the threshold-activation foils is covered in ASTM E XX3, "Measuring Foil Activities for Neutron Spectrum Unfolding."

1.4 The neutron spectrum $\phi(E)$ as measured by this method may have a wide variety of uses. Nevertheless, this method is specifically addressed to characterizing $\phi(E)$ in terms of a single parameter that gives a measure of its effectiveness in producing radiation damage in silicon semiconductor devices. The precision and accuracy of $\phi(E)$ are therefore expressed in terms of the 1-MeV equivalent fluence, ϕ_{eq}, for silicon, and in terms of the hardness parameter, ϕ_{eq}/ϕ. The calculation of these quantities is covered in ASTM Method E XX4, "Characterizing Neutron Spectra in Terms of 1-MeV Equivalent Fluence for Radiation Damage in Silicon."

1.5 As a corollary to measuring $\phi(E)$ and calculating ϕ_{eq}, a standard for measuring ϕ_{eq}/Monitor Count is proposed: ASTM Method E XX5, "Measuring 1-MeV Silicon Equivalent Fluence with Fast-Neutron Monitors."

1.6 A flow chart shown in Fig. 1 lists the sequence of operations that lead to $\phi(E)$, ϕ_{eq}, ϕ_{eq}/ϕ, and ϕ_{eq}/Monitor.

1.7 Periodic updating of nuclear data will improve the accuracy of the threshold-foil activation cross sections, branching ratios, and decay constants, as well as calculations of the damage function D(E). These must be utilized to update the input data for this method from time to time to improve its accuracy, which will require updating these standard methods.

1.8 All $E_t = 0$ foils (both 1/v and fission foils) are cadmium or ^{10}B covered, which excludes thermal-neutron measurements. This facilitates a more reliable solution at higher energies, where practically all of the radiation damage occurs in silicon.

1.9 Although codes other than SAND II, such as SPECTRA, CRYSTAL BALL, and OPTIMO [also available at Radiation Shielding Information Center (RSIC) (1)], can give results, the SAND II code was chosen because of the built-in feature of retarding the formation of spurious structure (see Sec. II.1). Also, it provides in convenient format the Δ_o's needed to evaluate the agreement between the foil data and the trial spectrum. This plays an important part in rejecting erratic foil data and in choosing a more realistic trial spectrum; a user interaction that is important to unfolding accuracy.

2. Significance

2.1 This method provides the neutron fluence $\phi(E)$ for general use, such as for calculating radiation damage to materials other than silicon, where the damage versus neutron energy, D(E), is known or is calculable from known neutron cross sections.

2.2 This method and the supporting methods (Sec. [illegible]) constitute a set of draft standards for characterizing divergent neutron fields in terms of ϕ_{eq}, the equivalent 1-MeV fluence for neutron radiation damage in silicon, and ϕ_{eq}/ϕ, the hardness parameter which specifies the fluence of 1-MeV neutrons required to produce the same radiation damage as a unit fluence of neutrons (above 0.01 MeV) having the spectral distribution $\phi(E)$. This characterization is of interest in planning irradiation schedules for parts screening or for sample-specification tests, and in comparing radiation damage studies carried out in different neutron fields.

3. Definitions

3.1 The description of terms relating to dosimetry are found in ASTM Definitions E 170, "Terms Relating to Dosimetry."

3.2 A_s is the saturated activity of the sample, as defined in ASTM Method E 261-70, "Standard Method for Measuring Neutron Flux by Radioactivation Techniques." R_m is the measured number of activations per nucleus produced by irradiating N_o target nuclei (of the isotope that can produce the reaction) for an irradiation time t_i. For constant reactor power, R_m is defined as the measured ratio $R_m = A_s t_i / N_o$.

4. Summary of the Method

4.1 A set of foils is selected with thresholds E_t that vary from 0 to 14 MeV, the foils are weighed, covered with cadmium or ^{10}B as necessary, and exposed to a neutron field having a spectral distribution ϕ (E). The resultant radioactivity is measured to determine the number N of radioactive atoms produced during the irradiation of N_o target atoms of the chosen isotope. For each foil species x,

$$N = N_o \int_{E_t}^{\infty} \sigma_x(E)\phi(E)\, dE \quad , \tag{1}$$

where $\sigma_x(E)$ is the cross section for the reaction being measured. The set of measured specific activities, given by the ratio $R_m(x) = (N/N_o)_x$, is used as input to the SAND II unfolding code, along with a trial spectrum $\phi_{tr}(E)$ that contains all the physical features. These features may include a 14-MeV spike with slowing-down component below 14 MeV, or a fission spectrum with 1/E moderated component (tail).

4.1.1 Using Eq. 1 with $\phi_{tr}(E)$ in place of ϕ (E), the SAND II code calculates the various $R_{tr}(x)$, utilizing the SAND II input library of cross sections $\sigma_x(E)$. In calculating the various $R_{tr}(x)$, the input spectrum $\phi_{tr}(E)$ is normalized so as to minimize the standard deviation S_o associated with the "zeroth iteration" differences $\phi_o(x) = (R_m - R_{tr})/R_m$ between the measured and calculated specific activities.

4.1.2 For foils where $\Delta_o(x)$ is largest, the SAND II code adjusts the spectrum in the energy interval above $E_t(x)$, so as to produce a first-iteration solution, $\phi_1(E)$, with reduced $\Delta_1(x)$ and, consequently, with reduced S_1. These iterations are continued until the n-th iteration, where $S_n \leq 5$ percent.

4.2 *SAND II Limitations*

4.2.1 The threshold-foil spectrometry method is not truly a spectrometry technique, but rather a mild perturbation technique. As such, it provides a reliable output only with considerable constraints applied, especially for the region below 1 MeV, where only one true threshold (^{237}Np, 0.5 MeV) exists. This constraint is that for reactor spectra, the epicadmium solution resembles a GODIVA spectrum with 1/E tail fitted (Sec. 6.1.2). Since this provides only one adjustable parameter, that of varying the 1/E fitting point until the solution resembles the trial spectrum, it is possible for this limiting case of reactor spectra to obtain a reliable solution with one real threshold, an artificial one at 10 keV (^{235}U or ^{239}Pu in boron), and a 1/v detector providing information below 1 MeV. This is carried out with some interaction with the code.

5. Interaction With SAND II Code

5.1 *Examination of $R_m(x)$ and $\phi_{tr}(E)$ via the $\Delta_o(x)$ Set of Indicators*

5.1.1 If the solution $\phi_n(E)$ is physically meaningful, it will have the same characteristics as ϕ_{tr}. This happens when no erroneous values of R_m are input to SAND II, and when the starting spectrum $\phi_{tr}(E)$ contains all the physical characteristics of the true spectrum. It is the task of the user to examine the set of $\Delta_o(x)$ to either reject single spurious values of the corresponding $R_m(x)$, or to adjust $\phi_{tr}(E)$ in regions above the threshold energy $E_t(x)$ where two or more corresponding values of $\Delta_o(x)$ are large and agree in sign and magnitude.

5.2 *Choosing $\phi_{tr}(E)$ for Unfolding Reactor Spectra*

5.2.1 Most reactor spectra used for radiation damage studies can be represented by a fission spectrum with properly normalized 1/E slowing-down component. The trial spectrum can be represented adequately in this case

by a fission spectrum with a fitted 1/E tail. A trial fitting is first used, and if the $\Delta_o(x)$ for the cadmium-covered 1/v detector (^{197}Au, ^{59}Co, or ^{55}Mn) and the ^{239}Pu or ^{235}U boron-covered fission detectors are large and positive (or negative), then the 1/E tail is normalized at a higher (or lower) energy to the fission spectrum, and SAND II rerun. Prescribed values are given in Sec. 6.1 for the 1/E normalizing point for three different fission spectra commonly used in radiation damage work.

5.2.2 If $\phi_{tr}(E)$ is too low in the energy region above a few MeV, for a reactor spectrum, the $\Delta_o(x)$ will be positive and may increase with E_t of the foils. For this case, there are enough foils used in this prescription for SAND II to achieve a good solution in only a few iterations, so that $\phi_{tr}(E)$ need not be adjusted here. A more common problem here is that one of the $\Delta_o(x)$ is erroneous, requiring many iterations to achieve a solution. This is seen as a physically unreal oscillation in the solution $\phi_n(E)$, in which case the spurious activation $R_m(x)$ must be removed and SAND II rerun without this activation.

5.3 *Choosing $\phi_{tr}(E)$ for Non-Reactor Spectra*

5.3.1 In this case, ϕ_{tr} should be obtained from a neutron-transport calculation containing the source term (say 14-MeV neutrons) and all the surrounding material. A simple one-dimensional approximation to the actual geometry is usually adequate.

5.4 *Recognition of a Well-Behaved Solution*

5.4.1 When the $R_m(x)$ and $\phi_{tr}(E)$ are self consistent, the SAND II perturbation code will converge in a few iterations (n = 1 to 10), and $\phi_n(E)$ will be much like $\phi_{tr}(E)$.

5.4.2 The prescriptions set forth in Section 6 are designed to achieve such a solution. It is most easily recognized by comparing plots of $\phi_{tr}(E)$ and $\phi_n(E)$ on log-log paper, but with $E*\phi(E)$ plotted instead of $\phi(E)$. In this way, the 1/E slowing-down region appears as a flat line, and the slope of $\phi(E)$ above a few MeV is not nearly as steep. Deviations of $\phi_n(E)$ from $\phi_{tr}(E)$ are therefore much more apparent in the $E*\phi(E)$ plots.

6. SAND II Operating Procedure

6.1 *SAND II Inputs*

6.1.1 The SAND II code is operated in the TIME INTEGRATED mode, which standardizes the activation-foil input format for both fast-burst and steady-state irradiations. The inputs are the trial spectrum ϕ_{tr}, the specific activities $R_m(x)$ of the foils, and the foil-cover data.

6.1.2 *Trial Spectrum* ϕ_{tr}

6.1.2.1 For a GODIVA-type reactor, select spectrum No. 5 of the SAND II library of trial spectra for a glory-hole spectrum.

6.1.2.2 For a spectrum at 50 cm from a GODIVA-type reactor ~1.5 meters above a concrete floor, use trial spectrum No. 5 with a 1/E component fitted at 10^{-2} MeV [this will be compatible with the 1/v foil (^{59}Co, ^{55}Mn, or ^{197}Au) and the boron-covered ^{235}U or ^{239}Pu low-energy fission foil, and will avoid distortions in the solution $\phi(E)$ for E >0.01 MeV that result from omitting the 1/E component].

6.1.2.3 For a TRIGA spectrum, fit the 1/E component at 0.15 MeV.

6.1.2.4 To obtain trial spectrum No. 5, first run SAND II with the trial spectrum No. 5 option called for. The SAND II output will include a printout of start spectrum No. 5 (620-point spectrum from 10^{-10} to 18 MeV). Normalize the 1/E spectrum at the proper point, as prescribed above, and input the resulting hybrid spectrum at $\Delta E/E$ = 10 percent energy intervals above the normalizing point energy (i.e., at 0.15, 0.015, 0.0015 MeV, etc., down to $\sim 10^{-10}$ MeV). The hybrid spectrum is input as SPECTRUM TABULAR, as described in the input instructions.

6.1.2.5 For cases other than the three mentioned above, choose a normalizing point at 0.03 MeV for the 1/E tail, and proceed with the fitting operation as described in Sec. 5.2.

6.1.3 *Threshold-Foil Data*

6.1.3.1 The threshold-foil isotope, the type of reaction, the specific activity R_m, and the foil-cover data are required inputs to the SAND II code. For example,

U235F BORON 0.101

and

AU197G CADMIUM 0.00480

correspond to the $^{235}U(n,f)$ reaction with the ^{235}U foil covered with 1.68 g/cm^2 of ^{10}B, and the $^{197}Au(n,\gamma)^{198}$ reaction with the ^{197}Au foil covered with a 0.1-cm-thick cadmium foil. A specific activation of 5.9-12 corresponds to $R_m(^{235}U) = 5.9 \times 10^{-12}$ fissions produced per ^{235}U atom present in the target. Whereas R_m is input for fission foils, for non-fission foils, R_m is multiplied by $\lambda = 0.693/T_{\frac{1}{2}}$ of the radioactive species for input to SAND II. Three or more 1/v detector foils such as ^{197}Au, ^{59}Co, and ^{55}Mn can be used with a SAND II trial run, but the one with the value of Δ_o most nearly the average of the three should be chosen for the final run of SAND II, the others being rejected to keep the number of iterations of SAND II (and therefore the spurious structure) to a minimum.

6.2 *Acceptance Criteria for a Good Solution $\phi_n(E)$*

6.2.1 If an $E^*\phi(E)$ plot of $\phi_n(E)$ shows the same general shape as a similar type plot of $\phi_{tr}(E)$, with $\phi_{tr}(E)$ selected as in Sec. 5.1.1, then $\phi_n(E)$ is likely to represent a good solution. This is usually accompanied by n being small, as mentioned in Sec. 5.4. If $\phi_n(E)$ exhibits a shape very much unlike ϕ_{tr}, the user must examine the $\Delta_o(x)$ (given by the SAND II printout) for spurious values of $\Delta_o(x)$, and, therefore, $R_m(x)$. Any spurious value is rejected and the SAND II code is rerun without this foil. On the other hand, when more than one foil in a given energy region of $E_t(x)$ shows a large positive value of $\Delta_o(x)$ and these values agree in sign, the $\phi_{tr}(E)$ must be increased in that region for positive $\Delta_o(x)$, and vice versa. In some cases, such as at high threshold energies where $\phi_{tr}(E)$ obtained from a calculation has often been found to be too low, the SAND II code may adjust the spectrum in very few iterations. This happens when the $\Delta_o(x)$ are progressively larger in magnitude with increasing $E_t(x)$ of the foil, and the activations $R_m(x)$ are consistent with a smooth, non-oscillating solution $\phi(E)$ in this region. In this case, the SAND II solution is valid [the code need not be rerun with $\phi_{tr}(E)$ adjusted].

7. Minimum Foil Set

7.1 Table I lists foils that have been successfully used. A 1/v foil is required for the low-energy region. ^{197}Au, cadmium covered, is suggested with appropriate epicadmium self-shielding correction. Use ^{235}U, or possibly ^{239}Pu, in ^{10}B as the "E_t = 10 keV" fission foil, along with ^{237}Np (E_t = 0.5 MeV), ^{238}U (corrected for ^{235}U impurity with the ^{235}U-foil data), ^{115}In, $^{54}Fe(n,p)^{54}Mn$, $^{60}Ni(n,p)^{60}Co$, $^{24}Mg(n,p)^{24}Na$, $^{27}A\ell(n,\alpha)^{24}Na$, and $^{90}Zn(n,2n)^{89}Zr$.

8. Availability of the SAND II Code and Cross-Section Library

8.1 The SAND II program tape, including a large catalog of trial spectra, is available from RSIC. Documentation of the code is also available at RSIC (1).

9. The SAND II Cross-Section Library

9.1 The present cross-section library tape contains an evaluated self-consistent set of cross-section data. This is referred to as the 1974 evaluated cross-section library tape, and constitutes part of this standard. When this tape, or any other foil-activation data, becomes updated, it is understood that these ASTM standard methods will similarly require updating.

10. Precision

10.1 Using the prescriptions outlined above and in the three accompanying ASTM Methods (E XX2, E XX3, and E XX4 mentioned in Sec. 1), both a glory-hole spectrum and a spectrum at 50 cm from a GODIVA-type reactor were measured (2,3) by two different experimental groups in an effort at evaluating the reproducibility of the method. Using different foil packets, but the same types of threshold foils, both spectra agreed within less than 2 percent in terms of the hardness parameter, ϕ_{eq}/ϕ. Different Ge(Li) gamma-ray detectors were used, each being cross calibrated with NBS standard gamma-ray sources having a quoted absolute

accuracy of 2 percent. A standard consisting of an 11-line source mixture was used at both laboratories, indicating the precision of NBS standard-source intensities is 1 percent for the 11 lines. Assuming the prescriptions in these ASTM standard methods are carefully followed, a precision of 10 percent should be easily achievable in ϕ_{eq}/ϕ, and 5 percent highly probable with additional work [such as checking activation ratios against those of similar spectra found in the literature (2) to help diagnose erratic foil activations].

11. Accuracy

11.1 The accuracy is specified here in terms of the 1-MeV equivalent flux, ϕ_{eq}, and the hardness parameter, ϕ_{eq}/ϕ. It was determined in a study wherein three different types of reactor spectra were measured (2). These spectra were found to belong to a parametric set, wherein they can be approximated by a GODIVA spectrum with 1/E tail fitted according to the degree of moderation present [see Sec. 6.1.1, selecting $\phi_{tr}(E)$]. The accuracy evaluation presented here is limited to spectra belonging to this set, which probably covers all reactor spectra used for silicon radiation damage studies. For other spectra, such as spectra deep in a reactor shield or well-moderated 14-MeV sources, additional studies are required.

11.2 *Comparison With Known Spectra*

11.2.1 The SAND II results, as obtained with $\phi_{tr}(E)$ generated according to Sec. 6.1.1, agreed with calculated values of $\phi(E)$ within better than 3 percent in ϕ_{eq}/ϕ. The calculations were verified by accurate time-of-flight measurements (2). In addition, the SAND II unfolding was carried out using the calculated $\phi(E)$ as the trial spectrum, ϕ_{tr}. In this case, the SAND II result agreed with the calculated spectrum to within ~1 percent in ϕ_{eq}/ϕ, indicating that the threshold-foil data were consistent with the calculation. This and other data show that the accuracy is very sensitive to the choice of $\phi_{tr}(E)$, especially for E <1 MeV, where only one useful threshold exists [^{237}Np(n,f)] above 10 keV.

11.2.2 It is not possible to check the accuracy of ϕ_{eq} against calculations without doing more exact calculations, geometrically, and more absolute flux monitoring.

11.3 *Sensitivity to Unfolding Method*

11.3.1 A reactor spectrum was unfolded with both the SAND II and the SPECTRA [also available at RSIC (1)] codes. The results agreed within 2 percent in ϕ_{eq}/ϕ, and 3 percent in ϕ_{eq}, indicating that the choice of codes is not a major factor. Most of the difference came from some spurious structure in the SPECTRA solution that is relatively suppressed in the SAND II method.

11.4 *Variational Studies on $\sigma_x(E)$ and $R_m(x)$*

11.4.1 The SAND II unfolding of a GODIVA-type spectrum was carried out by varying the input activations of individual foils, $R_m(x)$, and of pairs of foils (2). This simulates a bodily shift (or renormalization) in the cross-section curve, $\sigma_x(E)$. The results showed that for the spectrum at 50 cm from a GODIVA-type reactor, which was 165 cm above a concrete floor, a variation of 25 percent in the activation of any one foil with threshold below 2 MeV, where few thresholds exist, resulted in ≈2 percent increase of ϕ_{eq}/ϕ. For foils with thresholds between 2 and 6.5 MeV, where the neutron flux is high and many thresholds exist, a 25 percent change in $\sigma_x(E)$ of any single foil produced a 1 percent change in ϕ_{eq}/ϕ. Above 6.5 MeV, where the neutron flux is very low, the corresponding sensitivity was 0.5 percent for one foil. With two values of $\sigma_x(E)$ varied by 25 percent, ϕ_{eq}/ϕ changed by as much as 4 percent in one case [+25 percent for $^{238}U(n,f)$ and -25 percent for $^{24}Mg(n,p)$], and 2 percent in another (+25 percent for both ^{238}U and ^{24}Mg). A total of nine foils was used [$^{58}Ni(n,p)$, $^{24}Mg(n,p)$, $^{127}I(n,2n)$, $^{56}Fe(n,p)$, $^{239}Pu(n,f)$, $^{238}U(n,f)$, $^{235}U(n,f)$, $^{197}Au(n,\gamma)$, in Cd, and $^{237}Np(n,f)$].

11.4.2 The variations in ϕ_{eq} were appreciably greater than the corresponding variations in ϕ_{eq}/ϕ. They were $\Delta\phi_{eq}$ = +12 percent for the ^{239}Pu foil, 2.7 percent for ^{238}U, and <0.5 percent for foils with thresholds above 2 MeV. The ^{238}U and ^{24}Mg foils produced a 2 percent increase in ϕ_{eq} when both were raised by 25 percent, but ϕ_{eq} changed only 0.3 percent when the ^{238}U activation was increased 25 percent and the ^{24}Mg foil decreased by the same amount. The large sensitivity to changes in ^{239}Pu (or, similarly ^{235}U) activation (or cross section) arises from this being the foil with

the greatest sensitivity to neutrons between 0.01-MeV and the 0.5-MeV threshold of ^{237}Np. Fortunately, a cross-section data for fission foils such as ^{239}Pu and ^{235}U are accurately known, and a 25 percent uncertainty in either the cross section, or, equivalently, the foil count, is excessively large. Also, the specific activations are considerably greater than for the other fission foils, and are thus more accurately determined.

11.5 *Overall Accuracy Assessment*

11.5.1 The probable accuracy in ϕ_{eq} and ϕ_{eq}/ϕ, as estimated from the three contributing factors discussed above, is 10 percent for reactor spectra if the prescriptions outlined in these methods are carefully followed. An accuracy of 5 to 7 percent may be achievable with added effort, such as comparing activation ratios to those for similar spectra presented in the literature (2) to help detect erroneous values.

11.5.2 Other types of spectra, such as 14-MeV neutrons with considerable moderation, should be capable of equal or better accuracy, because foils with many threshold values E_t are available that cover the energy regions of high flux above 1 MeV. However, a complete assessment should be made, and must include accurate calculations of spectra in order to provide $\phi_{tr}(E)$ that contains all the physical neutron-transport characteristics (i.e., 14-MeV spike, slowing-down component, resonance "dips", and a fission-source term plus 1/E fail for neutron-multiplying media).

TABLE I Activation Foils (1.27 cm diameter)

Reaction	E_t (MeV)	E_γ (keV)	Gamma/Reaction (Fission Yield)	$T_{1/2}$	Foil Mass (g)	Isotopic Abundance (percent)	Notes
$^{197}Au(n,\gamma)^{198}Au$	0	412	0.95	2.696^{d}	0.056	100	a
$^{59}Co(n,\gamma)^{60}Co$	0	1173 1333	1.00 1.00	5.258^{y}	0.057	100	a,b
$^{55}Mn(n,\gamma)^{56}Mn$	0	847 1811	0.99 0.29	2.58^{h}	0.030	100	a,b
$^{235}U(n,f)^{140}La$	0(0.01)[i]	1593	0.96 (6.29)	40.23^{h}	0.281	100	a,c
$^{239}Pu(n,f)^{140}La$	0(0.01)[i]	1593	0.96 (5.24)	40.23^{h}	0.150	100	a,c
$^{237}Np(n,f)^{140}La$	0.5	1593	0.96 (5.69)	40.23^{h}	0.580	100	a,c
$^{237}Np(n,f)^{97}Zr$	0.5	743	0.92 (6.01)	16.8^{h}	0.580	100	a,d
$^{115}In(n,n')^{115m}In$	1.0	335	0.50	4.50^{h}	0.255	95.7	
$^{238}U(n,f)^{140}La$	1.45	1593	0.96 (6.02)	40.23^{h}	0.495	100	a,c
$^{232}Th(n,f)^{140}Ba$	1.75	537	0.256 (7.91)	12.8^{d}	1.066	100	a,e
$^{237}Th(n,f)^{97}Zr$	1.75	743	0.92 (4.12)	16.8^{h}	1.066	100	a,d
$^{54}Fe(n,p)^{54}Mn$	2.20	835	1.00	303^{d}	0.142	5.82	
$^{58}Ni(n,p)^{58}Co$	2.9	810	0.99	71.3^{d}	0.282	67.8	
$^{32}S(n,p)^{32}P$	2.9	betas	1.00β	14.3^{d}	4.10	95.0	h

(Continued)

TABLE I (Continued)

Reaction	E_t (MeV)	E_γ (keV)	Gamma/Reaction (Fission Yield)	$T_{1/2}$	Foil Mass (g)	Isotopic Abundance (percent)	Notes
$^{24}Mg(n,p)^{24}Na$	6.3	1369	1.00	15.0[h]	0.030	79	a
$^{56}Fe(n,p)^{56}Mn$	7.5	847 1811	0.99 0.29	2.58[h]	0.142	91.7	a,f
$^{27}Al(n,\alpha)^{24}Na$	8.7	1369	1.00	15.0[h]	0.257	100	a
$^{127}I(n,2n)^{126}I$	11.0	386 667	0.34 0.33	13.05[d]	0.657	100	
$^{90}Zr(n,2n)^{89}Zr$	14	910	0.99	78.4[h]	0.108	51.5	

[a] Cd cover 0.05 to 0.10 cm thick.

[b] Use ^{59}Co instead of ^{197}Au and ^{55}Mn for very long irradiations.

[c] 40.23-hour daughter of 12.80 day ^{140}B. Wait five days for maximum decay rate (ASTM E 393).

[d] Use ^{97}Zr for low fluence (3×10^{11} to 3×10^{12} n/cm^2). Use peak shape analysis or measure twice, seven days apart, to strip off 740 keV ^{99}Mo gamma ray ($T_{1/2}$ = 67 hrs).

[e] ^{232}Th radioactivity interferes with ^{140}La line.

[f] Maximum Mn impurity = 0.001 percent, Cd covered. Omit $^{56}Fe(n,p)^{56}Mn$ for long irradiations.

[g] Fission yields are for bombardment with fission-spectrum neutrons. For thermal and 14 MeV, (see Ref. 5).

[h] Requires separate detector, and calibration technique is complex.

[i] E_t = 0.01 MeV with ^{10}B sphere [important for soft (TRIGA) spectra where $\phi(E) < 0.01$ will otherwise dominate]. When ^{235}U or ^{239}Pu foil is ^{10}B covered, also cover ^{235}U and ^{237}Np foils so that accurate corrections can be made for ^{235}U and ^{239}Pu impurities in these high E_t foils.

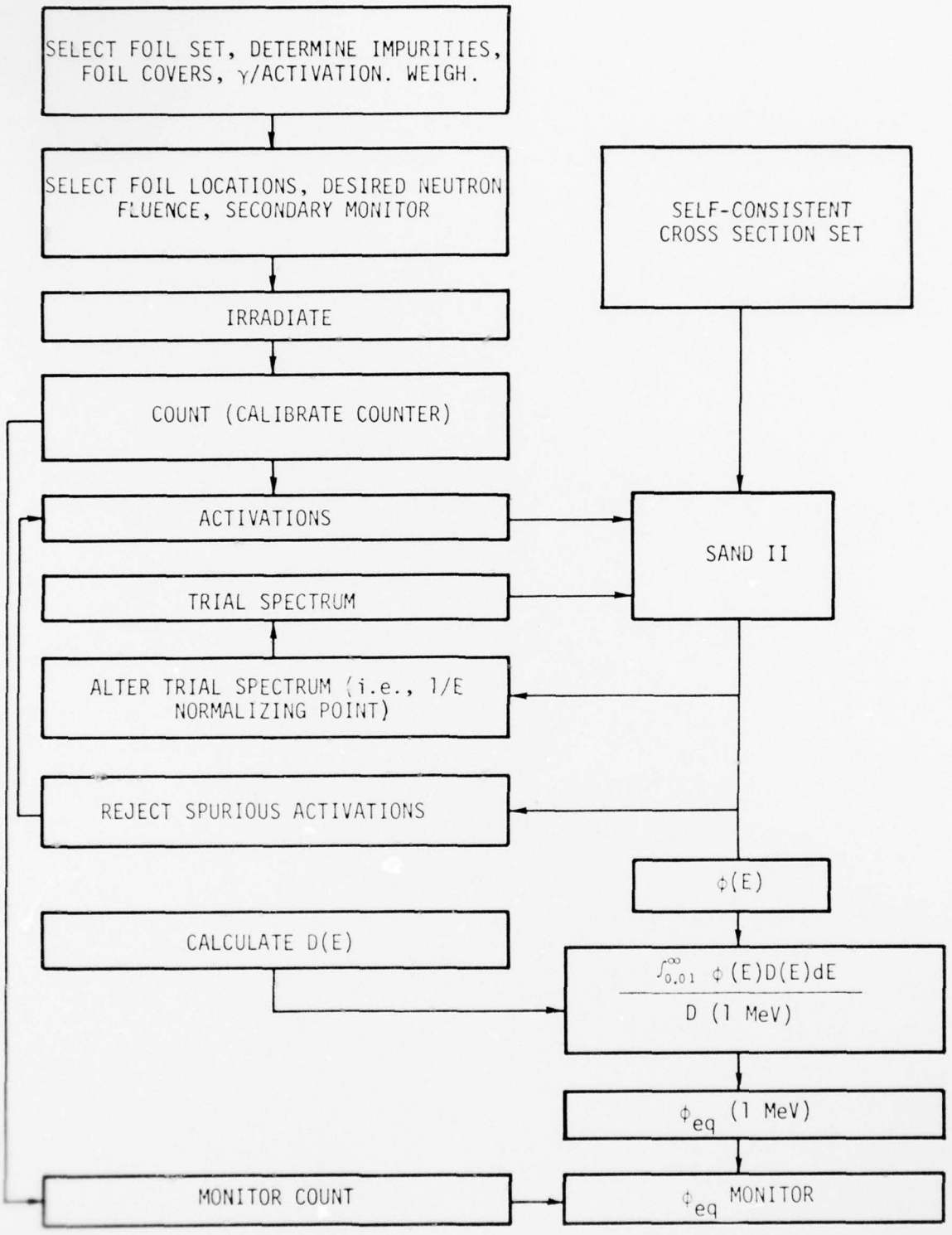

RT-12645

FIG. 1 Flow Chart for Measuring $\phi(E)$ and Calculating ϕ_{eq} and ϕ_{eq}/Monitor

References

(1) RSIC (Radiation Shielding Information Center), Oak Ridge National Laboratory, Oak Ridge, Tennessee.

(2) Verbinski, V. V., Lurie, N. A., and Rogers, V. C., "Threshold-Foil Measurements of Reactor Spectra for Radiation Damage Applications," (submitted for publication in Nucl. Sci. Eng.).

(3) Meason, J., Wright, H., Hogan, J., and Harvey, J., "The Neutron Spectral Distribution From a GODIVA-Type Critical Assembly," IEEE Trans. Nucl. Sci. NS-22, No. 6, 2330 (1975).

Designation: E XX2

Standard Method for

IRRADIATING A STANDARD SET OF
NEUTRON THRESHOLD ACTIVATION FOILS

1. Scope

1.1 This method describes a procedure for irradiating a standard set of threshold activation foils to be used for neutron spectrum unfolding covered in ASTM Method E XX1, "Standard Method for Unfolding Neutron Spectra." It is intended to be used in conjunction with ASTM Method E XX3, "Measuring Foil Activities for Neutron Spectrum Unfolding," for providing the foil-activation data used as input to the SAND II neutron spectrum unfolding code.

1.2 This method presents a standard set of foils that have been used at many facilities, and describes the flux-uniformity, the neutron self shielding, and flux-depression corrections that need to be considered in choosing the foil thickness, the covers, and the locations of the foils.

1.3 In this method, considerations that apply rather generally to neutron-activation detectors are discussed in ASTM Method E 261, "Measuring Neutron Flux by Radioactivation Techniques."

1.4 Background information on the detailed methods for individual threshold foil detectors of widest use is given in the following ASTM Methods.

E 262	Measuring Thermal Neutron Flux by Radioactivation Techniques
E 263	Measuring Fast-Neutron Flux by Radioactivation of Iron
E 264	Measuring Fast-Neutron Flux by Radioactivation of Nickel
E 265	Measuring Fast-Neutron Flux by Radioactivation of Sulfur
E 266	Measuring Fast-Neutron Flux by Radioactivation of Aluminum

E 343 Fast Neutron Flux by Analysis of Molybdenum-99 Activity from Uranium-238 Fission

E 393 Measuring Fast-Neutron Flux for Analysis for Barium-140 Produced by Uranium-238

E 419 Selection of Neutron Activation Detector Materials.

2. Apparatus

2.1 Precision balance (0.1 mg accuracy).

2.2 Cadmium covers (0.05 to 1 mm thick).

2.3 One-half inch i.d. aluminum "cup" with cover for ^{127}I (as ICH_2CONH_2).

3. Threshold Activation Foils

3.1 *Redundancy*

3.1.1 The set of foils listed in Table I is part of the self-consistent set that resides in the SAND II cross-section library. These foils were selected in an experimental evaluation program (1) in which three different "known" spectra were compared to corresponding threshold-foil spectrometry measurements unfolded with the SAND II code. This set contains two redundant 1/v foils [all three should be exposed, counted, and input to SAND II for a first-pass (ACTIVATION) run to select the average one], and a redundant E_t = 0 fission foil; ^{235}U and ^{239}Pu have very similar cross-section shapes. The ^{235}U foil presents much less of a safety hazard than ^{239}Pu, and is cheaper. It is very useful, when measuring soft (TRIGA) spectra, in determining the correction for the ^{235}U impurity in the ^{238}U foil (readily available with ~400 ppm ^{235}U impurity). Although the ^{32}S foil is widely used as a monitor foil, it is not part of the set because it requires an entirely different counter (for betas) and an involved calibration technique. It has about the same threshold as the $^{58}Ni(n,p)^{58}Co$ foil reaction, and should only be used when the Δ_o [the SAND II activation "error" as calculated for $\phi_{tr}(E)$ as input: see ASTM Method E XX1] of the two are within a few percent ($\lesssim$5 percent) of each other; otherwise, SAND II may be driven to many iterations in

trying to find a solution $\phi(E)$ that is compatible with both activations. This usually leads to an unacceptable solution.

3.2 *Foil Impurities*

3.2.1 Foil impurities are especially serious for a moderated source (TRIGA reactor) when the impurity leads to the same reaction product by way of thermal-neutron capture. Some of these foils (impurities) are ^{238}U (^{235}U), ^{27}Al (^{23}Na), ^{56}Fe (^{55}Mn). For a soft spectrum, such as the TRIGA J-tube spectrum (boral shielded), the ^{235}U fissions (Cd covered) were ≈100 times greater than the ^{238}U; therefore, the ^{238}U must have no more than ∿200 ppm of ^{235}U to reduce the error to 2 percent. Higher impurities can be tolerated for GODIVA-type reactors where the low-energy flux is much less intense, or with TRIGA-type reactors if the ^{235}U foil data are used for correcting the ^{238}U activity. In this case, the percent ^{235}U in ^{238}U must be accurately known. For the $^{56}Fe(n,p)^{56}Mn$ reaction, the ^{55}Mn impurity must be no more than 10 ppm (with Cd cover) for use with a TRIGA spectrum, and 100 ppm at 50 cm from a GODIVA-type reactor (∿2 meters off the concrete floor) for ≤2 percent background from the $^{55}Mn(n,\gamma)^{56}Fe$ reaction. Similarly, a manganese foil (Cd covered) can be used to correct the ^{56}Fe data if the impurity correction is small (≤20 percent of total n,p activation) and the percent Mn in Fe is accurately known.

3.3 *The Influence of Nuclear Data on the Selection of Foils*

3.3.1 Since the total number of interactions must be deduced from the absolute gamma-ray count with good accuracy (say 5 percent per foil), the foils selected must have gamma-ray yields known to a similar accuracy or better. These corrections include conversion-electron production, branching ratio to a given energy level, and fission yield.

3.3.2 The 1593-keV gamma-ray line from ^{140}La produced in ^{232}Th fission is not useful because of interference from ^{232}Th radioactivity. This has often led to the use of the 537-keV line from the ^{140}Ba precursor of ^{140}La, which is listed in the Table of Isotopes (2) as having an intensity of 0.34 gamma per ^{140}Ba decay. A recent evaluation (3) has shown this to be 25.7 percent, which is in much closer agreement with some work of Ref. 1, in which ^{235}U fission yields were compared by way

of four fission-product gamma rays (1593 keV for ^{140}La, 537 keV for ^{140}Ba, 743 keV for ^{97}Zr, and 668 keV for ^{132}I).

3.3.3 The choice of gamma-ray line thus directly influences the accuracy of determining the specific activity produced during the neutron irradiation. It also influences the final choice of foil thickness, in that the selection of a low-energy gamma-ray line may lead to a large gamma-ray self-absorption correction in counting. For example, the ^{232}Th foil of Table I has a maximum attenuation of 22 percent, or an average correction of ∿11 percent, for the 537-keV line. This represents an upper limit for foil thickness. Thus, the gamma scattering, as well as the neutron self shielding discussed below, will influence the foil selection.

3.4 *Foil Encapsulation*

3.4.1 All fission foils should be encapsulated in a hermetically sealed container to avoid oxidation and loss of materials, and for health-hazard requirements. The ^{239}Pu foil, if used instead of the much safer ^{235}U foil, will require special encapsulation and periodic wipes to check for leakage of the material. Copper encapsulation has been found satisfactory for ^{235}U, ^{238}U, ^{237}Np, and ^{232}Th foils. It is made ∿0.1 to 0.25 mm thick at the flat surfaces and is soldered at the periphery.

3.5 *Foil Diameter*

3.5.1 All foils are to be 1.27 cm (0.5 inch) in diameter to simplify foil-size effects in calibrating against point gamma-source standards (see ASTM Method E XX3).

4. Irradiation Procedures

4.1 *Foil Covers*

4.1.1 Cadmium covers of 0.1 cm thickness are prescribed for all fission foils and 1/v detectors, and for detectors such as ^{238}U, ^{56}Fe, ^{60}Ni, and ^{27}Aℓ, where traces of impurities (^{235}U, ^{55}Mn, ^{60}Co, and ^{23}Na) that yield the same reaction product via thermal-neutron capture can lead to unmanageably large corrections. When these corrections are greater than 5 percent, the irradiation should include cadmium-covered foils made of these impurities (^{238}U, ^{55}Mn, ^{60}Co, ^{23}Na, etc.). The corrections can

then be made with good accuracy if the percent impurity in the foil is accurately known. If not, a thermal-neutron activation-analysis type of irradiation will be required. Cadmium foils are not needed in the glory hole of a fast-burst reactor with little or no moderator material (<0.5 g, say) near or inside the cavity.

4.1.2 Covers of ^{10}B are useful on fission foils for the case of measuring a soft TRIGA spectrum, especially if a boral shield is used to surround the irradiation cavity. If the boral shield is a good 4π shield, and if a negligible amount of moderator is contained within the shield, the boral shielding can be properly accounted for by the SAND II unfolding code. In this case, the ^{10}B cover is not as important. The boral thickness is entered for each and every foil, and a 1/E spectrum is entered down to 3×10^{-7} MeV, the cadmium cutoff energy, or lower. If no ^{10}B cover is used, and if the cavity is only partially shielded, it will be difficult to predict the neutron spectrum from 10^{-3} MeV down to $\sim 3 \times 10^{-7}$ MeV, where the cadmium covers become effective. In this case, it is important to place all the 1/v foils, the foils with important 1/v impurities (see above), and all fission foils in a boral "box" or a ^{10}B cover. For best results, a ^{10}B cover of 1 to 1.8 g/cm^2 of (93 percent) ^{10}B is used. This cover thickness is then input to SAND II. In this way, the fraction of activations arising from 3×10^{-7} MeV to 10^{-2} MeV neutrons will be both greatly reduced and more accurately calculated for the SAND II unfolding process. The known spectrum outside the boral (a 1/E spectrum) is used down to 3×10^{-7} MeV or lower.

4.1.3 The ^{10}B covers may be replaced by cadmium covers for up to one meter from a GODIVA-type reactor that is a few meters above the concrete floor, or for the glory hole where no low-energy neutrons are found, and where the ^{10}B covers generally cannot be placed in any case. If the covers are used with a directional source, such as outside the GODIVA reactor, the fission-foil activation will require a correction for scattering by ^{10}B. The correction can either be done experimentally, with pure finite-threshold fission foils (^{237}Np or ^{232}Th) that contain negligible zero-threshold impurities which yield the same gamma-ray lines, or with a

sophisticated calculation that weights each inscattering by the track length through the material. These corrections are the order of 10 percent for a 1.65 g/cm^2 ^{10}B cover and a thin 1/2-inch-diameter fission foil (4).

4.2 *Foil Interferences*

4.2.1 A strong resonance absorber such as a thick ^{235}U foil cannot be placed in front of a 1/v absorber, and thick foils with their covers should not be stacked so as to result in a large and unmanageable scattering correction. For isotropic flux, the interfering foils should not scatter more than about 10 percent of the flux, as given by the simple hand calculation:

$$\phi = \phi_o \, e^{-\Sigma_t T} \quad , \tag{1}$$

where $\Sigma_t T$ is the sum of the products of the macroscopic total cross sections and thicknesses for those foils that are stacked in front of the deepest foil, i.e.,

$$\Sigma_t T = \Sigma_t(1)\ T_1 + \Sigma_t(2)\ T_2 + \cdots \quad . \tag{2}$$

For a beam geometry, the corresponding "interference" should be no more than ∿4 percent because of the more complex scattering correction.

4.2.1 *Foil Self Shielding*

4.2.1.1 The correction for self shielding is appreciable only for the 0.0025-cm-thick gold foil (with its highly absorbing resonance at ∿5 eV), being about a factor of two for epicadmium neutrons (5,6). The effect on the unfolded spectrum, $\phi(E)$, of varying the gold-foil activation by a factor of two was mostly local, appearing as a dip or bump at the 5-eV resonance, and changing ϕ_{eq} by only 1 percent.

4.3 *Flux Uniformity*

4.3.1 If the foils cannot all be located in the same region, or in a region of uniform flux (as determined from symmetry considerations), they can be spread out over a larger volume of varying flux but of constant neutron-spectrum shape. If the flux varies by more than 3 percent

from point to point, flux monitors should be used at the various cases. Around a GODIVA-type reactor, thick sulfur foils can be located near individual foils. Where space is more limited, thin nickel [$^{58}Ni(n,p)^{58}Co$], iron [$^{54}Fe(n,p)^{54}Mn$], or even aluminum [$^{27}Al(n,)^{24}Na$], monitors can be used; considerations discussed in ASTM Method E 261 apply.

4.4 *Flux Depression*

4.4.1 At low energies, flux depression is important for bare thermal-neutron detectors near cadmium-covered discs, if both are embedded in a moderator. At high energies, it is important for the same situation if the moderator contains reactor fuel. However, in sizeable cavities used for radiation damage studies, the cadmium covers, as well as the foils, generally subtend a negligibly small solid angle at the point of any surrounding moderator or fuel. For a GODIVA reactor glory hole, the foil-interference considerations discussed in Sec. 4.2 will completely dominate.

5. Foil Weighing

5.1 All foils should be weighed with a 0.1-mg precision balance that is checked against known weights over the range of the foil masses. The encapsulated foils are, of course, carefully weighed before encapsulation.

6. Purity Certification

6.1 The foil purity analysis results must be kept on permanent record for use in making foil impurity corrections. These impurities must be known to an accuracy dictated by the magnitude of the correction, which, in turn, will depend on the kind of neutron spectrum being measured (see Sec. 3.2). If, for example, the percentage impurity (say 400 ppm ^{235}U in ^{238}U) is known to an accuracy of 10 percent in a foil, and the separate impurity foil (^{235}U) is irradiated the same way as the other, then the impurity effect can be reduced to 10 percent of its stated value (40 ppm ^{235}U in ^{238}U, for this example) by calculating the correction. In this case, up to 2000 ppm of ^{235}U impurity could be tolerated for a TRIGA spectrum (see Sec. 3.2).

7. Precision

7.1 Foil weighing, neutron self shielding, and flux uniformity influence the precision of those aspects of the flux measurement to which this method is addressed. An estimated value of 3 percent is suggested as the effects of these corrections on the measurement of specific activities, assuming the scattering of the stack is kept to less than 10 percent for an isotropic flux, and to less than 4 percent for a directed flux. Assuming no thick ^{10}B covers are used in the directed-flux case, and secondary monitors such as thin $^{58}Ni(n,p)^{58}Co$ reaction foils are used when the foils are widely distributed in space, these factors will have only about a 1 percent effect on ϕ_{eq}.

8. Accuracy

8.1 The factors that affect the precision (see Sec. 7) will directly impact the accuracy. In addition, the selection of the foils and the gamma-ray line to be measured for each foil impact the accuracy by way of the uncertainties in gamma-ray intensity (gamma/reaction) and fission yield. These may be as large as 10 percent in individual cases, but should, on the average, contribute no more than 5 percent to the uncertainty in the specific activations. Assuming a reasonable amount of foil-to-foil randomness in this error, the contribution to the uncertainty of specifying ϕ_{eq} is estimated to be no more than 2 to 3 percent.

References

(1) Verbinski, V. V., Lurie, N. A., and Rogers, V. C., "Threshold-Foil Measurements of Reactor Spectra for Radiation Damage Applications" submitted for publication in *Nuclear Science and Engineering*.

(2) Lederer, C. M., Hollander, J. M., and Perlman, I., Table of Isotopes, John Wiley & Sons, Inc., New York, 6th Edition, 1967.

(3) Harvey, J. T., Meason, J. L., Hogan, J. C., and Wright, H. L., "Gamma-Ray Intensities for the Radioactive Decay of ^{140}Ba and ^{140}La," *Nuclear Science and Engineering* 58, 431 (1975).

(4) Wright, H. L., Applied Sciences Division, White Sands Missile Range, New Mexico 88002 (private communication).

(5) ANL 5800, Reactor Physics Constants, Argonne National Laboratory, Argonne, Illinois 60439, Feb. 1969.

(6) Sanford, G. S., and Secksinger, J. H., "Thickness Corrections for Neutron-Activated Gold Foils," ANL-7545, Argonne National Laboratory, Argonne, Illinois 60439.

(7) *Proceedings of the Consultants' Meeting on Nuclear Data for Reactor Neutron Dosimetry,* INDC(NDS)-56/U, IAEA, Vienna, September 10-12, 1973.

(8) Meek, M. E., and Rider, B. F., "Compilation of Fission Product Yields," NEDO-12154-1, Vallecitos Nuclear Center, Pleasanton, California 94566.

TABLE I Activation Foils (1.27 cm diameter)

Reaction	E_t (MeV)	E_γ (keV)	Gamma/Reaction (Fission Yield)	$T_{1/2}$	Foil Mass (g)	Isotopic Abundance (percent)	Notes
$^{197}Au(n,\gamma)^{198}Au$	0	412	0.95	2.696[d]	0.056	100	a
$^{59}Co(n,\gamma)^{60}Co$	0	1173 1333	1.00 1.00	5.258[y]	0.057	100	a,b
$^{55}Mn(n,\gamma)^{56}Mn$	0	847 1811	0.99 0.29	2.58[h]	0.030	100	a,b
$^{235}U(n,f)^{140}La$	0(0.01)[i]	1593	0.96 (6.29)	40.23[h]	0.281	100	a,c
$^{239}Pu(n,f)^{140}La$	0(0.01)[i]	1593	0.96 (5.24)	40.23[h]	0.150	100	a,c
$^{237}Np(n,f)^{140}La$	0.5	1593	0.96 (5.69)	40.23[h]	0.580	100	a,c
$^{237}Np(n,f)^{97}Zr$	0.5	743	0.92 (6.01)	16.8[h]	0.580	100	a,d
$^{115}In(n,n')^{115m}In$	1.0	335	0.50	4.50[h]	0.255	95.7	
$^{238}U(n,f)^{140}La$	1.45	1593	0.96 (6.02)	40.23[h]	0.495	100	a,c
$^{232}Th(n,f)^{140}Ba$	1.75	537	0.256 (7.91)	12.8[d]	1.066	100	a,e
$^{237}Th(n,f)^{97}Zr$	1.75	743	0.92 (4.12)	16.8[h]	1.066	100	a,d
$^{54}Fe(n,p)^{54}Mn$	2.20	835	1.00	303[d]	0.142	5.82	
$^{58}Ni(n,p)^{58}Co$	2.9	810	0.99	71.3[d]	0.282	67.8	
$^{32}S(n,p)^{32}P$	2.9	betas	1.008	14.3[d]	4.10	95.0	h

(Continued)

TABLE I (Continued)

Reaction	E_t (MeV)	E_γ (keV)	Gamma/Reaction (Fission Yield)	$T_{1/2}$	Foil Mass (g)	Isotopic Abundance (percent)	Notes
$^{24}Mg(n,p)^{24}Na$	6.3	1369	1.00	15.0 h	0.030	79	a
$^{56}Fe(n,p)^{56}Mn$	7.5	847 1811	0.99 0.29	2.58 h	0.142	91.7	a,f
$^{27}Al(n,\alpha)^{24}Na$	8.7	1369	1.00	15.0 h	0.257	100	a
$^{127}I(n,2n)^{126}I$	11.0	386 667	0.34 0.33	13.05 d	0.657	100	
$^{90}Zr(n,2n)^{89}Zr$	14	910	0.99	78.4 h	0.108	51.5	

[a] Cd cover 0.05 to 0.10 cm thick.

[b] Use ^{59}Co instead of ^{197}Au and ^{55}Mn for very long irradiations.

[c] 40.23-hour daughter of 12.80 day ^{140}B. Wait five days for maximum decay rate (ASTM E 393).

[d] Use ^{97}Zr for low fluence (3×10^{11} to 3×10^{12} n/cm^2). Use peak shape analysis or measure twice, seven days apart, to strip off 740 keV ^{99}Mo gamma ray ($T_{1/2}$ = 67 hrs).

[e] ^{232}Th radioactivity interferes with ^{140}La line.

[f] Maximum Mn impurity = 0.001 percent, Cd covered. Omit $^{56}Fe(n,p)^{56}Mn$ for long irradiations.

[g] Fission yields are for bombardment with fission-spectrum neutrons. For thermal and 14 MeV, (see Ref. 5).

[h] Requires separate detector, and calibration technique is complex.

[i] E_t = 0.01 MeV with ^{10}B sphere [important for soft (TRIGA) spectra where $\phi(E) < 0.01$ will otherwise dominate]. When ^{235}U or ^{239}Pu foil is ^{10}B covered, also cover ^{235}U and ^{237}Np foils so that accurate corrections can be made for ^{235}U and ^{239}Pu impurities in these high E_t foils.

Designation: E XX3

Standard Method for MEASURING FOIL ACTIVITIES

1. Scope

1.1 This method describes a standard procedure for measuring the absolute gamma-ray emission rate from a standard set of neutron threshold-activation foils used in spectrum measurements, and for calculating the specific activity of the foil from the gamma-ray data.

1.1.1 The measuring procedure takes into account corrections for finite foil size and thickness in detector calibration, count rate and pulse-pileup losses, and background measurements for complex decay schemes such as exist in some fission-foil lines.

1.1.2 The data processing takes into account complex background subtraction for fission-foil lines, corrections for irradiation, wait and count times, and corrections for gamma-ray branching ratios, conversion electrons, fission yields, and gamma-ray self absorption in the foils.

1.2 This method is intended to be used in conjunction with ASTM Method E XX2, "Irradiating a Standard Set of Neutron Threshold Activation Foils," for providing the foil-activation input data that are required in unfolding neutron spectra, as described in ASTM Method E XX1, "Unfolding Neutron Spectra." This method is part of the set of draft standards which include ASTM Method E XX4, "Characterizing Neutron Spectra in Terms of 1-MeV Equivalent Fluence for Radiation Damage in Silicon," and ASTM Method E XX5, "Measuring the Relative 1-MeV Silicon-Equivalent Fluence with Fast Neutron Monitors."

1.3 In this method, considerations that apply rather generally to neutron-activation detectors are discussed in ASTM Method E 261, "Measuring Neutron Flux by Radioactivation Techniques," while background information on the detailed methods for the individual threshold-foil detectors of widest use is given in the following ASTM Methods.

AD-A042 276 IRT CORP SAN DIEGO CALIF F/G 18/4
NEUTRON DOSIMETRY STANDARD.(U)
MAR 77 V V VERBINSKI DNA001-74-C-0163
UNCLASSIFIED INTEL-RT-8106-054 DNA-4128F NL

2 OF 2
ADA
042276

END

DATE
FILMED
8-77

E 262	Measuring Thermal Neutron Flux by Radioactivation Techniques
E 263	Measuring Fast-Neutron Flux by Radioactivation of Iron
E 264	Measuring Fast-Neutron Flux by Radioactivation of Nickel
E 265	Measuring Fast-Neutron Flux by Radioactivation of Sulfur
E 266	Measuring Fast-Neutron Flux by Radioactivation of Aluminum
E 343	Fast-Neutron Flux by Analysis of Molybdenum-99 Activity from ^{238}U
E 419	Selection of Neutron Activation Detector Materials.

2. Apparatus

2.1 *Ge(Li) or Intrinsic Germanium Gamma-Ray Detector*

2.1.1 10 percent or greater photopeak efficiency for ^{60}Co, referred to a 3 inch by 3 inch (7.62 cm) diameter NaI(Tℓ) detector, both at 25 cm from source. Multichannel analyzer, about 4000 channels total, 100 mHz or faster, 2 to 2.5 keV resolution. Precision tail-pulser, ∿60 cps, with inputs to gamma-ray detector preamplifier and to scaler.

2.2 *Foil and Source Holders*

2.2.1 For accurately positioning (and measuring) the center of each foil, and the center of the gamma-ray standard. Required precision is ∿0.2 mm or better in distance from face of detector, and 0.5 mm or better in lateral alignment. The apparatus must have provision for inserting a 1.27-cm-thick lead shield (see Sec. 2.3).

2.3 *Lead Slab*

2.3.1 A lead slab 1.27 cm thick, positionable against Ge(Li) or intrinsic germanium cryostat (flat face).

2.4 *NBS 11-Line Gamma-Ray Standard*

2.4.1 A NBS 11-line gamma-ray standard, less than one year old.

3. Detector Calibration

3.1 The detector must be calibrated to give the correct efficiency for gamma rays emitted from a 1.27-cm-diameter source, using a smaller diameter source as a standard. This is accomplished by measuring the count rate under each peak of the standard, first near the face of the detector cryostat, and then 10 cm farther back.

3.2 This measurement is made at both places with the 11-line NBS gamma-ray source. This gives the efficiency $\varepsilon(x)$ at some unknown distance x from the effective center of the detector, and $\varepsilon(10 + x)$ at 10 cm + x. (At 10 cm, the 1.27-cm-diameter foil size leads to a correction of <2 percent, as compared to the source which is ∿0.5 cm diameter.) Plot the efficiency at each position on log-log plotting paper and read off the efficiency at each position for an energy E_γ corresponding to one of the hottest foils, say $^{197}Au(n,)^{198}Au$ (412 keV), and calculate the ratio $R_{cal} = \varepsilon(x)/\varepsilon(10+x)$. Repeat the measurement at both positions with the gold foil and get R_{gold}. Multiply the $\varepsilon(x)$ by R_{gold}/R_{cal} to get the correct efficiency for a 1.27-cm-diameter foil at x. Repeat the procedure for one or two higher gamma-ray energies with another hot foil (say ^{56}Mn with gamma-ray lines at 847 and 1881 keV). Now slide the $\varepsilon(x)$ curve, as measured with the 11-line standard, to pass through these three corrected points. This represents the proper efficiency curve for a 1.27-cm-diameter foil at the distance x from detector "center."

3.3 From count-rate measurements at x and 10+x, it was found that the effective center of a particular 13 percent Ge(Li) gamma-ray detector (1) is 2.1 cm from the front face of the cryostat. Thus, the center of the standard source and of all the foils (the center being at half the foil thickness) must be located to within 0.2 mm to keep the positioning uncertainty down to 2%.

3.4 The above same calibration must be repeated for the ^{237}Np source behind the 1.27-cm lead shield.

3.5 A simpler approach can be used if the true axis of the detector is located. A careful measurement and x-y plot of count rate versus position at the cryostat face will accomplish this. The point source is

then simply moved off axis, 0.7 of the way to the periphery of the 1.27-cm-diameter foil. The efficiency measured here is approximately the area-weighted efficiency over the 1.27-cm-diameter foil.

4. *Counting Procedure and Area Analysis*

4.1 Set the amplifier gain so that 2 MeV corresponds to 4000 channels on the analyzer, and the 1-MeV point at about 2000 channels so that the zero-channel offset is small. Set the precision pulser so that it falls at ∿1.9 to 1.95 MeV, well above the ^{56}Mn 1811-keV line. Place the foil in the counting position. Run the analyzer on clock time with the pulser running. The ratio of the pulser events appearing in the peak at ∿1.9 to 1.95 MeV to the pulses generated gives the correction for the combination of analyzer deadtime and pulse-pileup losses from the peak. The analyzer can be run on live time instead, but in this case the true clock time must be measured. Alternatively, the pulser events can be counted with a scaler, care being taken that the analyzer and scaler are turned on and off together.

4.2 The peak analysis routine must be the same for pulses from the pulser as for those from both calibration and foil events. In one method, the counts are plotted for the peak and the nearby region (∿5 keV or more on each side). By fitting a straight line through the baseline, the baseline area can be subtracted from the peak area. In counting fission foils, the peak shape must be examined carefully for the presence of a very close neighboring peak, in which case peak-shape analysis must be used. The counting statistics must be very good for the peak-shape analysis to be accurate. The analysis can either be done by hand, or with the SAMPO code (2). The analyzer should be run, whenever possible, until the peak area is 10,000 counts or greater.

5. Backgrounds

5.1 *Room Background*

5.1.1 This must be kept to a minimum by selecting a low-background counting area, stacking a lead shield of at least 5-cm thickness around the detector, and moving away all sources not being counted. A room-background run is taken and is definitely required for long (overnight) counts, such as for the ^{90}Zr(n,2n)^{89}Zr reaction, which has a threshold

energy E_t at about 14 MeV, and consequently, a low specific activity, or for $^{60}Ni(n,p)^{60}Co$, where the half-life is very long.

5.2 *Fission-Foil Background*

5.2.1 Fission-foil backgrounds must be carefully measured because the foils are radioactive with a very complex gamma-ray emission spectrum, and because they are reused due to their high replacement cost. If they had been irradiated within several half-lives before the next planned irradiation (of at least the same or higher fluence), the background should be measured more than once to separate out the normal line [537, 745, or 1593 keV (see Table I)], with relatively short half-life, from any long-lived radioactivity contribution due to natural radioactivity (or to other fission fragments). The background peak area that will still be present during the counting time after the next irradiation is then calculated by adding the time-dependent area of the gamma-ray line with known half-life to that of the steady-state component.

6. Data Analysis

6.1 Correct the peak areas for analyzer deadtime losses and pulse-pileup losses by multiplying the area by the ratio of the number of precision pulses generated during the counting period to the number found in the pulser peak at ∿1.9 MeV. Divide by detector efficiency, gamma-ray intensity (gamma/reaction, Table I), and fission yield (for fission foils). Correct for gamma-ray self absorption by using the approximate expression

$$\phi_o = \phi e^{+\Sigma_t (M/2)} \qquad (1)$$

where ϕ is the measured activation decay rate at the time of counting, ϕ_o the corrected activation, Σ_t the macroscopic gamma-ray total cross section (cm^2/g), and M the thickness (g/cm^2) of the foil and encapsulation material. Equation (1) is accurate to ∿1 percent in ϕ_o for $\phi_o/\phi < 1.2$. The number N of atoms made radioactive by the neutron irradiation is then given by:

$$N = \frac{1}{\lambda} \frac{\dot{N}\, e^{\lambda t(w)} \left[1-e^{-\lambda t(i)}\right]^{-1} \left[1-e^{-\lambda t(c)}\right]^{-1}}{(\gamma/\text{reaction})\ (\text{fission yield})} \quad , \tag{2}$$

where N is the absolute gamma-ray disintegration rate, t(i) the neutron irradiation time, t(w) the wait time between the end of the irradiation interval and the beginning of the counting interval, and t(c) is the duration of the counting interval.

6.2 For the 1593-keV line of ^{140}La ($T_{\frac{1}{2}}$ = 40.23 hours), which is produced by the ^{140}Ba decays ($T_{\frac{1}{2}}$ = 12.8 days), Eq. 3 becomes

$$N_B = \frac{\dot{N}_L\ (\lambda_L-\lambda_B) \left[1-e^{-\lambda_B t(i)}\right]^{-1} \left[1-e^{-\lambda_B t(e)}\right]^{-1}}{\lambda_L\lambda_B\ (\text{fission field}) * 0.96 \left[e^{-\lambda_B t(w)} - e^{-\lambda_L t(w)}\right]} \quad , \tag{3}$$

where N_B, λ_B, and (fission yield) are the number of fissions produced, the decay constant for ^{140}Ba, and the fission yield for ^{140}Ba (see Table I), respectively, $\dot{N}_L$ is the emission rate for the 1593-keV ^{140}La gamma rays, λ_L the decay constant for ^{140}La, and 0.96 is the (γ/reaction) of ^{140}La.

6.3 For wait times of 10 days or more, Eq. 3 reduces to:

$$N_B = \frac{\dot{N}_L * (0.869)\ e^{\lambda_B t(w)} \left[1-e^{-\lambda_B t(i)}\right]^{-1} \left[1-e^{-\lambda_B t(c)}\right]^{-1}}{\lambda_B\ (\text{fission yield}) * 0.96} \quad , \tag{4}$$

with ∿1 percent error at 10 days.

6.4 The value of N (Eqs. 2, 3, or 4) is corrected for any significant neutron self-shielding or flux depression during irradiation, and $R = N/N_o$ (disintegrations per target atom) is computed from the measured target mass and isotopic abundance for the reaction (Table I).

7. Precision

7.1 The precision is limited by the counting statistics, by the reproducibility of the NBS calibration source and of the location of the foils and the standard source with respect to the detector, and by the

reproducibility of the peak-area-analysis routine used for the foil-counting and background measurement.

7.2 A calibration of one NBS 11-line source mix (88-, 122-, 165-, 279-, 392-, 514-, 662-, 898-, 1173-, 1333-, and 1836-keV lines) against another resulted in a standard deviation of 1 percent for the reproducibility of the calibration points. The source location (including source-size correction) leads to a precision uncertainty of ∿3 percent (if a good alignment scheme is employed for both distance and lateral alignment); because of the nearness of the foils to the detector, the weaker foils must be counted next to the face of the detector cryostat. Peak-area analysis and background subtraction are somewhat inseparable. If ∿1 percent or better counting statistics can be achieved, the associated precision is ∿2 percent for non-fission foils and 2 to 5 percent for fission foils, depending on the line chosen, the irradiation fluence, and the magnitude of the background.

7.3 An overall precision of 5 to 6 percent is suggested as the best achievable precision, combining all the above factors. If the 16.8-hour ^{97}Zr line of 743 keV (4) is used for analysis of ^{232}Th and ^{237}Np fission, the error may be much greater, unless shape fitting is utilized and measurements are made at different times to subtract out the effect of the ^{99}Mo gamma-ray line (67 hour), which has nearly the same gamma-ray energy (740 keV).

8. Accuracy

8.1 The accuracy of counting and data analysis reflects directly on the precision (see Sec. 7), and the accuracy of the nuclear data. At this time, it is felt that the uncertainty in the branching ratios of the gamma-ray decay schemes, including the conversion electron coefficient, is ∿5 percent for most cases, and may be as large as 10 percent for some individual cases. The fission yields are probably known to 5 percent. The half-lives are known to 1 percent for most cases, and will not be important except for waiting times of more than 2 to 3 half-lives. An overall accuracy of ∿10 percent is suggested as the value probably achievable for measuring specific activations, after some experience has

been achieved with the source-location and area-analysis schemes and reliable methods have been developed. A value of 15 percent is more likely, and will have about a 5 percent effect on the accuracy of measuring ϕ_{eq} (see ASTM Methods E XX1 and E XX4).

References

(1) Verbinski, V. V., Lurie, N. A., and Rogers, V. C., "Threshold-Foil Measurements of Reactor Spectra for Radiation Damage Applications", submitted to *Nuclear Science and Engineering*.

(2) Routti, J. T., "SAMPO, A Fortran IV Program for Computer Analysis of Gamma Spectra from Ge(Li) Detectors, and Other Spectra with Peaks," UCRL-19452 (1969).

(3) Wright, H. L., Applied Sciences Division, White Sands Missile Range, New Mexico 88002 (private communication).

(4) The value of 743 keV, given in the "Chart of Nuclides" (ERDA, Division of Isotopes Development, 1970) agrees with the measurements of Ref. 1. The value of 747 keV, listed in the "Table of Isotopes" does not (Lederer, C. M., Hollander, J. M., and Perlman, I., John Wiley & Sons, Inc., New York, 1967).

(5) Meek, M. E., and Rider, B. F., "Compilation of Fission Product Yields," NEDO-12154-1, Vallecitos Nuclear Center, Pleasanton, California 94566.

TABLE I (Continued)

Reaction	E_t (MeV)	E_γ (keV)	Gamma/Reaction (Fission Yield)	$T_{1/2}$	Foil Mass (g)	Isotopic Abundance (percent)	Notes
$^{24}Mg(n,p)^{24}Na$	6.3	1369	1.00	15.0 h	0.030	79	a
$^{56}Fe(n,p)^{56}Mn$	7.5	847 1811	0.99 0.29	2.58 h	0.142	91.7	a,f
$^{27}Al(n,\alpha)^{24}Na$	8.7	1369	1.00	15.0 h	0.257	100	a
$^{127}I(n,2n)^{126}I$	11.0	386 667	0.34 0.33	13.05 d	0.657	100	
$^{90}Zr(n,2n)^{89}Zr$	14	910	0.99	78.4 h	0.108	51.5	

[a] Cd cover 0.05 to 0.10 cm thick.

[b] Use ^{59}Co instead of ^{197}Au and ^{55}Mn for very long irradiations.

[c] 40.23-hour daughter of 12.80 day ^{140}B. Wait five days for maximum decay rate (ASTM E 393).

[d] Use ^{97}Zr for low fluence (3×10^{11} to 3×10^{12} n/cm^2). Use peak shape analysis or measure twice, seven days apart, to strip off 740 keV ^{99}Mo gamma ray ($T_{1/2}$ = 67 hrs).

[e] ^{232}Th radioactivity interferes with ^{140}La line.

[f] Maximum Mn impurity = 0.001 percent, Cd covered. Omit $^{56}Fe(n,p)^{56}Mn$ for long irradiations.

[g] Fission yields are for bombardment with fission-spectrum neutrons. For thermal and 14 MeV, (see Ref. 5).

[h] Requires separate detector, and calibration technique is complex.

[i] E_t = 0.01 MeV with ^{10}B sphere [important for soft (TRIGA) spectra where $\phi(E) < 0.01$ will otherwise dominate]. When ^{235}U or ^{239}Pu foil is ^{10}B covered, also cover ^{235}U and ^{237}Np foils so that accurate corrections can be made for ^{235}U and ^{239}Pu impurities in these high E_t foils.

TABLE I Activation Foils (1.27 cm diameter)

Reaction	E_t (MeV)	E_γ (keV)	Gamma/Reaction (Fission Yield)	$T_{1/2}$	Foil Mass (g)	Isotopic Abundance (percent)	Notes
$^{197}Au(n,\gamma)^{198}Au$	0	412	0.95	2.696^{d}	0.056	100	a
$^{59}Co(n,\gamma)^{60}Co$	0	1173 1333	1.00 1.00	5.258^{y}	0.057	100	a,b
$^{55}Mn(n,\gamma)^{56}Mn$	0	847 1811	0.99 0.29	2.58^{h}	0.030	100	a,b
$^{235}U(n,f)^{140}La$	$0(0.01)^{i}$	1593	0.96 (6.29)	40.23^{h}	0.281	100	a,c
$^{239}Pu(n,f)^{140}La$	$0(0.01)^{i}$	1593	0.96 (5.24)	40.23^{h}	0.150	100	a,c
$^{237}Np(n,f)^{140}La$	0.5	1593	0.96 (5.69)	40.23^{h}	0.580	100	a,c
$^{237}Np(n,f)^{97}Zr$	0.5	743	0.92 (6.01)	16.8^{h}	0.580	100	a,d
$^{115}In(n,n')^{115m}In$	1.0	335	0.50	4.50^{h}	0.255	95.7	
$^{238}U(n,f)^{140}La$	1.45	1593	0.96 (6.02)	40.23^{h}	0.495	100	a,c
$^{232}Th(n,f)^{140}Ba$	1.75	537	0.256 (7.91)	12.8^{d}	1.066	100	a,e
$^{237}Th(n,f)^{97}Zr$	1.75	743	0.92 (4.12)	16.8^{h}	1.066	100	a,d
$^{54}Fe(n,p)^{54}Mn$	2.20	835	1.00	303^{d}	0.142	5.82	
$^{58}Ni(n,p)^{58}Co$	2.9	810	0.99	71.3^{d}	0.282	67.8	
$^{32}S(n,p)^{32}P$	2.9	betas	1.00β	14.3^{d}	4.10	95.0	h

(Continued)

Designation: E XX4

Standard Method for

CHARACTERIZING NEUTRON SPECTRA IN TERMS OF 1-MeV EQUIVALENT FLUENCE FOR RADIATION DAMAGE IN SILICON

1. Scope

1.1 This method describes a standard procedure for characterizing a neutron field with spectrum $\phi(E)$ in terms of the ϕ_{eq}, the fluence of neutrons near 1 MeV required to produce the same radiation damage in some material x where the radiation damage function $D_x(E)$ is known.

1.2 This method describes a standard procedure for characterizing the shape of a neutron spectrum $\phi(E)$ in terms of the hardness parameter, ϕ_{eq}/ϕ. It is defined as the fluence of neutrons near 1 MeV required to produce the same radiation damage as one unit of fluence of neutrons of spectral distribution $\phi(E)$.

1.3 Although these standard procedures are applicable to characterizing the spectrum in terms of radiation damage to any material x where $D_x(E)$ is known, the prescriptions outlined here address themselves specifically to radiation damage in silicon; the damage function for silicon, $D_{Si}(E)$, is rapidly varying near 1 MeV. This method consequently prescribes alternative definitions for ϕ_{eq} (silicon).

1.4 This method is part of a set of standards dealing with neutron spectrometry, and is intended to serve as a means of characterizing different neutron spectra, $\phi(E)$, used in radiation damage studies and parts testing of electronic components. A standard method of deducing $\phi(E)$ by unfolding neutron threshold-foil activation data is covered in ASTM Method E XXI, "Standard Method for Unfolding Neutron Spectra." The procedures for selecting, irradiating and counting the foils, the tabulation of some of the required nuclear constants, and the method of calculating specific activations of the foils are presented in ASTM Methods E XX2, "Irradiating a Standard Set of Neutron Threshold Activation Foils," and E XX3, "Measuring Foil Activations." Once ϕ_{eq} and ϕ_{eq}/ϕ have been measured

and calculated, it is important for the user of a neutron irradiation facility to be able to measure ϕ_{eq} for subsequent irradiations. This is covered in ASTM Method E XX5, "Measuring the Relative 1-MeV Silicon-Equivalent Fluence with Fast-Neutron Monitors."

2. Significance

2.1 In neutron radiation damage studies, where the damage is neutron-energy dependent, it is convenient to parameterize a neutron field in terms of a single number called the 1-MeV equivalent fluence, $\phi_{eq} \pm \Delta\phi_{eq}$, which quantifies it by a single number and a standard deivation of that number. In addition, it is useful to assign a radiation-damage quality to a given spectral distribution, a parameter referred to here as the hardness parameter. This hardness parameter is simply ϕ_{eq}/ϕ, or the number of 1-MeV neutrons that produce the same radiation damage as a unit fluence of neutrons having the spectral distribution $\phi(E)$.

3. Summary of Method

3.1 The parameter ϕ_{eq} is defined as

$$\phi_{eq} = \frac{\int_{0.01\ \mathrm{MeV}}^{\infty} \phi(E)\ D(E)dE}{D(1\ \mathrm{MeV})} \quad , \tag{1}$$

where $\phi(E)$ is the spectral distribution of the neutrons and D(E) the radiation damage per unit fluence. D(1 MeV) is taken as the average $\bar{D}$(0.85-1.15 MeV) because D(E) is rapidly varying near 1 MeV. The integral does not include neutrons below 0.01 MeV because even for a soft TRIGA spectrum, less than 1 percent of the damage in bulk silicon is contributed by neutrons below this energy. The 0.01-MeV cutoff greatly simplifies the computation of the hardness parameter, ϕ_{eq}/ϕ:

$$\phi_{eq}/\phi = \frac{\int_{0.01\ \mathrm{MeV}}^{\infty} \phi(E)\ D(E)dE}{D(1\ \mathrm{MeV}) \int_{0.01\ \mathrm{MeV}}^{\infty} \phi(E)dE} \quad . \tag{2}$$

The "neutron count", given by the integral in the denominator of Eq. 2, includes only about half of the epicadmium neutron flux for a TRIGA-type reactor, and inclusion of the entire epicadmium flux would make ϕ_{eq}/ϕ very dependent on neutrons below 0.01 MeV, where almost no damage occurs. If the integral extended down very low energies, to include thermal neutrons, the situation would be much worse. The accurate assessment of the value of ϕ_{eq}/ϕ would then require an accurate measure of neutrons in the thermal region — an unnecessary complication and a great source of meaningless variation of ϕ_{eq}/ϕ, since a small amount of thermal-neutron shielding would change the parameter drastically without changing $\phi(E)$ above 0.01 MeV, where almost all the damage occurs!

4. Calculations

4.1 The output of the SAND II unfolding code is given as a 620-point spectrum, from 10^{-10} to 18 MeV, or 260 points in the region of 0.01 to 18 MeV. A recent calculation of the silicon displacement KERMA, D(E), has been carried out with the latest neutron cross sections for silicon (1,2), and is given at 200 energy points covering roughly the same neutron-energy interval. In folding $\phi(E)$ and D(E), a simple numerical integration is carried out as follows.

$$\int_{0.01}^{18\ \mathrm{MeV}} \phi(E)\ D(E)dE \;=\; \sum_{i=361}^{620} \phi(E_i)\ D(E_i)\Delta E_i \quad , \tag{3}$$

where i = 361 corresponds to E_i = 0.01 MeV of the SAND II output, and the $D(E_i)$ are the values given in Table I for the same energy mesh as the SAND II output above 0.01 MeV. They represent values obtained from the original table (1,2) by interpolation and some group averaging, where necessary.

4.2 The value given by Eq. 3 is divided by D(1 MeV) $\equiv \bar{D}$(0.85-1.15 MeV = 84 MeV $\cdot$mb) to provide ϕ_{eq} as per Eq. 1. ϕ_{eq}/ϕ is calculated by simply carrying the summation

$$\sum_{0.01\ \text{MeV}}^{18\ \text{MeV}} \phi_i \Delta E_i \qquad (4)$$

to obtain

$$\int_{0.01\ \text{MeV}}^{\infty} \phi(E)dE$$

in the denominator of Eq. 2. The error of the simple summation is less than 1 percent for the 620-point spectrum that vanishes at the upper limit of integration (18 MeV).

5. Problems

5.1 D(E) is strongly varying near 1 MeV. Its value, as given in Ref. 1, is 102 MeV·mb at 1 MeV, while the average value from 0.85 to 1.15 MeV is 84 MeV·mb. Although this difference does not impact inter-laboratory comparisons of silicon-damage effects if a standard value of D(1 MeV) is made, it leads to an unrealistically small value for ϕ_{eq}/ϕ; a fluence of 0.89 neutrons of 1 MeV becomes equivalent to a unit fluence of GODIVA-type neutrons (50 cm from reactor). The GODIVA 50-cm spectrum is the hardest of three spectra measured in an evaluation program (2) supporting these draft specifications. If, however, $\bar{D}$ (0.85 to 1.15 MeV) is used in Eq. 2 instead of D(1 MeV), the 1-MeV equivalent fluence per unit fluence now becomes 1.06; a much more intuitively meaningful figure for neutrons whose average energy is greater than 1.0 MeV, weighted with a damage function $D_{Si}(E)$ that increases with E.

6. Recommended Definition

6.1 Use $\bar{D}$(0.85 to 1.15 MeV) = 84 MeV·mb as D(1 MeV) in Eqs. 1 and 2.

6.2 Use Table I for $D(E_i)$, where the E_i mesh agrees with that of SAND II.

7. Precision

7.1 The estimated precision in calculating ϕ_{eq} and ϕ_{eq}/ϕ with the present method is appreciably better than 1 percent, assuming $\phi(E)$ and D(E) are exact, and that the SAND II 620-point spectrum is used in obtaining the fluence above 0.01 MeV (Eq. 2) (260 points above 0.01 MeV).

8. Accuracy

8.1 The accuracy of the numerical integration is estimated to be better than 1 percent. The accuracy of D(E) can be usefully discussed in three parts.

8.2 *Shape of D(E)*

8.2.1 In the calculation of ϕ_{eq} and ϕ_{eq}/ϕ, only the shape of the D(E) curve is important, as related to interlaboratory comparisons of these quantities, because D(E) appears in both the numerator and denominator of Eqs. 1 and 2. The shape of D(E) is probably known well enough to contribute no more than ~3 to 5 percent to the relative values of ϕ_{eq} and ϕ_{eq}/ϕ obtained for different spectra $\phi(E)$.

8.3 *The Absolute Value of D(E)*

8.3.1 The latest D(E) data (1,2) were obtained with the most recent evaluated cross-section set for silicon, which provides the total energy deposited in Si to an accuracy that would, in itself, impact ϕ_{eq} and ϕ_{eq}/ϕ by no more than a few percent (say 2 to 3 percent) because of its effect on the shape of D(E). However, the calculation of the partition of this energy between ionization and displacement is much less well known. The partition was calculated with the Lindhard theory (3,4), which has not been modified to agree with experimental results (5). Consequently, the D(E) values may change by the order of 10 percent when appropriate adjustments are made to obtain good agreement with past and future measurements.

8.4 *D(1 MeV)*

8.4.1 The value of ϕ_{eq} and ϕ_{eq}/ϕ will vary about 20 percent, depending upon the interval over which $\bar{D}(1\ \text{MeV} \pm \Delta E)$ is averaged. There is a great deal of arbitrariness in the absolute value of ϕ_{eq} and ϕ_{eq}/ϕ in this respect, in that the definition does not influence intercomparisons of these quantities for most reactor-type spectra used in radiation damage

studies. The interval 0.85 to 1.15 MeV was chosen as a compromise between a very wide energy interval, over which $\phi(E)$ may encounter significantly large variations, and a delta function that results in an intuitively low value for ϕ_{eq}/ϕ because of the rapidly varying (and therefore unrepresentative) value of D(E) at or very near 1 MeV (see Discussion, Sec. 5).

References

(1) Rogers, V. C., Harris, Jr., L. Steinman, D. K., and Bryan, D. E. "Silicon Ionization and Displacement KERMA for Neutrons from Thermal to 20 MeV," IEEE Trans. Nucl. Sci. NS-22, No. 6, 2326 (1975), Erratum, ibid. NS-23, No. 1, 875 (1976).

(2) Verbinski, V. V., Lurie, N. A., and Rogers, V. C., "Threshold-Foil Measurements of Reactor Spectra for Radiation Damage Applications," submitted for publication in *Nuclear Science and Engineering*.

(3) Radiation Effects in Semiconductors, edited by F. L. Vook, Plenum Press, New York, 1968 (*Proceedings of the Santa Fe Conference on Radiation Effects in Semiconductors*, October 3-5, 1967).

(4) Lindhard, J., Nielsen, V., Scharff, M., and Thompsen, P. V., *Kgl. Danske Vindenskab, Nat. Fys. Medd.* 33, No. 10 (1963).

(5) van Lint, V. A. J., Mission Research Corporation (private communication).

TABLE I D(E) in MeV·mb (E in MeV)

E	D	E	D	E	D	E	D
1.000-2	1.054	9.600-2	5.356	9.20-1	96.1	5.20+0	193.3
1.050-2	1.086	1.000-1	5.298	9.60-1	104.8	5.30+0	188.1
1.100-2	1.112	1.050-1	5.269	1.00+0	72.5	5.40+0	182.5
1.150-2	1.144	1.100-1	5.182	1.10+0	62.6	5.50+0	176.4
1.200-2	1.164	1.150-1	4.803	1.20+0	44.0	5.60+0	170.6
1.275-2	1.208	1.200-1	4.367	1.30+0	69.9	5.70+0	175.5
1.350-2	1.252	1.275-1	3.784	1.40+0	92.6	5.80+0	181.9
1.425-2	1.287	1.350-1	3.202	1.50+0	98.7	5.90+0	188.6
1.500-2	1.322	1.425-1	2.911	1.60+0	101.9	6.00+0	196.5
1.600-2	1.377	1.500-1	2.911	1.70+0	120.5	6.10+0	189.2
1.700-2	1.429	1.600-1	7.569	1.80+0	96.6	6.20+0	177.6
1.800-2	1.479	1.700-1	16.30	1.90+0	168.8	6.30+0	166.5
1.900-2	1.563	1.800-1	66.95	2.00+0	177.0	6.40+0	155.7
2.000-2	1.572	1.90-1	101.9	2.10+0	184.8	6.50+0	147.3
2.100-2	1.630	2.00-1	105.7	2.20+0	142.6	6.60+0	151.4
2.200-2	1.688	2.10-1	91.1	2.30+0	133.0	6.70+0	155.7
2.300-2	1.747	2.20-1	81.5	2.40+0	154.3	6.80+0	161.0
2.400-2	1.805	2.30-1	71.3	2.50+0	157.2	6.90+0	165.3
2.550-2	1.913	2.40-1	64.6	2.60+0	142.6	7.00+0	170.9
2.700-2	1.965	2.55-1	59.4	2.70+0	157.2	7.10+0	175.0
2.800-2	2.038	2.70-1	55.6	2.80+0	197.9	7.20+0	177.3
3.000-2	2.140	2.80-1	54.4	2.90+0	185.4	7.30+0	179.3
3.200-2	2.212	3.00-1	53.0	3.00+0	142.6	7.40+0	181.1
3.400-2	2.387	3.20-1	52.1	3.10+0	127.5	7.50+0	183.4
3.600-2	2.515	3.40-1	51.5	3.20+0	123.4	7.60+0	183.1
3.800-2	2.678	3.60-1	51.2	3.30+0	118.8	7.70+0	181.4
4.000-2	2.887	3.80-1	52.1	3.40+0	122.3	7.80+0	180.2
4.250-2	3.057	4.00-1	52.7	3.50+0	124.6	7.90+0	178.7
4.500-2	3.348	4.25-1	53.6	3.60+0	123.4	8.00+0	177.3
4.750-2	3.581	4.50-1	54.7	3.70+0	122.6	8.10+0	176.1
5.000-2	3.930	4.75-1	55.6	3.80+0	121.7	8.20+0	175.0
5.250-2	4.221	5.00-1	59.7	3.90+0	121.7	8.30+0	174.7
5.500-2	4.512	5.25-1	80.1	4.00+0	123.1	8.40+0	174.4
5.750-2	5.094	5.50-1	147.0	4.10+0	124.3	8.50+0	173.8
6.000-2	5.706	5.75-1	113.5	4.20+0	129.8	8.60+0	173.2
6.300-2	6.404	6.00-1	61.1	4.30+0	148.5	8.70+0	172.9
6.600-2	6.986	6.30-1	55.0	4.40+0	168.8	8.80+0	173.2
6.900-2	7.248	6.60-1	56.8	4.50+0	180.2	8.90+0	177.3
7.200-2	7.132	6.90-1	59.4	4.60+0	185.4	9.00+0	181.6
7.600-2	6.783	7.20-1	64.6	4.70+0	188.6	9.10+0	186.6
8.000-2	6.462	7.60-1	78.6	4.80+0	192.7	9.20+0	190.4
8.400-2	6.171	8.00-1	92.6	4.90+0	195.0	9.30+0	195.0
8.800-2	5.822	8.40-1	96.0	5.00+0	194.5	9.40+0	198.2
9.200-2	5.560	8.80-1	82.7	5.10+0	193.9	9.50+0	200.3

(Continued)

TABLE I (Continued)

E	D	E	D
9.60+0	199.4	1.41+1	214.8
9.70+0	198.8	1.42+1	214.8
9.80+0	198.0	1.43+1	214.8
9.90+0	197.1	1.44+1	214.8
1.00+1	196.5	1.45+1	215.1
1.01+1	195.6	1.46+1	215.1
1.02+1	195.0	1.47+1	215.1
1.03+1	195.3	1.48+1	215.4
1.04+1	195.6	1.49+1	215.7
1.05+1	196.2	1.50+1	216.3
1.06+1	196.5	1.51+1	216.6
1.07+1	196.8	1.52+1	217.2
1.08+1	197.1	1.53+1	217.5
1.09+1	197.4	1.54+1	218.0
1.10+1	198.0	1.55+1	218.6
1.11+1	199.1	1.56+1	218.9
1.12+1	200.6	1.57+1	219.5
1.13+1	202.0	1.58+1	219.8
1.14+1	203.5	1.59+1	220.1
1.15+1	204.9	1.60+1	220.6
1.16+1	206.4	1.61+1	220.7
1.17+1	207.8	1.62+1	220.7
1.18+1	209.6	1.63+1	220.7
1.19+1	210.5	1.64+1	220.7
1.20+1	210.8	1.65+1	220.9
1.21+1	211.0	1.66+1	220.9
1.22+1	211.6	1.67+1	220.9
1.23+1	211.9	1.68+1	220.9
1.24+1	209.6	1.69+1	221.2
1.25+1	212.5	1.70+1	221.2
1.26+1	212.8	1.71+1	221.2
1.27+1	213.1	1.72+1	221.2
1.28+1	213.4	1.73+1	222.1
1.29+1	213.7	1.74+1	222.7
1.30+1	213.7	1.75+1	223.3
1.31+1	213.7	1.76+1	223.9
1.32+1	214.0	1.77+1	224.4
1.33+1	214.0	1.78+1	224.7
1.34+1	214.2	1.79+1	225.3
1.35+1	214.2	1.80+1	226.2
1.36+1	214.5		
1.37+1	214.5		
1.38+1	214.8		
1.39+1	214.8		
1.40+1	214.8		

Designation: E XX5

Standard Method for

MEASURING THE RELATIVE 1-MeV SILICON EQUIVALENT FLUENCE WITH FAST-NEUTRON MONITORS

1. Scope

1.1 This method describes the measurement of ϕ_{eq}/Monitor, the 1-MeV equivalent neutron fluence per unit monitor count, for a neutron field where the spectrum $\phi(E)$ has been measured and the 1-MeV equivalent fluence for silicon radiation damage has been calculated.

1.2 This method is part of, and follows as a corollary to, the four ASTM methods that are addressed to measuring the neutron spectrum $\phi(E)$, and with it, calculating ϕ_{eq}. These are as follows.

E XX1	Unfolding Neutron Spectra
E XX2	Irradiating a Standard Set of Neutron Threshold Activation Foils
E XX3	Measuring Foil Activities
E XX4	Characterizing Neutron Spectra in Terms of 1-MeV Equivalent Fluence for Radiation Damage in Silicon

2. Significance

2.1 This method is user oriented, in that it is addressed to measuring ϕ_{eq}/Monitor for neutron irradiations subsequent to the one in which $\phi(E)$ was measured. It provides ϕ_{eq}/Monitor for a variety of options, depending on (a) the access to the results of the SAND II code used to deduce $\phi(E)$ from the threshold data, and (b) the availability of the apparatus and facilities required for calibrating various types of monitor foils.

3. Apparatus

3.1 Nickel or iron foils and gamma-ray detector as in ASTM Method E XX3.

3.2 Sulfur foils, beta counter, aluminum foil, Ge(Li) or intrinsic germanium detector, NBS gamma-ray sources (calibration standards), and access to 14-MeV neutron generator.

4. Determining ϕ_{eq} per Unit Monitor Count

4.1 *By Measurement*

4.1.1 During the course of measuring $\phi(E)$ to obtain ϕ_{eq}, a monitor foil may be placed in the same neutron field as the set of threshold activation foils (Position A), or in some more convenient location (Position B), thus obtaining ϕ_{eq}/Monitor directly. Subsequent monitor counts will then predict the absolute flux in Position A in terms of ϕ_{eq} if no shields or nearby moderators or scatterers are changed. Thus, a "retractable" GODIVA-type reactor, calibrated at, say 2 meters above the floor, must be subsequently relocated in height to within ∿0.1 meter if the monitor foils are located at the same distance from the reactor as the irradiation samples (∿50 cm), and within a few centimeters if the monitors are approximately a factor of two nearer (or farther). Scatterers must not be moved to change the flux by more than a few percent. An upper limit on the inscattering effect of any materials, such as sample holders or nearby stands, can be estimated (a) by using a rough average of the total cross section in the vicinity of 1 MeV for reactor neutrons, (b) by assuming isotropic scattering, and (c) by taking into account the flux at the scatterer and the solid angle subtended at the detector. For thick materials such as concrete, a fast neutron albedo of 10 percent can be used.

4.1.2 Most shielding materials in front of either sample or monitor must be kept constant in thickness within ∿2 mm for less than a 5 percent change in flux [2 mm for polyethylene and water (1)].

4.1.3 While 2 or 3 grams of additional moderator alongside a fast neutron monitor will make little difference, a few tenths of a gram of moderator adjacent to the cadmium-covered zero-threshold detectors can be important (i.e., 1/v detectors, and ^{235}U or ^{239}Pu foils).

4.1.4 The monitor is generally chosen with a threshold high enough to make it insensitive to neutrons below ∿0.01 MeV whose contribution to the radiation damage is negligibly small. Sulfur is usually selected because of the high threshold value for the reaction, the convenient half-life of the resultant ^{32}P radioactivity (beta rays), and the ease of purifying sulfur. However, the $^{54}Fe(n,p)^{54}Mn$ or $^{58}Ni(n,p)^{58}Co$ reactions

are preferable if a Ge(Li) or intrinsic germanium detector is available; the absolute activations can then be measured by simply cross calibrating against NBS standard gamma-ray sources, providing the absolute value of $\phi(E)$ if a spectral-shape measurement is available.

4.1.5 The ϕ_{eq}/Monitor may be measured at a different time, if either a reliable secondary monitor is used (such as a fission chamber in a steady-state reactor, or a thermometer in a fast-burst irradiation). If not, one of the threshold foils used in measuring $\phi(E)$ can be placed in Position A, defined above, for calibration during exposures subsequent to measuring $\phi(E)$.

4.2 *By Calculation*

4.2.1 If a standard monitor foil such as sulfur [$^{32}S(n,p)^{32}P$] is not included in the set of foils irradiated to measure $\phi(E)$, then the ^{32}S activation can be calculated with the SAND II code. The code is rerun with a trial value of $R_m(^{32}S)$ added, and $R_m(^{32}S)$ is adjusted until Δ_o (see Method E XXI) becomes zero. If the $^{58}Ni(n,p)^{58}Co$ reaction had been used in determining $\phi(E)$, the ^{32}S activation can be estimated from the resultant ^{58}Co activity. The two reactions have nearly the same threshold, and it was found that $R_m(^{32}S) \cong 0.56\ R_m(^{58}Ni)$ for three different reactor spectra (fast burst reactor glory hole, 50 cm from the FBR, and TRIGA J-tube). Once $R_m(^{32}S)$ is calculated, the sulfur-foil counter must be calibrated in terms of absolute ^{32}P beta-ray activity resulting from the $^{32}S(n,p)^{32}P$ reaction. One such technique utilizes 14-MeV neutrons to irradiate Aℓ and S, the absolute 14-MeV neutron flux (and therefore the absolute ^{32}P activity) being given by the $^{27}Aℓ(n,\alpha)^{24}Na$ reaction. The cross sections for both reactions are accurately known at 14 MeV. Alternatively, a known amount of ^{32}P (NBS source) can be mixed in with a sulfur pellet. This cross calibration of ^{32}S is, of course, unnecessary if the $^{58}Ni(n,p)^{58}Co$ reaction, the $^{54}Fe(n,p)^{54}Mn$ reaction, or some other well-known reaction leading to a gamma-ray emitter is used for monitoring ϕ_{eq}.

5. Precision

5.1 The precision for measuring ϕ_{eq}/Monitor is the combination of the precision of measuring ϕ_{eq} and of measuring the monitor count. The accuracy of measuring ϕ_{eq} is treated in ASTM Method E XX4, and will not be covered here. The precision of measuring the $^{58}Ni(n,p)^{58}Co$ and $^{54}Fe(n,p)^{54}Mn$ activations is about 3 percent if counting statistics and calibration techniques allow. The foil location, the fluence of each irradiation, and the counting times will determine the counting statistics, and these factors are largely subject to the choice of the user. The precision for beta counting of sulfur foils is about the same as for the nickel and iron monitor foils, if the sulfur foils are thick enough to make the count-rate thickness independent. Many of the sulfur counting considerations are discussed in ASTM Method E 265-70, "Measuring Fast-Neutron Flux by Radioactivation of Sulfur."

6. Accuracy

6.1 If ^{58}Ni and ^{54}Fe foils are used, an accuracy of $\sim$5 percent can be achieved on the absolute activation if counting statistics are not a consideration (see Sec. 5). For sulfur monitoring, the accuracy is $\sim$5 percent if the sulfur is exposed simultaneously with the threshold activation foils. If not, and the sulfur activation must be calibrated indirectly, the accuracy is in this case estimated to be 10 percent.

References

(1) Goldstein, Herbert, Fundamental Aspects of Reactor Shielding, Addison-Wesley (1959).

DISTRIBUTION LIST

DEPARTMENT OF DEFENSE

Defense Communication Engineer Center
ATTN: Code R410, James W. McLean

Director
Defense Communications Agency
ATTN: Code 930, Monte I. Burgett, Jr.

Defense Documentation Center
12cy ATTN: TC

Director
Defense Nuclear Agency
ATTN: STVL
ATTN: DDST
ATTN: RAEV
3cy ATTN: STTL, Tech. Library
2cy ATTN: RAEV, Major W. Adams
ATTN: STSI

Director of Defense Research & Engineering
ATTN: DD/S&SS

Commander
Field Command, DNA
ATTN: FCPR

Director
Interservice Nuclear Weapons School
ATTN: Document Control

Director
Joint Strat. Tgt. Planning Staff, JCS
ATTN: JLTW-2

Chief
Livermore Division, Field Command, DNA
ATTN: FCPRL

DEPARTMENT OF THE ARMY

Project Manager
Army Tactical Data Systems
U.S. Army Electronics Command
ATTN: Dwaine B. Huewe

Commander
BMD System Command
ATTN: BDMSC-TEN, Noah J. Hurst

Commander
Frankford Arsenal
ATTN: SARFA-FCD, Marvin Elnick

Commander
Harry Diamond Laboratories
ATTN: DRXDO-EM, R. Bostak
ATTN: DRXDO-RC, Robert B. Oswald, Jr.
ATTN: DRXDO-EM, J. W. Beilfuss
ATTN: DRXDO-EM, Robert E. McCoskey
ATTN: DRXDO-NP, Francis N. Wimenitz
ATTN: DRXDO-TR, Edward E. Conrad
ATTN: DRXDO-RB, Joseph R. Miletta
ATTN: DRXDO-TI, Tech. Library

DEPARTMENT OF THE ARMY (Continued)

Commanding Officer
Night Vision Laboratory
U.S. Army Electronics Command
ATTN: CPT Allan S. Parker

Commander
Picatinny Arsenal
ATTN: SMUPA-ND-N-E
ATTN: SMUPA-ND-W

Commander
Redstone Scientific Information Center
U.S. Army Missile Command
3cy ATTN: Chief, Documents

Secretary of the Army
ATTN: ODUSA or Daniel Willard

Commander
TRASANA
ATTN: ATAA-EAC, Francis N. Winans

Chief
U.S. Army Communications Sys. Agency
ATTN: SCCM-AD-SV, Library

Commander
U.S. Army Electronics Command
ATTN: DRSEL-GG-TD, W. R. Werk
ATTN: DRSEL-TL-IR, Edwin T. Hunter
ATTN: DRSEL-PL-ENV, Hans A. Bomke

Commander-in-Chief
U.S. Army Europe and Seventh Army
ATTN: ODCSE-E AEAGE-PI

Commander
U.S. Army Materiel Dev. & Readiness Command
ATTN: DRCDE-D, Lawrence Flynn

Commander
U.S. Army Missile Command
ATTN: DRCPM-PE-EA, Wallace O. Wagner
ATTN: DRCPM-LCEX, Howard H. Henriksen
ATTN: DRCPM-MDTI, CPT Joe A. Sims
ATTN: DRSMI-RGD, Vic Ruwe

Commander
U.S. Army Mobility Equip. R & D Center
ATTN: AMSEL-NV-SD, J. H. Carter
ATTN: STSFB-MW, John W. Bond, Jr.

Chief
U.S. Army Nuc. and Chemical Surety Gp.
ATTN: MOSG-ND, Maj Sidney W. Winslow

Commander
U.S. Army Nuclear Agency
ATTN: ATCN-W, LTC Leonard A. Sluga

Commander
White Sands Missile Range
ATTN: STEWS-TE-NT Marvin P. Squires

DEPARTMENT OF THE ARMY (Continued)

Commander
U.S. Army Test and Evaluation Command
ATTN: DRSTE-EL, Richard I. Kolchin
ATTN: DRSTE-NB, Russell R. Galasso

Commanding General
U.S. Army Electronics Command
ATTN: DRSEL-TL-I, Robert A. Gerhold

DEPARTMENT OF THE NAVY

Commander
Naval Electronic Systems Command
Naval Electronic Systems Command, Hqs.
ATTN: Code 5032, Charles W. Neill
ATTN: PME 117-21
ATTN: Code 50451
ATTN: Code 504511, Charles R. Suman
ATTN: ELEX 05323, Cleveland F. Watkins
ATTN: Larry W. Sumney

Director
Naval Research Laboratory
ATTN: Code 5210, John E. Davey
ATTN: Code 2627, Doris R. Folen
ATTN: Code 6601, E. Wolicki
ATTN: Code 5216, Harold L. Hughes

Commander
Naval Sea Systems Command
ATTN: SEA-9931, Samuel A. Barham
ATTN: SEA-9931, Riley B. Lane

Commander
Naval Surface Weapons Center
ATTN: Code WA50, John H. Malloy
ATTN: Code 244
ATTN: Code 431, Edwin B. Dean
ATTN: Code WA501, Navy Nuc. Prgms. Off.

Naval Electronics Laboratory
ATTN: Charles E. Holland, Jr.

Commander
Naval Weapons Center
ATTN: Code 533, Tech. Library

Commanding Officer
Naval Weapons Support Center
ATTN: Code 7024, James Ramsey
ATTN: Code 70242, Joseph A. Munarin

Director
Strategic Systems Project Office
ATTN: NSP-27331, Phil Spector
ATTN: NSP-230, David Gold
ATTN: NSP-2342, Richard L. Coleman
ATTN: SP 2701, John W. Pitsenberger

Naval Air Station
ATTN: Charles D. Caposell

DEPARTMENT OF THE AIR FORCE

AF Aero-Propulsion Laboratory, AFSC
ATTN: POE-2, Joseph F. Wise

AF Institute of Technology, AU
ATTN: ENP, Charles J. Bridgman

DEPARTMENT OF THE AIR FORCE (Continued)

AF Materials Laboratory, AFSC
ATTN: LTE

AF Weapons Laboratory, AFSC
ATTN: ELP TREE Section
ATTN: ELA
ATTN: SAS
ATTN: ELP, Capt John G. Tucker
ATTN: SAT
ATTN: SAB
ATTN: SUL

AFTAC
ATTN: TFS, Maj Marion F. Schneider

RADC (ETSD)
ATTN: Even Rooslid

Commander
ASD
ATTN: ASD-YH-EX, Lt Col Robert Leverette

Headquarters
Electronic Systems Division, AFSC
ATTN: DCD/SATIN IV
ATTN: YSEV
ATTN: YWEI

Commander
Foreign Technology Division, AFSC
ATTN: ETET, Capt Richard C. Husemann

Commander
Rome Air Development Center, AFSC
ATTN: RBRP, Jack S. Smith
ATTN: RBRAC, I. L. Krulac
ATTN: R. W. Thomas

SAMSO/DY
ATTN: DYS, Maj Larry A. Darda

AFAL/DHE
ATTN: H. H. Steenberg

SAMSO/IN
ATTN: IND, I. J. Judy

SAMSO/MN
ATTN: MNNH
ATTN: MNNG, Capt David J. Strobel
ATTN: MNNG

SAMSO/RS
ATTN: RSSE, Lt Col Kenneth L. Gilbert

SAMSO/SK
ATTN: SKF, Peter H. Stadler

Commander in Chief
Strategic Air Command
ATTN: NRI-STINFO Library
ATTN: XPFS, Maj Brian G. Stephan

ENERGY RESEARCH AND DEVELOPMENT ADMIN

Sandia Laboratories
ATTN: Doc. Con. for 3141, Sandia Rpt. Coll.
ATTN: Doc. Con. for Org. 2110, J. A. Hood
ATTN: Doc. Con. for Org. 1933, F. N. Coppage

ENERGY RESEARCH AND DEVELOPMENT ADMIN
(Continued)

University of California
Lawrence Livermore Laboratory
ATTN: Tech. Info. Dept. L-3
ATTN: Lawrence Cleland, L-156
ATTN: Hans Kruger, L-96
ATTN: Joseph E. Keller, Jr., L-125

Los Alamos Scientific Laboratory
ATTN: Doc. Con. for J. Arthur Freed

OTHER GOVERNMENT AGENCIES

Department of Commerce
National Bureau of Standards
ATTN: Judson C. French

DEPARTMENT OF DEFENSE CONTRACTORS

Aerojet Electro-Systems Co. Division
Aerojet-General Corporation
ATTN: Thomas D. Hanscome

Aeronutronic Ford Corporation
Aerospace & Communications Ops.
Aeronutronic Division
ATTN: Tech. Info. Section
ATTN: Ken C. Attinger

Aeronutronic Ford Corporation
Western Development Laboratories Division
ATTN: Samuel R. Crawford, M.S. 531

Aerospace Corporation
ATTN: Irving M. Garfunkel
ATTN: J. Benveniste
ATTN: Julian Reinheimer
ATTN: S. P. Bower

Avco Research & Systems Group
ATTN: Research Library, A830, Rm 7201

The BDM Corporation
ATTN: T. H. Neighbors

The Bendix Corporation
Communication Division
ATTN: Document Control

The Bendix Corporation
Research Laboratories Division
ATTN: MGR Program. Dev. Donald J. Niehaus
ATTN: Max Frank

The Bendix Corporation
Navigation and Control Division
ATTN: George Gartner

Bell Telephone Laboratories
ATTN: G. E. Smith

The Boeing Company
ATTN: David L. Dye, M.S. 87-75
ATTN: Aerospace Library
ATTN: Howard W. Wicklein, M.S. 17-11
ATTN: Robert S. Caldwell, 2R-00

Booz-Allen and Hamilton, Inc.
ATTN: Raymond J. Chrisner

DEPARTMENT OF DEFENSE CONTRACTORS
(Continued)

California Institute of Technology
Jet Propulsion Laboratory
ATTN: J. Bryden
ATTN: A. G. Stanley

Charles Stark Draper Laboratory, Inc.
ATTN: Kenneth Fertig

Computer Sciences Corporation
ATTN: Richard H. Dickhaut

Cutler-Hammer, Inc.
ATTN: Central Tech. Files, Anne Anthony

The Dikewood Corporation
ATTN: L. Wayne Davis

E-Systems, Inc.
ATTN: Library 8-50100

Effects Technology, Inc.
ATTN: Edward John Steele

Fairchild Camera and Instrument Corp.
ATTN: Sec. Dept. for 2-233, David K. Myers

Fairchild Industries, Inc.
Sherman Fairchild Technology Center
ATTN: MGR Config. Data & Standards

Garrett Corporation
ATTN: Robert E. Weir, Dept. 93-9

General Dynamics Corp.
Electronics Division
ATTN: D. W. Coleman

General Electric Company
Space Division
ATTN: Larry I. Chasen
ATTN: John L. Andrews
ATTN: Joseph C. Peden, VFSC, Rm 4230M

General Electric Company
Re-Entry & Environmental Systems Division
ATTN: John W. Palchefsky, Jr.
ATTN: Robert V. Benedict

General Electric Company
Ordnance Systems
ATTN: Joseph J. Reidl

General Electric Company
TEMPO-Center for Advanced Studies
ATTN: Royden R. Rutherford
ATTN: DASIAC
ATTN: M. Espig

General Electric Company
ATTN: CSP 0-7, L. H. Dee

General Electric Company
Aircraft Engine Group
ATTN: John A. Ellerhorst, E-2

Georgia Institute of Technology
Georgia Tech. Research Institute
ATTN: R. Curry

DEPARTMENT OF DEFENSE CONTRACTORS
(Continued)

General Electric Company
Aerospace Electronics Systems
ATTN: Charles M. Hewison, Drop 624
ATTN: W. J. Patterson, Drop 233

General Electric Company—TEMPO
ATTN: DASIAC for William Alfonte

Grumman Aerospace Corporation
ATTN: Jerry Rogers, Dept. 533

GTE Sylvania, Inc.
Electronics Systems Grp.—Eastern Division
ATTN: Leonard L. Blaisdell
ATTN: James A. Waldon
ATTN: Charles A. Thornhill, Librarian

GTE Sylvania, Inc.
ATTN: H & V Group, Mario A. Nurefora
ATTN: Herbert A. Ullman

Gulton Industries, Inc.
Engineered Magnetics Division
ATTN: Engnmagnetics Division

Harris Corporation
Harris Semiconductor Division
ATTN: Wayne E. Abare, M.S. 16-111
ATTN: T. L. Clark, M.S. 4040
ATTN: Carf F. Davis, M.S. 17-220

Hazeltine Corporation
ATTN: Tech. Info. Center, M. Waite

Honeywell, Incorporated
Government and Aeronautical Products Division
ATTN: Ronald R. Johnson, A1622

Honeywell, Incorporated
Aerospace Division
ATTN: Harrison H. Noble, M.S. 725-5A
ATTN: Stacey H. Graff, M.S. 725-J

Honeywell, Incorporated
Radiation Center
ATTN: Technical Library

Hughes Aircraft Company
ATTN: John B. Singletary, M.S. 6-D133
ATTN: Billy W. Campbell, M.S. 6-E110
ATTN: Kenneth R. Walker, M.S. D157

Hughes Aircraft Company
Space Systems Division
ATTN: Edward C. Smith, M.S. A620
ATTN: William W. Scott, M.S. A1080

IBM Corporation
ATTN: Frank Frankovsky

IIT Research Institute
ATTN: Irving N. Mindel

Intl. Tel. & Telegraph Corporation
ATTN: Alexander T. Richardson

DEPARTMENT OF DEFENSE CONTRACTORS
(Continued)

IRT Corporation
ATTN: Ralph H. Stahl
ATTN: R. L. Mertz
ATTN: Leo D. Cotter
ATTN: MDC
ATTN: V. V. Verbinski

Jaycor
ATTN: Robert Sullivan
ATTN: Catherine Turesko

Johns Hopkins University
Applied Physics Laboratory
ATTN: Peter E. Partridge

Kaman Sciences Corporation
ATTN: Albert P. Bridges
ATTN: Donald H. Bryce

Litton Systems, Inc.
Guidance & Control Systems Division
ATTN: John P. Retzler
ATTN: Val J. Ashby, M.S. 67

Lockheed Missiles & Space Co., Inc.
ATTN: Benjamin T. Kimura, Dept. 81-14
ATTN: Edwin A. Smith, Dept. 85-85
ATTN: G. H. Morris, Dept. 81-01
ATTN: L. Rossi, Dept. 81-64
ATTN: Samuel I. Taimuty, Dept. 85-85

Lockheed Missiles and Space Company
ATTN: Tech. Info. Center, D. Coll.

LTV Aerospace Corporation
Vought Systems Division
ATTN: Technical Data Center

LTV Aerospace Corporation
ATTN: *Tech. Library*

M.I.T. Lincoln Laboratory
ATTN: Leona Loughlin, Librarian, A-082

Martin Marietta Aerospace
ATTN: Mona C. Griffith, Library MP-30
ATTN: Jack M. Ashford, MP-537
ATTN: William W. Mras, MP-413

McDonnell Douglas Corporation
ATTN: Tech. Library
ATTN: Tom Ender

Mission Research Corporation
ATTN: William C. Hart

Mission Research Corporation
ATTN: V. A. J. Van Lint

National Academy of Sciences
ATTN: National Materials Advisory Board for
R. S. Shane, Nat. Materials Advsy.

Palisades Inst. for Rsch. Services, Inc.
ATTN: Records Supervisor

DEPARTMENT OF DEFENSE CONTRACTORS
(Continued)

Northrop Corporation
Electronic Division
ATTN: Boyce T. Ahlport
ATTN: Vincent R. DeMartino

Northrop Corporation
Northrop Research and Technology Center
ATTN: Orlie L. Curtis, Jr.
ATTN: J. R. Srour
ATTN: David N. Pocock

Power Physics Corporation
ATTN: Mitchell Baker

R & D Associates
ATTN: S. Clay Rogers

Raytheon Company
ATTN: Gajanan H. Joshi, Radar Sys. Lab.

Raytheon Company
ATTN: Harold L. Flescher

RCA Corporation
Government & Commercial Systems
Astro Electronics Division
ATTN: George J. Brucker

RCA Corporation
David Sarnoff Research Center
ATTN: K. H. Zaininger
ATTN: Gerald B. Herzog

RCA Corporation
ATTN: E. Van Keuren, 13-5-2

Research Triangle Institute
ATTN: Eng. Div., Mayrant Simons, Jr.

Rockwell International Corporation
ATTN: James E. Bell, HA10
ATTN: N. J. Rudie, FA53
ATTN: K. F. Hull
ATTN: L. Apodaca, FA53
ATTN: George C. Messenger, FB61

Rockwell International Corporation
ATTN: T. B. Yates

Rockwell International Corporation
Electronics Operations
ATTN: Dennis Sutherland
ATTN: Alan A. Langenfeld
ATTN: Mildred A. Blair

Sanders Associates, Inc.
ATTN: Moe L. Aitel, NCA 1-3236

Science Applications, Inc.
ATTN: J. Robert Beyster
ATTN: Larry Scott

Simulation Physics, Inc.
ATTN: Roger G. Little

DEPARTMENT OF DEFENSE CONTRACTORS
(Continued)

The Singer Company
ATTN: Tech. Info. Center

Sperry Flight Systems Division
Sperry Rand Corporation
ATTN: D. Andrew Schow

Sperry Rand Corporation
Univac Division
Defense Systems Division
ATTN: James A. Inda, M.S. 41T25

Sperry Rand Corporation
Sperry Division
Sperry Gyroscope Division
Sperry Systems Management Division
ATTN: Charles L. Craig, EV
ATTN: Paul Marraffino

Stanford Research Institute
ATTN: Philip J. Dolan

Sundstrand Corporation
ATTN: Curtis B. White

Texas Instruments, Inc.
ATTN: Donald J. Manus, M.S. 72
ATTN: H. D. Toombs

TRW Systems Group
ATTN: Robert M. Webb, R1-2410
ATTN: Barry Dunbridge
2cy ATTN: R. K. Plebuch, R1-2078
ATTN: H. H. Holloway, R1-2036
2cy ATTN: O. E. Adams, R1-1144
ATTN: Tech. Info. Center, S-1930
ATTN: Jerry I. Lubell, R1-1144

TRW Systems Group
ATTN: Earl W. Allen, 520/141
ATTN: F. B. Fay, 527/710

TRW Systems Group
ATTN: Donald W. Pugsley

United Technologies Corporation
Hamilton Standard Division
ATTN: Raymond G. Giguere

Westinghouse Electric Corporation
Defense and Electronic Systems Center
ATTN: Henry P. Kalapaca, M.S. 3525

Jack S. Kilby